Elucidating the Role of the Iron-Sulfur Cluster in the Nuclease/Helicase Dna2

DISSERTATION
ZUR
ERLANGUNG DER NATURWISSENSCHAFTLICHEN DOKTORWÜRDE
(Dr. sc. nat.)
VORGELEGT DER
MATHEMATISCH-NATURWISSENSCHAFTLICHEN FAKULTÄT
DER
UNIVERSITÄT ZÜRICH
VON

RICHARD EDWARD LUTZ

AUS
GEORGIA, VEREINIGTE STAATEN von AMERIKA

PROMOTIONSKOMMISSION:

PROF. DR. KERSTIN GARI (VORSITZ UND LEITUNG DER DISSERTATION)
PROF. DR. JOSEF JIRICNY
DR. PETR CEJKA
PROF. DR. ORLANDO SCHÄRER
PROF. DR. LORENZA PENENGO

ZÜRICH, 2018

-To Mom and Dad-

Table of Contents

Abstract

The genetic blueprint of all living organisms, whether unicellular (e.g. bacteria) or multicellular (e.g. human) is encoded by its genome. One of the most fundamental challenges of the cell is to accurately copy and transmit its genome to daughter cells. In addition, during their life cycle cells are often exposed to many forms of DNA replication stress and DNA damage, and combat this *via* the complex network of interconnected pathways, named the DNA damage response (DDR). If this process goes awry, genomic instability develops and, depending on specific mechanisms involved, presents in various forms and represents a major hallmark of cancer. Over the years, a number of critical proteins in DNA replication and repair have been shown to coordinate an FeS cluster (i.e. DNA2, DNA primase, Polα, Polδ, Polε, MUTYH, XPD, RTEL1, FANCJ, and ChlR1). These findings were rather surprising, given that upon FeS cluster oxidation, free iron atoms can generate dangerous reactive oxygen species that may interfere with DNA integrity and lead to genomic instability. So far, the function of FeS clusters in these proteins is largely unknown.

Since all known FeS cluster proteins interact with MMS19/MIP18, core members of the Cytoplasmic Iron-sulfur Assembly (CIA) machinery, we reasoned that new FeS proteins may be amongst the interaction partners of MMS19/MIP18, previously identified by mass spectrometry. In this study we focused on Replication Factor C subunit 5 (RFC5) since it not only associates with MMS19/MIP18, but also displays synthetic lethality with *mms19*Δ in yeast, a feature observed for multiple FeS proteins. Using co-immunoprecipitation interaction studies with the CIA machinery and ^{55}Fe incorporation assays, our data show that while RFC5 interacts with both MMS19 and MIP18, it is unlikely to coordinate an FeS cluster. Additional studies will be required to identify the functional relevance of RFC5's interaction with the CIA machinery.

In our second study, we aimed to further characterize the role of the FeS cluster in the nuclease/helicase Dna2, a known FeS cluster protein. The role of the FeS cluster in Dna2 had been previously studied, where it was shown that loss of the FeS cluster eliminated Dna2's nuclease activity and reduced ATPase activity. Considering the fragile nature of FeS clusters and the threat of oxidation, coupled with advancements in protein purification and FeS cluster biology, we asked whether the integrity of the FeS cluster was maintained during purification in the latter study. Therefore, using recombinant Dna2 WT and mutants purified using an optimized protocol, we characterized Dna2's nuclease and helicase activities. Our *in vitro* data suggest that potent nuclease activity depends on the FeS cluster, but is not completely abolished in the FeS binding mutant, in contrast to previously reported data. Furthermore, the helicase activity is highly reduced upon loss of the FeS cluster, despite the helicase domain being distant from the FeS binding domain. In

addition, we characterized the role of Dna2's FeS cluster in Okazaki fragment maturation with nuclease- and replication-based assays. Our data suggests that the FeS cluster in Dna2 regulates its cleavage site *in vitro*, with WT Dna2 being able to cleave at the base of an Okazaki fragment, while the FeS binding mutant is unable to cleave at the base, which prevents the formation of a ligatable substrate and the completion of Okazaki fragment maturation. Taken together, our data suggest a critical role of the FeS cluster in Dna2 in regulating its cellular activities.

Zusammenfassung

Der genetische Bauplan aller lebender Organismen, ob unizellulär (z.B Bakterien) oder multizellulär (z.B der Mensch), ist in deren Genom codiert. Eine der grössten Herausforderungen einer Zelle ist es, ihr Genom zuverlässig zu verdoppeln und möglichst akkurat an ihre Tochterzellen weiterzugeben. Unterdessen sind Zellen im Laufe ihres Lebenszyklus häufig verschiedenen Formen von DNA-Replikationsstress und DNA-Schäden ausgesetzt. Diese initiieren die Aktivierung eines komplexen Netzwerks aus Signalwegen, das kollektiv als DNA-Schadensantwort bezeichnet wird. Ein Scheitern dieses Prozesses kann zu genomischer Instabilität führen, die sich abhängig von den involvierten Mechanismen auf verschiedene Art und Weise manifestieren kann und ein Schlüsselmerkmal von Krebserkrankungen darstellt. In den letzten Jahren wurde gezeigt, dass einige Proteine, die an der DNA-Replikation und -Reparatur beteiligt sind, ein Eisen-Schwefel (FeS)-Cluster koordinieren (z.B. DNA2, DNA Primase, Polα, Polδ, Polε, MUTYH, XPD, RTEL1, FANCJ und ChlR1). Diese Erkenntnis war überraschend, da infolge einer Oxidation des FeS-Clusters freie Eisenatome gefährliche reaktive Sauerstoffspezies generieren, welche die DNA schädigen und so genomische Instabilität verursachen können. Bis heute ist die Funktion der FeS-Cluster in diesen Proteinen weitestgehend unbekannt.

Weil alle bekannten FeS-Cluster-Proteine mit MMS19/MIP18, den zentralen Mitgliedern der zytoplasmatischen Eisen-Schwefel-Cluster-Assembly (CIA) Maschinerie, interagieren, vermuteten wir, dass sich bisher unbekannte FeS-Cluster-Proteine unter den Interaktionspartnern von MMS19/MIP18 befinden, die zuvor mit Hilfe von Massenspektrometrie identifiziert wurden. In dieser Studie haben wir uns mit Replikationsfaktor C Untereinheit 5 (RFC5) beschäftigt, weil diese nicht nur mit MMS19/MIP18 assoziiert, sondern zusätzlich in Hefe eine synthetische Letalität mit *mms19*Δ aufweist, eine Eigenschaft die bei mehreren FeS-Cluster-Proteinen beobachtet wurde. Durch Co-Immunpräzipitation mit der CIA-Maschinerie und ^{55}Fe-Inkorporationsassays konnten wir zeigen, dass RFC5 zwar sowohl mit MMS19 als auch MIP18 interagiert, jedoch wahrscheinlich kein FeS-Cluster koordiniert. Zusätzliche Studien sind erforderlich, um die funktionale Relevanz der Interaktion zwischen RFC5 und der CIA-Maschinerie zu analysieren.

Unsere zweite Studie hatte das Ziel, die Rolle des FeS-Clusters in der Nuklease/Helikase Dna2, einem schon bekannten FeS-Cluster-Protein, zu charakterisieren. Die Rolle des FeS-Clusters in Dna2 wurde zuvor in einer Studie untersucht, in der gezeigt wurde, dass der Verlust des FeS-Clusters Dna2's Nukleaseaktivität eliminiert, sowie dessen ATPase-Aktivität reduziert. Die Fragilität des FeS-Clusters, das Risiko einer Oxidation, sowie den Fortschritt

bei Proteinaufreinigungsmethoden und der FeS-Cluster Biologie berücksichtigend, haben wir infrage gestellt, ob die Integrität des FeS-Clusters während der genannten Studie sichergestellt wurde. Deshalb haben wir die Nuklease- und Helikaseaktivität von rekombinantem Dna2, das mit Hilfe eines optimierten Protokolls aufgereinigt wurde, charakterisiert. Die Ergebnisse unserer *in vitro* Studien deuten darauf hin, dass die Nukleaseaktivität vom FeS-Cluster abhängt, im Gegensatz zu den publizierten Daten jedoch in einer Mutante, die das FeS-Cluster nicht mehr binden kann, nicht komplett eliminiert wird. Des Weiteren ist auch die Helikaseaktivität nach Verlust des Clusters stark reduziert, obwohl die Helikase-Domäne weit entfernt von der Domäne liegt, die das FeS-Cluster bindet. Zusätzlich haben wir die Rolle von Dna2's FeS-Cluster bei der Okazaki-Fragment-Reifung mit Nukleaseassays und Replikationsassays untersucht. Unsere Daten weisen darauf hin, dass das FeS cluster *in vitro* die Schnittposition von Dna2 beeinflusst, wobei Wildtyp-Dna2 in der Lage ist, an der Basis eines Okazaki-Fragments zu schneiden, während die FeS-Bindemutante nicht an der Basis scheiden kann, was die Bildung eines ligierbaren Substrates und somit die Volllendung der Okazaki-Fragment-Reifung verhindert. Zusammenfassend zeigen unsere Daten, dass das FeS-Cluster eine wichtige Rolle bei der Regulation der zellulären Aktivitäten von Dna2 spielt.

Acknowledgements

I would like to express my gratitude to Prof. Dr. Kerstin Gari for giving me the opportunity to work and study in her research group and involving me in such a exciting and fulfilling project. Furthermore, I would like to thank her for all of her support in and out of the lab, I have truly learned a lot from her and moving forward in life I will be able to take the skills she has taught me and apply them in whatever career I may find myself in. Above all, I would like to thank her for her patience and understanding as I navigated through some difficult moments in life, it made hard times easier.

I would also like to thank the members of my thesis committee: Prof. Dr. Josef Jiricny, Dr. Petr Cejka, Prof. Dr. Orlando Schärer, and Prof. Dr. Lorenza Penengo for all of the fruitful scientific discussions and support during the duration of PhD studies.

Furthermore, I would like to thank the entire Institute of Molecular Cancer Research, for creating a wonderful and stimulating working environment, it has been a pleasure to work alongside you these past years. In addition I would like to thank the technical and administrative staff, for taking care of all us in the institute and for keeping everything moving so seamlessly, especially Farah Mhamedi, Odete Alves, Danielle Luterbacher, and Annica Mandola.

It goes without saying, but I want to give a huge thanks to all the members of the Gari group, it has been a great privilege to work and grow scientifically with you. I am very grateful for your support and friendship and will always look back fondly on our time together. In addition, I would like to thank Dr. Maryna Levikova and Dr. Cosimo Pinto for all of your assistance and guidance on the Dna2 project, it wouldn't of gotten off the ground without your help. Moreover, I want to thank all of my friends from back home and the new ones I've met in Europe, for your support and friendship, it truly means a lot.

I dedicate my thesis to my parents Ae Sun and Richard Lutz, thank you for all of the support through the years as I chased after my academic goals. I am very grateful to have parents that have always supported me, even when I left the continent. Furthermore, I would like to thank my sisters Kimberly and Jennifer for always being the best and supportive sisters in the world. In addition, I would like to thank Birgit and Frank Meyer for all of their support as I moved, first to Germany and then to Switzerland, I am so grateful to have you in my life.

Last, but not least, I want to thank my partner Susanne Meyer, for always being there for me, supporting me and following me as I chased my academic goals. I wouldn't be where I am today with out your steadfast support and love.

1. Introduction

1.1 Genome Instability and Cancer

The genetic blueprint of all living organisms, whether unicellular (e.g. bacteria) or multicellular (e.g. human) is encoded by its genome. One of the most fundamental challenges of the cell is to accurately copy and transmit its genome to daughter cells. Replicating the entire genome is no simple task; eukaryotic genomes are quite large, ranging from 10^7 to > 10^9 base pairs (bp), and are organized into multiple chromosomes. The basic machinery utilized during semi-conservative DNA replication is conserved from prokaryotes to eukaryotes, all working together in co-ordinated actions to promote replication fidelity. Moreover, the fidelity of this process is dependent on the precision of regulatory mechanisms that couple DNA replication to cell cycle progression (DePamphilis et al., 2006).

During their life, cells are exposed to many forms of DNA replication stress and DNA damage (*Figure 1.1)*, and combat this *via* the complex network of interconnected pathways, named the DNA damage response (DDR). If this process goes awry, genomic instability develops and, depending on specific mechanisms involved, presents in various forms (Abbas et al., 2013). Therefore, genome instability can result from point mutations and microsatellite instability (MSI) that is characterized by the expansion or contraction of the number of nucleotide repeats present in microsatellite sequences, and defective nucleotide or base excision repair (NER/BER), or mismatch repair (MMR). Additionally, genome instability may also result from gross chromosomal rearrangements, aneuploidy (i.e. the loss or gain of copies in genes or chromosomal regions that differ from the wild type), hyper-recombination, loss of heterozygosity (LOH) and, most commonly, chromosomal instability (CIN), which is in general defined by the elevated rates by which chromosome structure and number changes over time in cancer cells compared with normal cells (Abbas et al., 2013; Aguilera & García-Muse, 2013; Negrini et al., 2010).

The mechanisms underlying the causes of these instabilities still remain elusive, but two major hypotheses attempt to explain the driving force of tumor initiation and progression through genomic instability. The first, named the mutator hypothesis, establishes the idea that genomic instability present in pre-cancerous lesions is due to mutations in caretaker genes (i.e. DNA repair genes and mitotic checkpoint genes) and this helps them drive tumorigenesis by enhancing the accumulation of spontaneous mutations (Loeb, 2011). In hereditary cancers, the presence of genomic instability is clearly linked to mutations in DNA repair genes. Indeed, it was shown that germline mutations in breast cancer susceptibility type 1 (BRCA1), BRCA2, NBS1, Werner syndrome (WRN) helicase, BLM, and the Fanconi anemia genes, all involved in double-strand break (DSB) or DNA interstrand cross link repair, increase the risk for the development of various cancers, such

as breast and ovarian cancer, leukemias and lymphomas as predicted by the mutator hypothesis (Negrini et al., 2010).

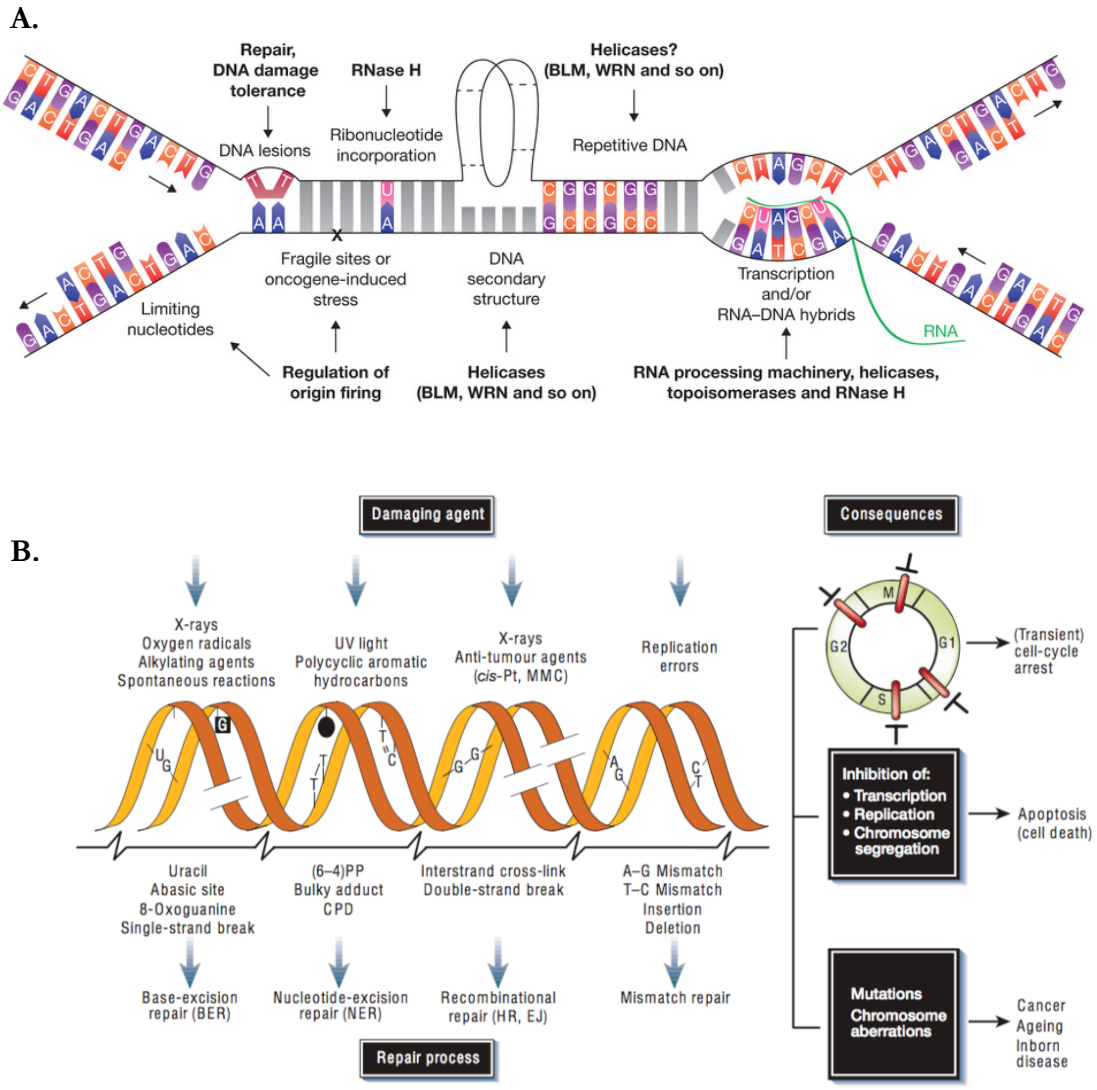

Figure 1.1 Sources of replication stress and DNA damage. (A.) There are a number of conditions that can cause replication stress as noted above, some of the key resolution pathways are indicated in bold. Figure modified from (Zeman & Cimprich, 2014) (B.) There are a variety of DNA damaging agents (top), that induce a variety of DNA lesions (middle), which are addressed by dedicated repair mechanisms (bottom). Any unresolved DNA damage may lead to cell death, and disease. Figure modified from (Hoeijmakers, 2001)

In contrast to hereditary cancers, the molecular basis of genomic instability in sporadic (non-hereditary) remains unclear. Although sporadic cancers exhibit genomic instability and mutations in a large number of genes, they very often do not have mutations in the caretaker genes. The genomic instability exhibited in these cancers can be explained by the oncogene-induced DNA replication stress model (Halazonetis et al., 2008). In this model, tumor development results from oncogene-induced collapse of DNA replication forks, especially at common fragile sites, followed by the formation of DSBs and activation of the DDR pathway. Breaks at common fragile sites can drive genomic instability and constitutively activated DDR also leads to elevated levels of errors during DNA repair, which in turn favors the transition of a precancerous lesion into cancer (Bartkova et al., 2005; Gorgoulis et al., 2005; Yao & Dai, 2014). Furthermore, mutations in *p53* and *ATM,* vital genes in cell cycle control and DNA repair, raise the support of oncogene-induced DNA replication stress, as they cause gross misregulation of DNA replication and repair. Therefore, mutations in *p53* and *ATM* can be attributed to the development of genomic instability and oncogene-induced DNA damage (Yao & Dai, 2014).

In spite of the tremendous advances made in our understanding of the causes of genomic instability and its role in the development of cancer, more studies are required to clearly identify the mechanism of tumor initiation. The hypotheses presented above may both be legitimate in specific settings, but regardless of the driving force of tumor initiation, the management of DNA replication stress and DNA damage in a timely manner is critical, as they are major threats in maintaining genome integrity and stability and represent major hallmarks of cancer (*Figure 1.2)* (Abbas et al., 2013; Negrini et al., 2010).

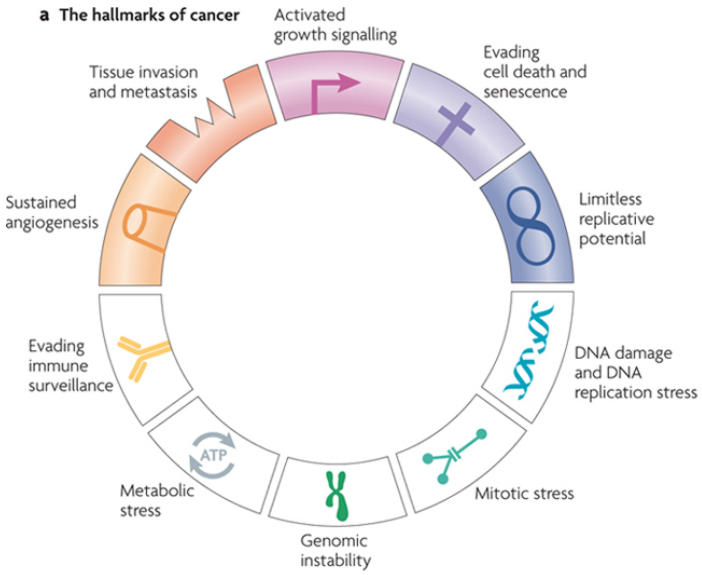

Figure 1.2 The hallmarks of cancer. First described by Douglas Hanahan and Robert Weinberg in 2000, details the multiple characteristics cells acquire in the development of cancer. (Negrini et al., 2010)

1.2 Eukaryotic Cell Cycle

The most basic function of the cell cycle is to accurately duplicate the entire genome and then segregate the copies into two genetically identical daughter cells. These activities define the two major phases of the cell cycle, *S phase* (S for DNA synthesis) where chromosome duplication occurs and *M phase* (M for mitosis) where chromosome segregation and cell division occurs. In addition, the cell cycle contains two gap phases G_1 (between M- and S phase) and G_2 (between S phase and mitosis) (*Figure 1.3)*. During the gap phases, the cells monitor the internal and external environment to ensure all the conditions are met for the major processes of S phase and mitosis. In the event that conditions are not met, cells can delay the progress of G_1 and enter a specialized resting state called G_0 (Alberts et al., 2015, pp. 1054-1055). Furthermore, the cell cycle is highly regulated to ensure that all stages occur in the correct order and that each phase is completed before the next one commences (Sclafani & Holzen, 2007). If the cell cycle's regulatory mechanisms are compromised, this leads to the accumulation of DNA damage or in some cases catastrophic damage that induces apoptosis, due to the misregulation of repair pathways. However, if corrupted cells escape apoptosis, they may proliferate unchecked and replicate DNA without pausing to repair the damage, which contributes to genome instability and the development of cancer (Alberts et al., 2015, p. 1074).

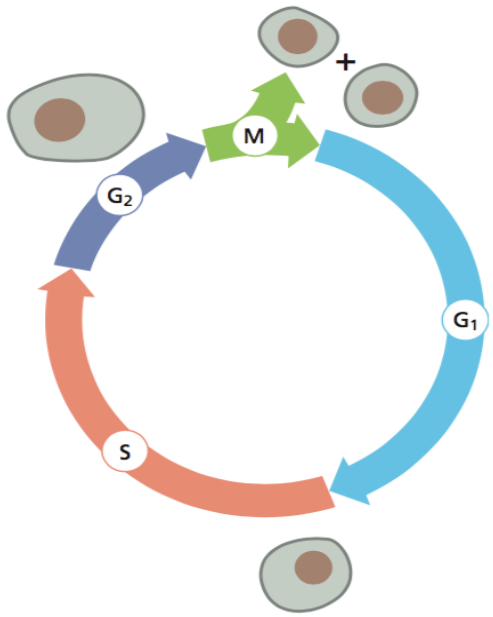

Figure 1.3 Eukaryotic Cell Cycle
Divided in discrete phases and progression regulated by cell cycle checkpoints, that help ensure the DNA is replicated faithfully and only once and that the cell is prepared for division. (Alberts et al., 2015)

1.3 Eukaryotic DNA Replication

Eukaryotic DNA replication is a complex process that involves the coordination of multiple protein complexes to initiate, synthesize and process the DNA (Burgers & Kunkel, 2017). The initial steps of DNA replication occur as early as G_1 phase of the cell cycle, when pre-initiation replication complexes assemble at the origins of replication. The origins of replication are distributed throughout the genome and are strictly regulated to ensure a single firing per replication cycle. The origin recognition complex (ORC), a multi-component complex, is then recruited to the origin. Next, Cdc6 recruits the minichromosome maintenance (MCM) proteins 2-7, joining the ORC to form the pre-replicative complex (pre-RC). Pre-RCs are then activated to generate active replication forks (Masai et al., 2010). DNA synthesis always occurs in the 5' to 3' direction, but due to the anti-parallel nature of DNA, moving replication forks can only synthesize one of the two strands continuously. DNA synthesis in the direction of DNA unwinding occurs continuously and is termed leading strand replication. In contrast, the other strand is synthesized discontinuously in small sections, which is termed lagging strand replication. Initiation of DNA replication is associated with the formation of the replicative CMG helicase (Cdc45, MCM 2-7, GINS) and the association of the replicative polymerases (*Table 1.1)* at the pre-RC (Burgers & Kunkel, 2017). In humans, Pol α/primase initiates *de novo* synthesis on both the leading and lagging strands by incorporating ~10 nucleotides (nt) of initiator RNA followed by ~20 nt of initiator DNA (Burgers, 2009). Subsequently, the replication factor C (RFC) complex binds to the RNA/DNA primer and loads proliferating cell nuclear antigen (PCNA), which assists in the switching of Pol α/primase for the more processive Pol δ and/or Pol ε. Thereafter, elongation takes place on the leading strand *via* RFC, PCNA, and Pol ε, whereas, on the lagging strand, the small sections of DNA, termed Okazaki fragments, are extended by RFC, PCNA, and Pol δ (Garg & Burgers, 2005). However, the consensus view of the division of labor between Pol ε and Pol δ on extending the leading and lagging strand has been challenged in recent years, with studies providing evidence that Pol δ functions as the main DNA polymerase in replication with Pol ε playing a more auxiliary role (Georgescu et al., 2014; Johnson et al., 2015).

Table 1.1 Eukaryotic replicative DNA polymerases

DNA Polymerases	Function
α (alpha)	Initiates DNA replication in conjunction with primase
δ (delta)	Replication of the lagging strand during S phase
ε (epsilon)	Replication of the leading strand during S phase

1.4 Lagging Strand Replication

As noted above, DNA replication can only occur continuously on the leading strand, which is elongated by Pol ε. In contrast, the lagging strand is synthesized in small sections (Okazaki fragments ~150-190 nt) by Pol δ. Upon encountering the previously-synthesized Okazaki fragment, Pol δ displaces the downstream RNA/DNA primer into a 5' flap *via* strand displacement synthesis. This 5' flap must be removed in order to create a ligatable nick that can be processed into a continuous DNA strand (Balakrishnan & Bambara, 2011). Failure to join the fragments compromises the integrity of the genome.

1.4.1 Lagging Strand Replication: FEN1 Only Pathway

Based on the available biochemical data, the nuclease thought to be responsible for digesting the majority of the displaced flaps is Flap Endonuclease 1 (FEN1; Rad27 in *S. cerevisiae)*. FEN1 is a 5' to 3' endonuclease that belongs to a class of structure-specific flap nucleases that recognize and cleave at the 5' junction between ssDNA and dsDNA to generate a nick (Balakrishnan & Bambara, 2013). The nick left by FEN1 is sealed by DNA ligase I, resulting in a mature Okazaki fragment that is part of the continuous DNA complex *(Figure 1.4)*. However, genetic studies have shown that the deletion of FEN1 is still viable but the *rad27*Δ strain exhibits temperature-sensitive growth, defects in DNA replication, high rates of recombination and methyl methanesulfonate (MMS) sensitivity (Reagan et al., 1995; Sommers et al., 1995). In addition, during the course of strand displacement, the 5' flaps can become longer and coated by the ssDNA binding protein, Replication Protein A (RPA). These longer RPA-coated 5' flaps are unable to be processed by FEN1 (Bae et al., 2001). These findings questioned FEN1 as the sole nuclease involved in Okazaki fragment maturation, making it likely that overlapping pathways evolved to maintain such an essential process.

1.4.2 Lagging Strand Replication: The Two Nuclease Pathway

The secondary pathway for Okazaki fragment processing was first proposed by Seo and colleagues, in which the longer 5' RPA coated flaps require the action of a second nuclease, Dna2. In this pathway, the binding of RPA to the long flap intermediates inhibits FEN1, creating a requirement for Dna2, which is stimulated by RPA to cleave the flap. This generates a shorter flap (~5-7 nt) that can no longer be bound by RPA, freeing FEN1 to generate a substrate for ligation (Bae et al., 2001) *(Figure 1.4)*. Dna2 was originally discovered in a genetic screen for genes involved in DNA replication in yeast and was later shown to be involved in Okazaki fragment maturation *via* genetic and biochemical interactions with several known Okazaki fragment processing proteins (Budd & Campbell, 1995; Budd & Campbell, 1997; Kuo et al., 1983). Furthermore, Dna2 was found to be an

essential gene with several temperature-sensitive mutants being identified to study the consequences of impaired Dna2 activity. Two Dna2 mutants in particular have been well characterized; the *dna2-1* (nuclease deficient) and *dna2-2* (helicase deficient) strains (Budd & Campbell, 1995; Budd et al., 1995). As mentioned above, the *rad27*Δ strain is viable, but can not survive without Dna2 function, as *dna2-1*Δ and *rad27*Δ are synthetically lethal. In addition, it was shown that overexpression of Dna2 suppresses the temperature-sensitive growth defects of the *rad27Δ* strain, suggesting that Dna2 may compensate for the loss of function of FEN1 in Okazaki fragment maturation (Budd & Campbell, 1997). These observations were later supported by *in vitro* experiments, which demonstrated that Dna2 processes RNA-DNA flaps more efficiently than DNA-only flaps, making it well suited for the processing of long flaps generated during Okazaki fragment maturation (Bae & Seo, 2000). However, the observation that Dna2 would only degrade a portion of the flap but not entirely, leaving behind a smaller flap (~5-7 nt), suggested that it functions in concert with FEN1 to produce a ligatable nick to complete Okazaki fragment maturation (Ayyagari et al., 2003; Bae et al., 2001). Interestingly, *dna2-1*Δ is lethal in combination with a mutation in Pol δ (*pol3-01)* that stimulates strand displacement synthesis. In a similar fashion, deletion of the Pol32 subunit, which limits strand displacement synthesis of Pol δ *in vitro*, suppresses the growth defects of the *dna2-1*Δ strain (Budd et al., 2005; Garg et al., 2004; Gerik et al., 1998; Johansson et al., 2004). Taken together, these observations suggest that Dna2 is critical under conditions that promote the formation of long flaps and works in coordinated actions with FEN1 to produce a ligatable nick. This pathway for Okazaki fragment processing is now known as the "two-nuclease pathway", however a recent study has challenged this notion, demonstrating that Dna2 can act as the sole nuclease in Okazaki fragment maturation *in vitro*, without the need for further FEN1 processing (Levikova & Cejka, 2015). In this study, Levikova and Cejka propose that Dna2 processes the majority of Okazaki fragments, with FEN1 functioning downstream of Dna2 in cases of inaccurate cleavage by Dna2, or if strand displacement synthesis occurs again before ligation can be completed. This hypothesis is further supported by the fact that Dna2 is essential *in vivo*, whereas FEN1 is dispensable under certain growth conditions.

Further work done in *Saccharomyces cerevisiae* demonstrated a genetic interaction between PIF1 and Dna2 (Budd et al., 2006). PIF1 is a 5' to 3' helicase involved in telomere maintenance and mitochondrial DNA replication. However, it was later shown that the selective inactivation of the nuclear PIF1 isoform suppressed the lethality of *dna2Δ* , pointing to a role for PIF1 in Okazaki fragment maturation by promoting long flap formation (Budd et al., 2006; Stith et al., 2008). Subsequent studies demonstrated *in vitro* that the PIF1 helicase directly stimulates the strand displacement synthesis activity of Pol δ, indicating that DNA flaps are extended in the presence of PIF1, which in turn makes

the function of Dna2 required to complete Okazaki fragment maturation (Pike et al., 2009; Rossi et al., 2008).

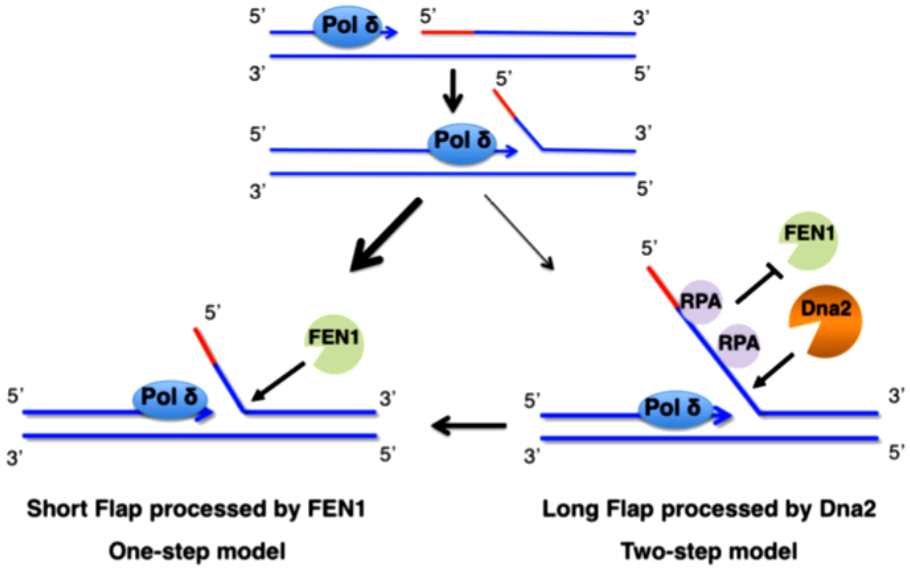

Figure 1.4 Two Models for Okazaki Fragment Maturation. During the course of synthesis on the lagging strand, Pol δ encounters the terminal end of the previous fragment and begins strand displacement synthesis. If the displaced 5' flap does not become too large and coated by RPA, it is processed solely by FEN1 (*left side).* However, in the event the 5' flap becomes large and coated by RPA, the flap requires of a second nuclease Dna2 *(right side).* First, Dna2 cuts along the flap leaving behind a smaller flap, that is then further processed by FEN1, completing Okazaki fragment maturation. In recent years, this model has been challenged by the observed ability of Dna2 to cut at the base and its essential nature in cells. Figure Adapted from (Bae et al., 2001; Ayyagari et al., 2003)

1.5 DNA Replication Stress

Remarkably, despite its size, the genome is duplicated faithfully during each cell cycle. However, DNA replication isn't an unchallenged process. Deregulation of internal cellular processes or exogenous sources that may interfere with replication can cause cells to undergo replication stress. Until now, due to a lack of unambiguous markers that can be used to definitively detect this cellular event, replication stress remains insufficiently characterized. However, a defining characteristic of replication stress is the slowing or stalling of replication forks and/or DNA synthesis (Zeman & Cimprich, 2014). There are a number of conditions or replicative challenges that can slow or stall DNA replication, including reduced dNTPs pools, DNA lesions, ribonucleotide incorporation, repetitive DNA sequences, DNA-protein crosslinks, DNA secondary structures, fragile sites and oncogene-induced stress (*Figure 1.1A)* (Zeman & Cimprich, 2014). If replication stress is not dealt with in a timely manner, it can lead to DNA damage that can exacerbate the stresses that challenge fork progression, provoking their collapse. In addition, several

studies have shown that pre-cancerous lesions display DNA damage, purportedly due to alterations of the replication process (Técher et al., 2017).

1.6 DNA Damage

DNA damage may result from both endogenous and exogenous challenges, for example, various environmental agents, such as ultraviolet (UV) light, ionizing radiation (IR) and genotoxic agents that can disrupt DNA integrity. Furthermore, normal metabolic processes, such as cellular respiration, can indirectly damage DNA through the production of reactive oxygen species (ROS). Altogether, it is estimated that every cell experiences up to 10^5 DNA lesions per day (Hoeijmakers, 2001). However cells have evolved specific repair mechanisms to address the different DNA lesions inflicted on the cell (*Figure 1.1B)* (Hoeijmakers, 2009). The abundant causes of replication stress and DNA damage highlight the challenges the cell faces during DNA replication. However, as noted above, under normal conditions there are multiple repair pathways dedicated to DNA damage signaling, repair and cell cycle control, that efficiently overcome these replicative obstacles (Ciccia & Elledge, 2010).

1.7 DNA Damage Response (DDR)

To maintain genomic integrity, DNA must be safeguarded from damage induced by environmental agents and/or generated spontaneously during normal DNA metabolism. Therefore, to avoid the consequences of DNA damage, cells have evolved a complex network of interconnected pathways, named the DDR. The DDR is a multifaceted system that has the ability to sense DNA damage and, most importantly, transduce this information to influence the cellular response to it (Ciccia & Elledge, 2010). As noted in *Figure 1.1B*, there are a variety of repair mechanisms for each specific form of damage. However, they are usually controlled by a common signaling program. Furthermore, the DDR is made up of an arsenal of strictly-regulated enzymatic tools, which cells use to remodel and repair DNA (Ciccia & Elledge, 2010). Errors occurring during the detection and repair process may lead to the introduction of mutations in the genomic information. In general, any mutation may lead to detrimental effects, such as cell death and the acquisition of various disorders including cancer (Salk et al., 2010). Therefore, it is unsurprising that genetic predisposition to mutations in DDR factors increase the overall rate of mutations, which in turn increases genome instability, paving the way for the development of cancer (Negrini et al., 2010).

The detection of DNA damage leads to the activation of one of the three apical kinases, belonging to the family of phosphatidylinositol 3−kinase−like protein kinases (PIKKs) (Shiloh, 2003). ATM (ataxia telangiectasia mutated) and DNA-PK (DNA-

dependent protein kinase) become activated following detection of DSBs by the Mre11-Rad50-Nbs1 (MRN) complex or the Ku70-Ku80 heterodimer, respectively (Andegeko et al., 2001; Carson et al., 2003; Gottlieb & Jackson, 1993). The ATR (ataxia telangiectasia and Rad3-related) kinase is activated by ssDNA coated by RPA and requires the presence of the ATR-interacting protein (ATRIP), Rad17 and the 9-1-1 (Rad9, Rad1, Hus1) complex (Yang & Zou, 2006; Zou & Elledge, 2003). Furthermore, proteomics analysis showed that DNA-PK activity is restricted to few proteins, whereas ATM and ATR target more than 700 substrates, orchestrating the majority of DDR events (Kotula et al., 2013; Matsuoka et al., 2007). Both ATM and ATR are activated by DNA damage and DNA replication stress, but they have distinct damage specificities and non-redundant functions. However, ATM and ATR often work in tandem to signal DNA damage and regulate a wide range of downstream cellular processes critical for genome stability, including DNA replication, DNA repair, and cell cycle control (Awasthi et al., 2015; Maréchal & Zou, 2013).

1.8 Double-Strand Break Repair

As noted above, DNA damage may result from a variety of different sources that inflict different DNA lesions, which are addressed by different and specific repair mechanisms (*Figure 1.1B)* (Hoeijmakers, 2009). Although occurring much less frequently than other DNA lesions, double-strand breaks (DSBs) are cytotoxic lesions formed when both strands of the DNA duplex are broken. DSBs can form as a result of endogenous metabolic reactions and replication stress or from exogenous sources like radiation and chemotherapeutics (Mehta & Haber, 2014). In addition, DSBs are essential intermediates during programmed recombination events, in particular meiosis, yeast mating-type interconversion and lymphocyte development (Symington & Gautier, 2011). However regardless of their source, its been shown that defective DSB repair is associated with a number of developmental, immunological and neurological disorders, and a major driver of carcinogenesis (Chapman et al., 2012). Cells have evolved two mechanistically-distinct pathways to repair DSBs: non-homologous end joining (NHEJ) and homologous recombination (HR), with pathway selection being mostly influenced by the stage of the cell cycle (Abbas et al., 2013).

1.8.1 Non-homologous End Joining

As the name implies, NHEJ involves the direct ligation of the broken ends and represents the simplest mechanism to repair DSBs and restore chromosome integrity (Symington & Gautier, 2011). Although NHEJ can operate during all phases of the cell cycle, its function is critical in the G_1 phase, where the initial step in HR, the 5' to 3' resection of DSB ends is blocked. In addition, G_1 cells lack the homologous sister

chromatid, which is used as a template to repair the DSB *via* HR (Mehta & Haber, 2014). Due to the direct ligation of the broken ends, NHEJ is considered an error-prone process, that often results in small insertions, deletions, substitutions at the break site, and translocations if DSBs from different parts of the genome are joined together (Chapman et al., 2012).

NHEJ is initiated when the two DSB ends are recognized and bound by the Ku70/Ku80 (Ku) heterodimer. The Ku heterodimer serves as a scaffold to recruit the other NHEJ factors to the site of the damage, including the DNA-dependent protein kinase catalytic subunit (DNA-PKcs), X-ray cross complementing protein 4 (XRCC4), DNA Ligase IV, and XRCC4-like factor (XLF) (Davis & Chen, 2013). Together, these proteins work in a sequential order to (i) recognize a DSB and protect it from degradation, (ii) process non-ligatable ends, and (iii) stimulate and complete end joining (*Figure 1.5*) (Iyama & Wilson III, 2013). Despite being an error-prone process, NHEJ is critical in maintaining genome stability. Indeed, it has been shown that loss of NHEJ factors leads to an increase in chromosomal aberrations and non-reciprocal translocations (Davis & Chen, 2013)

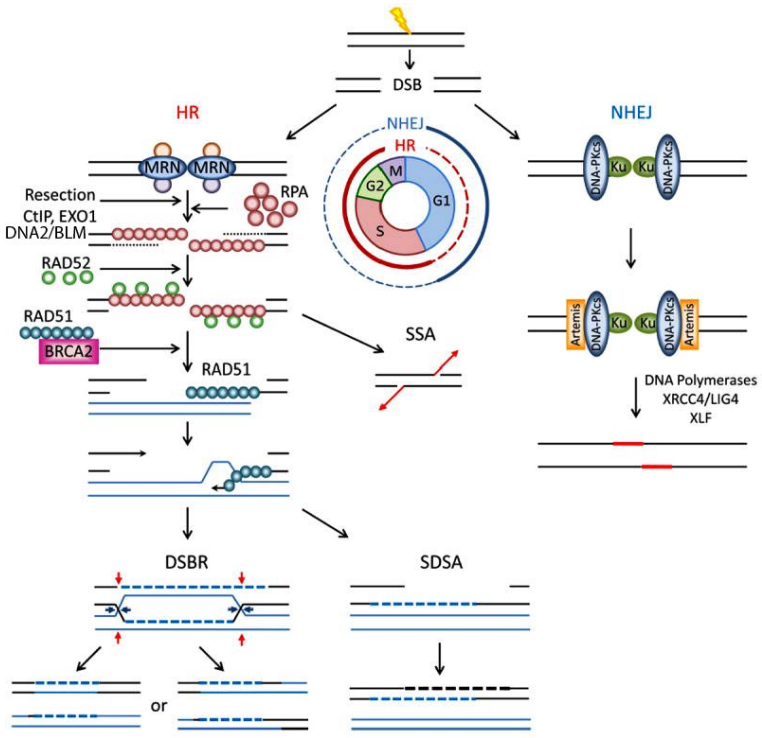

Figure 1.5 DSB Repair: HR & NHEJ. DSB repair is divided into two major pathways: HR & NHEJ. Repair pathway choice is in one part dependent on the phase of the cell cycle. HR is initiated by recognition of the DSB by MRN and the initial end resection. Further resection is carried out by EXO1 and/or DNA2/BLM, which generates a long 3' strand overhang that is rapidly coated by RPA. RAD52 assists RAD51 along with mediator protein BRCA2, in replacing RPA with RAD51 to form a nucleoprotein filament. In SSA, recombination is RAD51 independent. Next, the RAD51 nucleoprotein filament promotes homology search and invasion, which generates a D-loop, that can be resolved in pathways that result in Co and NCO products, *via* normal DSBR or SDSA. Figure modified from (Iyama & Wilson III, 2013)

1.8.2 Homologous Recombination

DNA DSBs can be repaired by several varying HR pathways. Single-strand annealing (SSA) is the most basic HR mechanism, which involves the annealing of homologous repeat sequences that flank a DSB, which causes a deletion rearrangement between the repeats (Bhargava et al., 2016). However in general, HR depends on the recognition and pairing of broken DNA ends with intact homologous sequences on a sister chromatid or, less commonly, the homologous chromosome and is largely considered an error-free process (Mehta & Haber, 2014). In contrast to NHEJ which can operate throughout the cell cycle, HR is generally restricted to the S- and G_2 phase following DNA replication, mainly due to the availability of the sister chromatid (Chapman et al., 2012).

HR is initiated when the DSB is recognized by the MRN (MRE11, RAD50, and Nijmegen breakage syndrome 1 (NBS1)) complex. Next, the MRN complex associates with the C-terminal binding protein (CtBP)-interacting protein (CtIP). Together, they perform the initial 5' to 3' end resection, generating the required 3' ssDNA overhang for strand exchange. As noted above, NHEJ is active during all phases of the cell cycle, so during S- and G_2 phase NHEJ and HR factors "compete" for substrates. The MRN-dependent DNA resection acts as a control point and commits the cell to repair the DSB *via* HR (Jasin & Rothstein, 2013). Next, the 3' overhang is further processed by either Exonuclease 1 (EXO1), which cleaves mononucleotides, or DNA2 in conjunction with the Bloom syndrome (BLM) helicase, that cleaves off short oligonucleotides from the 5' strand (Cejka et al., 2010; Huertas et al., 2008; Mimitou & Symington, 2008; Zhu et al., 2008). Immediately following the end resection, the ssDNA tails are bound by RPA to remove disruptive secondary structures and prevent degradation. This activates ATR *via* an interaction with ATR-interacting protein (ATRIP) that signals the full checkpoint response (Iyama & Wilson III, 2013). In turn, RAD52 is recruited and promotes replacement of RPA with the RAD51 recombinase. Along with mediator protein Breast cancer type 2 susceptibility protein (BRCA2), RAD51 replaces RPA and forms a nucleoprotein filament on the ssDNA strand. Once the RAD51 nucleoprotein filament is formed, it promotes homology search and strand invasion on the intact homologous DNA region, providing the genetic instructions for error-free repair (Mehta & Haber, 2014). Here, RAD51 facilitates the contact between the invading ssDNA and the homologous DNA duplex in a so-called displacement loop (D-loop) (Krejci et al., 2012). Next, repair synthesis is performed, where the invading 3' strand acts as a primer, while the donor duplex acts as the template. The required DNA polymerase remains elusive *in vivo*, but the extension is most likely mediated by DNA Pol η (eta) or Pol δ (McVey et al., 2016). There are two predominant models that have been proposed for D-loop resolution, of which endonucleolytic cleavage can lead to crossover (CO) and/or non-crossover (NCO)

products. The first model involves the formation of a double 4-way junction intermediate structure known as a double Holliday junction (dHJ). In this model, dHJs are resolved in one of three ways: (i) symmetrical cleavage by the endonucleases GEN1, Slx1/Slx4, (ii) asymmetric cleavage by endonuclease Mus81/Eme1, which leads to CO products (Schwartz & Heyer, 2011) or, (iii) dissolution of the HJ to generate exclusively NCO products. This is mediated by the BLM helicase, topoisomerase III α and the RMI1-2 complex, which work in tandem to permit branch migration and decatenation of the linked strands of the two HJs (Bizard & Hickson, 2014). In the second model, designated the synthesis-dependent strand annealing (SDSA) pathway, DSB repair is completed *via* NCO products without Holliday junction formation. In SDSA, the newly-synthesized strand is displaced and re-annealed to the second DNA end (*Figure 1.5)* (Jasin & Rothstein, 2013).

1.9 Iron-Sulfur (FeS) Cluster Proteins

Iron-Sulfur (FeS) clusters are ancient inorganic cofactors, remnants of an anaerobic world. FeS clusters present a particular problem in an aerobic world, because FeS cluster proteins are particularly sensitive to oxidation, which frequently leads to the destruction of the cluster and the subsequent inactivation of the protein. Despite this, cells have gone through a lot of effort to maintain them, and they are required to sustain fundamental life processes (Imlay, 2006). FeS cluster proteins are involved in cellular processes as diverse as DNA replication and repair, RNA modification, gene regulation, electron carriers in redox reactions, regulatory sensors, protein stability and iron metabolism (Barras, 2017). The biogenesis of eukaryotic FeS cluster proteins is mediated by the mitochondrial iron-sulfur cluster assembly (ISC) and the cytosolic FeS protein assembly (CIA) machineries. Both the ISC and CIA machineries are specifically involved in cytosolic and nuclear FeS protein maturation, whereas the ISC machinery alone is required for the maturation of all other cellular FeS proteins (Lill & Mühlenhoff, 2008).

1.9.1 Structure of FeS Clusters

The most common and simplest FeS clusters are of the rhombic [2Fe-2S] and cubic [4Fe-4S] types (*Figure 1.6)* (Rees & Howard, 2003). Furthermore, in several FeS proteins, one iron of a [4Fe-4S] cluster may be lost to form a [3Fe-3S] cluster, or undergo metal substitutions to generate mixed-metal clusters (Lill & Mühlenhoff, 2008). [4Fe-4S] clusters can alter their oxidation states between +2 and +3, due to the fact that iron exists as Fe^{2+} or Fe^{3+}, while sulfur always exists in the -2 oxidation state (S^{2-}). FeS clusters are typically coordinated in proteins by four conserved cysteine-sulfur residues, however, coordination with nitrogen atoms of histidine and arginine, serine residues or small molecules (e.g. CN^-, homocitrate) has been observed (Rees, 2002). Another important

aspect of FeS clusters are their versatile electrochemical properties with redox potentials ranging from +300 mV to -500 mV, which makes them excellent electron donors/ acceptors. Furthermore, the binding motifs for FeS cluster proteins are not highly conserved and can differ radically. However, some consensus motifs have been described in some mammalian and plant ferredoxins, but an ubiquitous FeS binding motif has yet to be identified (Lill & Mühlenhoff, 2008).

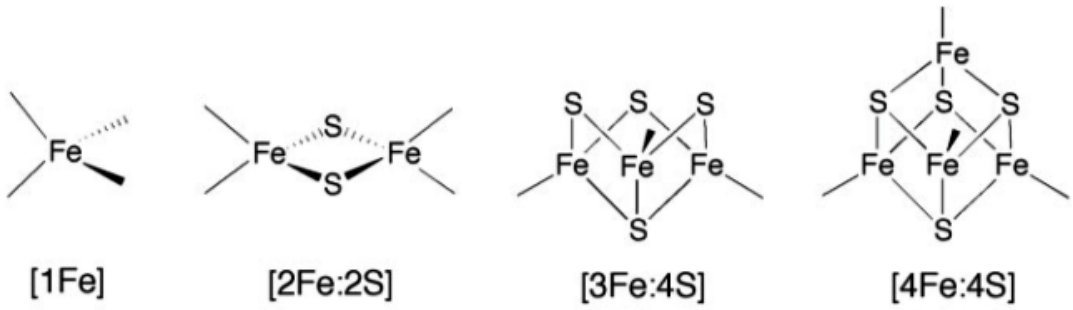

Figure 1.6 Basic FeS Clusters. Schematic representations of the basic types of FeS clusters containing one to four iron atoms. Figure modified from (Rees, 2002)

1.9.2 Iron-Sulfur Cluster Proteins Involved in DNA Repair and Replication

The most common function for FeS cluster proteins is in electron transfer during cellular respiration. However, a growing number of proteins involved in DNA replication and repair have been shown to bind an FeS cluster (i.e. DNA2, Primase, Pol α, Pol ε, Pol δ, MutYH, XPD, RTEL1, FANCJ, and ChlR1) (Netz et al., 2012; Wu & Brosh, 2012) (*Table 1.2).* These findings were rather surprising, given that upon FeS cluster oxidation, free iron atoms can generate dangerous ROS that may interfere with DNA integrity and lead to genomic instability. Moreover, the FeS cluster is predicted to be crucial for the protein functions, but its precise molecular role is largely unknown (Paul & Lill, 2015).

1.9.3 Potential Roles of the FeS Cluster in Genome Maintenance Proteins

Despite the inherent danger to oxidation and degradation, FeS clusters are crucial for the function of proteins involved in DNA replication and repair activities. For the majority of these genome maintenance proteins, their FeS cluster has been thought to play a non-catalytic role in stabilizing the structure of the protein (White & Dillingham, 2012). However, a model proposed by the Barton group suggests that the redox-active FeS clusters of DNA glycosylases are used to scan the genome for DNA damage (Boal et al., 2007; Boal et al., 2009). Their model is based on the fact that electron transport can occur over long molecular distances within the DNA duplex due to π-stacking (Kelley & Barton, 1999; Núñez et al., 1999) and that the presence of damage or mismatched bases causes a

significant disruption in electron transport within the duplex (Boon et al., 2000). This model therefore, proposes that through DNA-mediated charge transfer, genome maintenance proteins use their FeS clusters to scan DNA and distinguish between intact and damaged DNA (Boal et al., 2005). However, not all FeS proteins are involved in damage detection, it is therefore likely that the FeS cluster in other proteins may be utilized in different ways. Indeed, recent studies have shown a critical role of the FeS cluster in DNA polymerases in the formation of active replicative complexes and in DNA primase as an on/off switch for DNA binding and efficient RNA primer synthesis (Netz et al., 2012; O'Brien et al., 2017).

1.9.4 Conserved Family of FeS Cluster Binding Helicases Linked to Human Disease

XPD (Rad3 in *S. cerevisiae)* is the founding member of a superfamily 2 (SF2) of helicases that includes RTEL1, FANCJ, and ChlR1. Key characteristic of all family members is binding of an FeS cluster *via* four conserved cysteine residues and 5' to 3' helicase activity (White, 2009). Furthermore, all family members are linked to human diseases (*Table 1.2).* XPD is part of the transcription initiation factor (TFIIH) complex that plays a critical role in basal transcription and NER. Mutations within *XPD* have been linked to three genetic disorders, namely xeroderma pigmentosum (XP), Cockayne syndrome (CS) and Trichothiodystrophy (TTD). These diseases are all characterized by skin hypersensitivity to sun exposure, a result of defective NER (Lehmann, 2003). Interestingly, a common point mutation in TTD patients (arginine to histidine; R211H) which lies just outside of the FeS cluster binding domain, exhibits abolished helicase activity and is unable to stably bind an FeS cluster (Rudolf et al., 2006). RTEL1 is an essential anti-recombinase that is required for limiting meiotic recombination, removing toxic recombination intermediates and regulating telomere integrity (Vannier et al., 2014). Single-nucleotide polymorphism (SNPs) variants in *RTEL1* have been shown to increase susceptibility to high-grade glioma and mutations within *RTEL1* have been identified in individual patients with Hoyeraal-Hreidarsson syndrome, a severe variant of dyskeratosis congenita (DC), characterized by early onset bone marrow failure, immunodeficiency and developmental defects, due to dysfunctional telomeres (Le Guen et al., 2013; Wrensch et al., 2009). FANCJ was identified as the gene mutated in the J complementation group of Fanconi anemia (FA), a genome instability disorder with elevated risk of cancer development that functions in DSB repair and interstrand crosslink repair (Paul & Lill, 2015). One *FANCJ* point mutation commonly found in FA patients (alanine to proline; A349P), located immediately adjacent to one of the conserved cysteine residues of the FeS binding domain, exhibits abolished FeS cluster binding and defects in helicase activity and displacing DNA-bound proteins (Wu et al., 2010). *DDX11* (ChlR1) mutations are associated with the rare genetic

disorder Warsaw breakage syndrome (WABS), characterized by congenital abnormalities and - on a cellular level - defects in sister chromatid cohesion (van der Lelij et al., 2010). Interestingly, the WABS patient point mutation (arginine to Glutamine; R263Q), which is also located just outside of the FeS binding domain, abolishes helicase activity and DNA-dependent ATP hydrolysis (Capo-Chichi et al., 2013). Taken together, these findings illuminate the essential role the FeS cluster plays in this SF2 helicase family and genome stability.

Table 1.2 FeS cluster binding DNA repair and replication proteins

Human DNA metabolism FeS cluster binding proteins and their yeast counterparts, and associated disease. Table modified from (Paul & Lill, 2015)

Human	Yeast	Function	Associated Disease
CHLR1	Chl1	Helicase, sister chromatid cohesion, heterochromatin organization	Warsaw breakage syndrome
DNA2	Dna2	Helicase/nuclease, DNA repair, Okazaki fragment maturation, telomere maintenance	
FANCJ	-	Helicase, DNA interstrand crosslink repair	Fanconi Anemia
MutYH	-	DNA glycosylase, base excision repair	
Pol α	Pol α	DNA replication	
Pol δ	Pol δ	DNA replication	
Pol ε	Pol ε	DNA replication	
Primase	Primase	DNA replication and DSB repair	
RTEL1	-	Helicase, regulation of telomere length, anti-recombinase	Hoyeraal-Hreidarsson syndrome, high-grade glioma
XPD	Rad3	Helicase, nucleotide excision repair	Xeroderma pigmentosum, Cockayne syndrome, Trichothiodystrophy

1.9.5 Biogenesis of FeS cluster proteins

As noted above, the biogenesis of all cytosolic and nuclear FeS cluster proteins requires the assistance of both the ISC and CIA machineries (Lill, 2009). In general, FeS cluster biogenesis can be divided into two main steps, (i) the *de novo* assembly and transient binding of an FeS cluster on the CIA scaffold complex, and (ii) the transfer of the FeS cluster from the scaffold to target apoproteins (Lill, 2009). In the first step, in conjunction with the mitochondrial ISC machinery, an unknown sulfur-containing compound (X-S) is generated and transferred to the cytosol by the ABC7 transporter protein, where it is transported to the CIA scaffold complex made up of NTPases (CFD1/NBP35) (Netz et al., 2007). Next, at the CIA scaffold complex, an unknown iron donor is taken up and is assembled into an FeS cluster in the cytosol, which is supported by the lack of evidence of intact FeS clusters crossing the inner mitochondrial membrane (Rouault, 2015). Once assembled, the FeS cluster is transferred to the CIA targeting complex, which is made up of MMS19 nucleotide excision repair protein homolog (MMS19), MIP18 family protein FAM96B (MIP18) and cytosolic iron-sulfur assembly component 1 (CIAO1), and iron-only hydrogenase like protein (IOP1) (Paul & Lill, 2015). The core CIA members MMS19, MIP18 and CIAO1 mediate the insertion of the FeS cluster into apoproteins, producing the mature holoprotein (*Figure 1.7)* (Netz et al., 2013). In addition, IOP1 has also been shown to be essential to this process, but was suggested to act outside of the core CIA members, but possibly acts to connect the early- and late-acting components of the CIA machinery *via* an unknown mechanism (Paul & Lill, 2015; Seki et al., 2013).

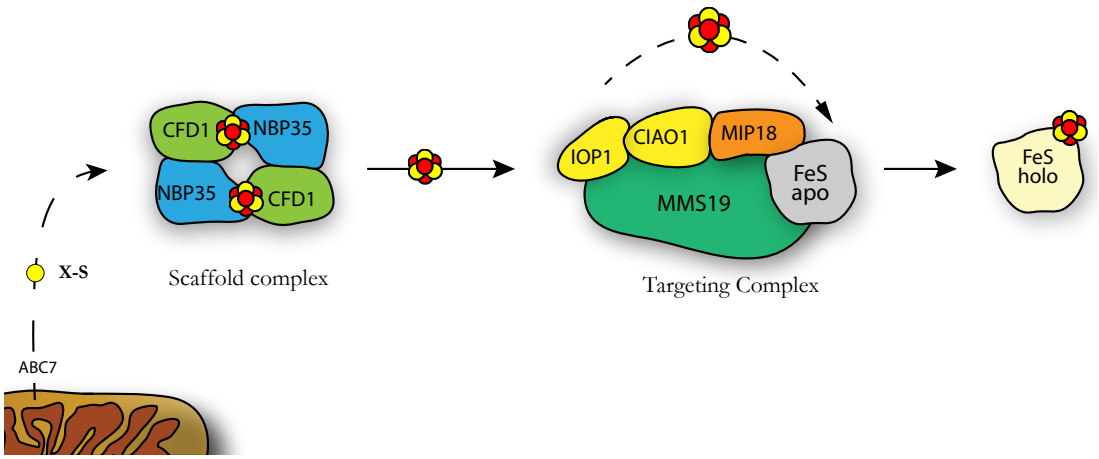

Figure 1.7 Cytosolic and Nuclear FeS cluster Protein Biogenesis via CIA . Cytosolic and Nuclear FeS cluster protein maturation occurs in the cytoplasm. (i) *via* ISC machinery in the mitochondria, a sulfur donor is released to the cytoplasm where it meets an unknown Fe donor and (ii) on the CIA scaffold complex the FeS cluster is assembled. In the last step, (iii) the FeS cluster is transferred to the CIA targeting complex, where through the specific actions of MMS19, MIP18, and CIAO1 the FeS cluster is inserted into the apoproteins.

1.9.6 Iron-Sulfur Cluster Biogenesis and the Link with Genome Stability

The maturation of these FeS cluster binding DNA metabolizing proteins requires both the ISC and CIA assembly machineries. Both genetic and biochemical studies have shown that all stages of FeS cluster biogenesis are intimately linked with the maintenance of genome stability. Namely, defects in FeS cluster biogenesis factors prevents the upstream maturation of critical proteins in DNA repair and replication, leading to genomic instability (Paul & Lill, 2015). Since the identification of MMS19 as a component of the CIA targeting complex, functional studies have shown that MMS19 depletion in both yeast and human cells causes sensitivity to hydroxyurea, S-phase defects during the cell cycle and inhibits XPD incorporation into the transcription factor IIH (TFIIH) complex, which is required for transcription and nucleotide excision repair (Gari et al., 2012; Paul & Lill, 2015; Stehling et al., 2012; Zhang, 2014). Furthermore, MMS19 has also been shown to interact directly with all known nuclear FeS cluster proteins, linking it to various DNA metabolic pathways and, in an indirect way, making it an essential component in maintaining genome stability (Paul & Lill, 2015).

1.10 Identifying and Characterizing Novel Nuclear Iron-Sulfur Cluster Proteins

To date, there are no defined motifs for FeS cluster binding; in fact most FeS cluster proteins were discovered by chance. This is in part due to the fact that essential factors of the FeS cluster biogenesis pathways have only been recently discovered and characterized. Furthermore, the discovery of these factors *via* genetic screens was not possible due to their necessity for cell survival (Dos Santos & Dean, 2017). However, two independent studies showed that MMS19 is a crucial member in the CIA targeting complex, and that interaction with MMS19 is a critical step in FeS cluster biogenesis for all FeS cluster proteins involved in DNA repair and replication (Gari et al., 2012; Stehling et al., 2012). In addition, later studies identified MIP18 as a CIA targeting complex member, and it was shown to bind to both CIA targeting complex members and FeS proteins, and specifically binds to the FeS cluster coordinating regions in FeS proteins (Stehling et al., 2012; van Wietmarschen et al., 2012). Taken together, these findings show that CIA targeting complex members play a central role in FeS cluster insertion into FeS apoproteins. These new discoveries opened up the possibility of identifying novel nuclear FeS cluster proteins *via* their interaction with MMS19/MIP18. In addition, novel FeS cluster proteins may be identified *via* the observed synthetic lethality of yeast *mms19*Δ with the deletion of multiple FeS proteins (e.g. Polδ) (Collins et al., 2007).

1.11 Aim of Studies: Identifying and Characterizing Novel and Known Nuclear FeS Cluster Proteins

As summarized above, a growing number of essential proteins involved in DNA repair and replication have been shown to bind an FeS cluster and in some cases are linked to human disease (*Table 1.2)*. Due to the identification of crucial CIA members (i.e. MMS19 & MIP18), we reasoned that it may be possible to identify potential unknown FeS cluster proteins *via* interactome analysis. Previously, FeS proteins were discovered serendipitously. Through the duration of my doctoral studies, we set out to confirm whether our candidate protein, RFC5 (*see 1.10*) is a *bona fide* nuclear FeS cluster protein and characterize the function(s) it may play in its cellular activities. In our second aim, we investigate the role the FeS cluster plays in the nuclease/helicase Dna2 *(See 1.11)*, a known FeS cluster binding protein involved in both DNA repair and replication. Considering the crucial role that many of these proteins play in DNA repair and replication, we aim to characterize the role of the FeS cluster in known proteins, in order to elucidate its precise molecular function. It is clear that the FeS cluster likely plays a role in protein stability, but other, more intricate, biochemical functions are expected, such as redox sensing of DNA damage (Paul & Lill, 2015). Together, these studies will allow us to paint a clearer picture of the role(s) FeS cluster proteins have on global genomic stability.

1.12 Aim 1: Identifying Potential Novel Nuclear FeS Cluster Proteins: RFC5

The 36 kDa RFC5 subunit, consisting of 340 amino acids, was found to bind to MMS19 by mass spectrometry (Stehling et al., 2012). Further, deletion of Rfc3, the yeast counterpart to RFC5, was found to be synthetic lethal with *mms19*Δ (Collins et al., 2007). RFC5 is part of an evolutionarily-conserved AAA+ ATPase (ATPases Associated with diverse cellular Activities family) protein complex that is composed of five distinct subunits (RFC1-5) *(Figure 1.8)*. Like all of the other RFC subunits, RFC5 possesses several conserved domains: AAA+ ATPase domain containing Walker A, Walker B, Sensor I, Sensor II motifs and the trans-acting arginine finger, and an RFC C-terminal domain. The Replication Factor C complex (RFC), the eukaryotic clamp loader, is highly-conserved from yeast to human (Hedglin et al., 2013). The clamp tethers DNA polymerases to DNA to increase the processivity of synthesis, as well as the efficiency of replication (Thompson et al., 2012).

As noted above, RFC's canonical function couples the energy from ATP binding and hydrolysis to the loading of the DNA replication processivity clamp protein, PCNA, onto DNA (Johnson et al., 2006). Additionally, the *alternative* RFC complexes and their functions have begun to be unraveled. It has been shown that CTF18-RFC acts in cohesion establishment and replication checkpoint activation (Skibbens, 2005). The RAD17-RFC

(Rad24 in *S. cerevisiae*) complex has been shown to act on the PCNA-like 9-1-1 complex (RAD9-RAD1-HUS1; Rad17-Mec3- Ddc1 in *S. cerevisiae*) placing it at sites of DNA damage (Bermudez et al., 2003). Lastly, the ATAD5-RFC (Elg1 in *S. cerevisiae*) complex has been recently shown to act in unloading PCNA during DNA replication, preventing the accumulation of PCNA on chromatin, which if left bound could lead to genomic instability (Kubota et al., 2013; Lee et al., 2013).

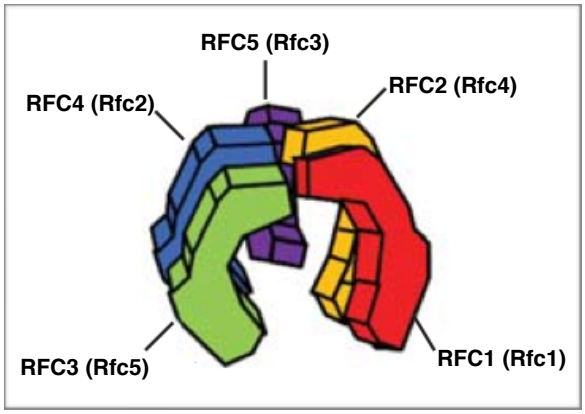

Figure 1.8 Structure of the RFC Complex. Basic structure of the RFC complex with yeast counterparts in parentheses. RFC1, represents the largest subunit and is thought to be the determinant in RFC function between the other alternative complexes. RFC5 along with RFC2 and RFC4, make up a central "core" of the complex. Figure modified from (Hedglin et al., 2013)

It has been widely assumed that the sole determinant of specificity and function of the RFC complexes was the large subunit. Although each complex differs only in the large subunit, recent studies have shown that the smaller subunits (RFC2-5) also play a role in specificity and that the ATP sites work in unison to promote the conformational changes in the clamp-loading reaction (Marzahn et al., 2014). Moreover, these studies suggest that the smaller subunits may play a larger role in the function of the holocomplex and that each subunit could possibly have a unique function in the clamp-loading reaction (Daee & Myung, 2010). Therefore, we hypothesized that an FeS cluster in RFC5 could potentially play a role in its DNA-related activities, complex formation and regulation of alternative-RFC complexes.

1.13 Aim 2: Elucidating the Role of the Iron-Sulfur Cluster in the Nuclease/Helicase Dna2

In our second aim, we investigate the role of the FeS cluster in DNA replication ATP-dependent nuclease/helicase DNA2 (Dna2). As noted above, Dna2 is an essential protein that was found to be required for DNA replication *in vivo*. The *Saccharomyces cerevisiae* Dna2 has a size of 172 kDa and contains an unstructured N-terminal regulatory domain, a RecB family nuclease domain and a superfamily I (SF1) helicase domain (*Figure 1.9)*. Four cysteine residues (a.a. 516, 768, 771, 777) located within the nuclease domain coordinate an

FeS cluster that is thought to play a role in protein stabilization. Dna2 is highly conserved, present in eukaryotes from yeast to human; however, the N-terminal regulatory domain is very poorly conserved (Wanrooij & Burgers, 2015). In addition, Dna2 belongs to a novel class of proteins with a nuclease domain and a conserved FeS cluster that includes the bacterial AddAB nuclease/helicase (Yeeles et al., 2009).

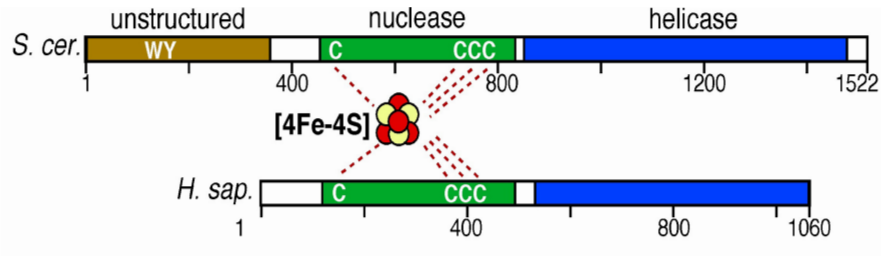

Figure 1.9 Structure of Yeast and Human Dna2/DNA2. Dna2 is highly conserved from yeast to humans, apart from the N-terminal domain which is absent higher eukaryotes. Key features: RecB family nuclease domain, SF1 helicase domain, and FeS cluster coordinated within the nuclease domain. Figure modified from (Wanrooij & Burgers, 2015).

1.13.1 Cellular Roles of Dna2

Dna2 is a multifunctional protein that possesses both nuclease and helicase activities that require a free unblocked ssDNA end for loading (Bae & Seo, 2000; Bae et al., 1998; Balakrishnan et al., 2010). Dna2 contains ssDNA-specific endonuclease, 5' to 3' helicase and DNA-dependent ATPase activities. The nuclease activity can be either 5' to 3' or 3' to 5', where RPA stimulates the former and inhibits the latter (Cejka et al., 2010; Lee et al., 2000; Wanrooij & Burgers, 2015). The helicase activity of Dna2 has been considered weak, mostly owing to the fact that its nuclease activity auto-inhibits its helicase. However, it was recently shown that Dna2 possesses potent helicase activity in a nuclease-dead background (Levikova et al., 2013). Even so, studies of separation-of-function mutants have shown that the nuclease activity of Dna2 is essential for cell survival, whereas helicase-dead mutants are viable. That being said, helicase-dead mutants exhibit growth defects, sensitivity to methyl methanesulfonate (MMS) and IR, which indicates the helicase activity still contributes to Dna2 function *in vivo* (Budd & Campbell, 2000; Budd et al., 1995, 2000; Formosa & Nittis, 1999). Dna2 preferentially binds to and acts on 5'-flap structures, binding to the 5'-flap, threading over its 5' end and moving down the flap in order to cleave its substrate, leaving 3-4 nt from the base of the flap (Balakrishnan et al., 2010; Stewart et al., 2010). As noted above, Dna2 has various essential cellular roles, such as Okazaki fragment processing, repair of DSBs in conjunction with BLM helicase (Sgs1 in *S. cerevisiae)*, telomere maintenance, prevention of replication fork reversal and checkpoint activation (*Figure 1.10)* (Wanrooij & Burgers, 2015).

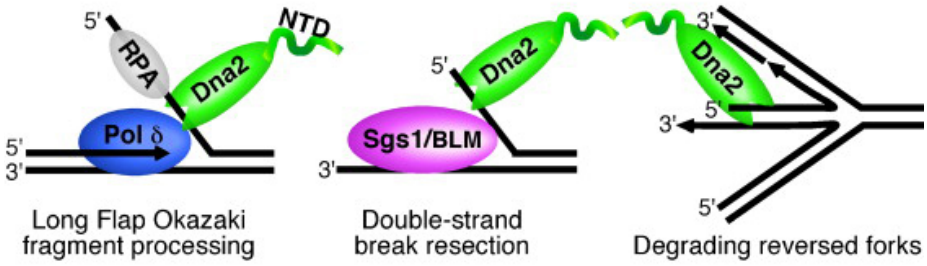

Figure 1.10 Dna2 at the nexus of DNA replication and repair *Left Panel:* Dna2 acts during DNA lagging strand replication, processing Okazaki fragments in conjunction with Fen1 generating cleavable nicks. *Middle Panel:* Dna2 works in conjunction with Sgs1/BLM in a DSB end resection pathway. *Right Panel:* Dna2 prevents replication fork reversal Figure modified from (Wanrooij & Burgers, 2015).

1.13.2 The FeS cluster in Dna2

As noted above, Dna2 is part of a novel class of proteins that have a nuclease domain and conserved FeS cluster. Dna2 was first identified as a potential member of this family, when sequence comparison with the AddAB nuclease/helicase revealed a potential FeS binding domain within its nuclease domain (Yeeles et al., 2009). Later, a study by Pokharel and Campbell, confirmed yeast Dna2 as a *bona fide* FeS cluster protein. Furthermore, their biochemical analysis revealed that loss of the FeS cluster is detrimental to its nuclease activity but, in contrast to AddAB, did not affect DNA binding and protein structure, as indicated by limited protease digestion experiments. Interestingly, the loss of the FeS cluster also reduced its ATPase activity, even though the ATPase domain is located in the C-terminal helicase domain (Pokharel & Campbell, 2012).

Considering the fragile nature of FeS clusters and the threat of oxidation, coupled with advancements in protein purification and FeS cluster biology, we asked whether the integrity of the FeS cluster was maintained during purification in earlier studies. For example, in a recent study, Dna2 purified from an optimized protocol, was shown to be more active and able to function as the sole nuclease during Okazaki fragment processing, challenging the accepted "two nuclease" model (Levikova & Cejka, 2015). These data suggest, that Dna2 can cut at or near the base, acting as the sole nuclease in Okazaki fragment maturation and that Fen1 may only function in a specific subset of fragment processing. Moreover, Dna2's helicase activity was considered to be weak due to the auto-inhibitory effects of the nuclease activity. However, in a nuclease-deficient background, Dna2 exhibits potent helicase activity (Levikova et al., 2013). Therefore, it is tempting to speculate whether the redox state of the FeS cluster plays a role in regulating nuclease/helicase activity. Taking into account Dna2's various cellular roles, we hypothesized that perhaps the FeS cluster in Dna2 may be responsible for regulating the balance between its activities *in vivo*. Therefore, we set out to address whether the FeS cluster plays a larger role

in regulating Dna2's cellular activities and structural stability, as mutations to its FeS binding domain are not likely to be tolerated.

2. Materials and Methods

2.1 General Buffers, Solutions, and Media

LB Medium	Yeast-extract 10g/l Tryptone 10g/l NaCl 10g/l *LB medium according to Miller; pH adjusted to 7.5 and autoclaved*
LB Agar	LB medium agar (2% wt/vol)
Yeast Medium	1x Standard synthetic medium (Lacking appropriate amino acids) 1x Nitrogen Base Glucose or Galactose (2% vol/vol)
Yeast Agar	Yeast Medium agar (2% wt/vol)
SOC medium	Tryptone (2% wt/vol) Yeast extract (0.5% wt/vol) 10 mM NaCl 2.5 mM KCl 10 mM $MgCl_2$ 20 mM Glucose
TSB Buffer	PEG-3350 (10% wt/vol) DMSO (5% vol/vol) 10 mM $MgCl_2$ 10 mM $MgSO_4$ *Prepared in LB medium*
5x KCM Buffer	100 mM KCl 30 mM $CaCl_2$ 50 mM $MgCl_2$ *Used at 1x.*
5x Laemmli Buffer	0.25M Tris-HCl (pH 6.8) Glycerol (50% vol/vol) SDS (8% vol/vol) 0.5M DTT Bromophenol blue (0.1% wt/vol) *Used at 1x.*
10x DNA Loading Buffer	Ficoll 400 (20% wt/vol) 100 mM EDTA SDS (1% vol/vol) Bromophenol blue (0.25% wt/vol) Xylene Cyanol (0.25% wt/vol) *Used at 1x.*
10x TBE	108 g Tris base 55 g Boric acid 40 ml 0.5M EDTA (pH 8.0) *For 1 liter, diluted to 1x for use.*
10x TBS	121 g Tris base 88 g NaCl *For 1 liter, diluted to 1x for use; pH adjusted to 8.0 with HCl*
PBS	instamed PBS Dulbecco w/o Mg^{2+} and Ca^{2+}

1x TBS-Tween®20	1x TBS Tween®20 (0.01% vol/vol)
10x SDS-PAGE Running Buffer	30 g Tris base (25 mM) 144 g Glycine (190 mM) 10 g SDS (10% wt/vol) *For 1 liter, diluted to 1x for use.*
10x Western Blot Transfer Buffer	30 g Tris base (25 mM) 144g Glycine (190 mM) Ethanol (20% vol/vol) *For 1 liter, diluted to 1x for use.*
Ponceau-S Statin	Ponceau-S (0.1% wt/vol) Acetic Acid (5% vol/vol)
2x Stop Buffer	Formamide (95% vol/vol) 20 mM EDTA Bromophenol blue (0.1% wt/vol) *Used at 1x.*
2x Helicase Stop Buffer	Ficoll 400 (7% wt/vol) 20 mM Tris-HCl (pH 7.5) 20 mM EDTA SDS (0.2% vol/vol) *Used at 1x.*
2% Replication Assay Stop Solution	150 mM EDTA SDS (2% vol/vol) Glycerol (30% vol/vol) Bromophenol blue (0.1% wt/vol)
10x DNA Annealing Buffer	100 mM Tris-HCl (pH 8.0) 500 mM NaCl 100 mM $MgCl_2$ *Used at 1x.*
2x HBS	280 mM NaCl 50 mM HEPES 1.5 mM Na_2HPO_4
Lysis Buffer	50 mM Na-Phosphate pH 7.0 150 mM NaCl Glycerol (10% vol/vol) NP-40 (0.1% vol/vol) 1 mM TCEP 0.5 mM EDTA
EB Buffer (Qiagen)	10 mM Tris-Cl, pH 8.5

2.2.1 DNA Cloning

The Gateway® cloning technology (Invitrogen) permits the easy transfer of insert sequences into a wide number of expression vectors using two site specific recombination reactions. Initially, the insert sequence is cloned into a donor plasmid (pDONOR221) that is flanked by recombination sites. Likewise, acceptor plasmids encode for different recombination sites, which permits the specific transfer of the insert from donor to acceptor plasmid.

To begin, the gene of interest was flanked by attB sites, introduced by PCR. In the first recombination reaction ("BP reaction"), the attB flanked gene of interest is inserted into the pDONOR221 plasmid, mediated by BP Clonase® II. The resulting plasmid serves as the DNA bank to be subsequently transferred into the different destination vectors. Thereafter, all pDONOR221 plasmids were verified via Sanger sequencing. The subcloning into the destination vectors is mediated by the LR Clonase® II ("LR reaction"). The resulting plasmids were verified *via* restriction digest. In general, both BP and LR reactions are assembled in a 5 µl reaction (*Table 2.1)*, incubated for 3 hours at 25 °C, followed by the addition of 1 µl Proteinase K (20 mg/ml) and 10 minute incubation at 37°C. The complete reaction is then used for plasmid propagation *via* bacterial transformation (*See 2.2.4*).

Table 2.1: BP and LR Reaction Composition

BP Reaction	Amount	LR Reaction	Amount
PCR product (100 ng/µl)	1 µl	pDEST_ "Tag" (100 ng/ µl)	1 µl
pDONOR 221 (100 ng/µl)	1 µl	pDONOR221_ "gene" (100 ng/µl)	1 µl
BP Clonase® II	1 µl	LR Clonase® II	1 µl
EB Buffer	2 µl	EB Buffer	2 µl
	5 µl TOTAL		5 µl TOTAL

2.2.2 Polymerase Chain Reaction (PCR)

DNA was amplified using the high fidelity Phusion® Hot Start II polymerase enzyme (New England BioLabs) in a 50 µl reaction volume and assembled as outlined in *Table 2.2*. All analytical and preparative PCRs used 25-35 cycles, while Site-directed mutagenesis PCRs used 12-18 cycles, depending on the gene of interest or flanking DNA sequence. All oligonucleotides used in this study were synthesized by Microsynth and are listed in *Table 2.3*. All PCRs were separated on 0.8% TBE agarose gels (100V; 1 hour).

Furthermore, PCR products from attB-flanking PCRs were purified using the QIAquick Gel Extraction Kit (Qiagen).

Table 2.2: PCR Reaction Composition

Component	50 µl Reaction	Final Concentration
Template DNA	Variable	< 250 ng
5X Phusion HF Buffer	10 µl	1X
10 mM dNTPs	1 µl	200 µM
10 µM Forward Primer	2.5 µl	0.5 µM
10 µM Reverse Primer	2.5 µl	0.5 µM
DMSO	1.5 µl	3%
Phusion Polymerase*	0.5 µl	1.0 units/50 µl PCR
Nuclease-free H_2O	up to 50 µl	

** Phusion Polymerase Extension Time: 15-30s per kb*

PCR Protocol

Step	Temperature	Duration
1. Initial Denaturation	98 °C	5 min
2. Denaturation	98 °C	45 sec
3. Annealing	Variable	45 sec
4. Extension	72 °C	Variable
5. Final Extension	72 °C	10 min
6. Pause	4 °C	∞

Step 2-4 Cycles: Analytical and preparative 25-35X / SDM: 12-18 X

Table 2.3: DNA Oligonucleotides used in PCR

Name	Sequence (5' - 3')
oRL 1	**GGGGACAAGTTTGTACAAAAAAGCAGGCTTCACCATGGAGGTGGAGGCCGTC**
oRL 2	**GGGGACCACTTTGTACAAGAAAGCTGGGTCCTAACTGGCCACCGGGGC**
oRL 3	**GGGGACAAGTTTGTACAAAAAAGCAGGCTTCACCATGAGCCTCTGGGTGGAC**
oRL 4	**GGGGACCACTTTGTACAAGAAAGCTGGGTCTCAGAACATCATGCCTTCCAATC**
oRL 5	**GGGGACAAGTTTGTACAAAAAAGCAGGCTTCACCATGCAAGCATTTCTTAAAGGTAC**
oRL 6	**GGGGACCACTTTGTACAAGAAAGCTGGGTCTTAACAATTCTGAGATAACTGCTGC**
oRL 7	**ATGGAGACCTCAGCACTCAAGC**
oRL 8	**CACCGCATGTTAGAAGACTTCCTCTGCCCTCACCGCTGCCGGCCTCTGCAACAATCAGCTC**
oRL 9	**GGAAGTCTTCTAACATGCGGTGACGTGGAGGAGAATCCCGGCCCTATGGAGGTGGAGGCCGTC**
oRL 10	**CTAACTGGCCACCGGGGC**
oRL 11	**TCTACATCTCCACAAGTAAGTAGGCTGCCCCTACCTTCACCGCTGCCACTGGCCACCGGGGCCATTG**
oRL 12	**TACTTACTTGTGGAGATGTAGAAGAAAACCCTGGTCCCATGCAAGCATTTCTTAAAGGTAC**
oRL 13	**TTAACAATTCTGAGATAACTGCTGC**
oRL 60	**GACTTGCAAGTACAGTTCACAAATCGG**
oRL 61	**CCGATTTGTGAACTGTACTTGCAAGTC**
oRL 63	**GGGGACAAGTTTGTACAAAAAAGCAGGCTTCACCTCACGATCCGCGGGCACCCGCTTAGC**
oRL 66	**GGGGACCACTTTGTACAAGAAAGCTGGGTCCTAGACCGTTGCAATACACTGATTTATTATCTG**

2.2.3 Site-directed Mutagenesis (SDM)

Site-directed mutagenesis was performed based on the QuikChange® Site-Directed Mutagenesis kit from Stratagene. Using a plasmid with gene of interest as the DNA template, long PCR primers containing the desired point mutation in the center are used in a PCR reaction (*See 2.2.2)* with the high fidelity Phusion® Hot Start II polymerase, to avoid extra mutations. Following the PCR, the amplified DNA fragments are digested with 10U of DpnI (1-2 hours at 37˚C) (New England BioLabs) to degrade parental DNA. The last step is propagation by bacterial transformation (*See 2.2.4).* The isolated plasmid was then checked to verify the desired point mutation and any accumulation of extra mutations by Sanger sequencing at Microsynth.

2.2.4 Bacterial Cell Preparation and Transformation

Chemically competent *Escherichia coli* DH10B or DH10bac cells were prepared by growing a suspension culture in LB medium to an OD_{600} = ~ 0.5-0.6, pelleted cells were gently resuspended in ice-cold TSB buffer, aliquoted and stored at -80˚C until use. Transformations were performed in a 100 µl reaction volume by mixing 1-100 ng DNA in 5X KCM buffer and 50 µl competent bacteria. Transformation reactions were incubated for 10 minutes on ice and subsequently incubated for an additional 15 minutes at RT˚C. Next, the reactions were supplemented with 400 µl of SOC medium and incubated at 37˚C with shaking for 1 hour (DH10B) or 4 hours (DH10bac), plated on LB-agar plates supplemented with appropriate selection antibiotics and incubated overnight at 37˚C.

2.2.5 Isolation of Plasmid DNA

After the successful bacterial transformation, 6 ml (mini-prep) or 80 ml (midi-prep) of LB medium supplemented with appropriate selection antibiotics were inoculated with a single colony and grown overnight at 37˚C on a shaker. The following day the cells were centrifuged at 4000 RPM for 10 minutes. Plasmid DNA was isolated using the Qiagen Plasmid Mini or Plasmid Midi Kit, which is based on a modified alkaline lysis procedure, followed by the adsorption of DNA onto a silica-based membrane in the presence of high salt. Finally, the bound DNA was washed two times with an ethanol based solution and eluted from the membrane with 50 µl (mini-prep) or 200 µl (midi-prep) low salt elution buffer according to the manufacturer's instructions. DNA concentrations were determined using the NanoDrop Spectrophotometer (ThermoFisher Scientific).

2.2.6 Yeast Transformation

To begin, a 50 ml culture of the yeast strain to be transformed was grown overnight at 30˚C in a standard synthetic medium lacking the appropriate amino acids and supplemented with 2% glucose (vol/vol). The following morning, the culture was diluted to $OD_{600=}$ 0.2 and grown to its exponential phase around $OD_{600=}$ 0.6-0.8. Next, the culture was spun down and washed with 25 ml of sterile water to remove the residual growth medium. The culture was then spun down again and resuspended in 1 ml of sterile water, 100 µl of which was used for each transformation. Next, each transformation was spun down and the supernatant was removed and assembled as outlined in *Table 2.4*. Once assembled, each transformation was incubated at RT˚C for 1 hour, followed by heat shock at 42˚C for 15 minutes. Then, 1 ml of appropriate synthetic yeast medium was added to the transformation and incubated at 30˚C for 2-4 hours. Following the incubation, each transformation was spun down and resuspended in 100 µl of sterile water, plated on appropriate selection plates and grown at 30˚C for 2-3 days.

Table 2.4: Yeast Transformation Assembly

Component	Amount
DNA: Plasmid: 500 ng PCR: 3-5 µg	Variable
PEG 3550 50%	240 µl
LiAC 1M	36 µl
ssDNA Carrier Salmon Sperm (10mg/ml)	10 µl
d.d. H_2O	up to 360 µl

2.2.7 Reverse Transcription- PCR (RT-PCR)

To begin, total RNA was isolated from two 25 ml suspension cultures of Sf9 insect cells, one infected with a shRNA Sf9 MIP18 baculovirus and one infected with a control baculovirus and grown for 48 hours. After 48 hours, the cells were counted and ~5.0 $x10^6$ cells were taken for RNA isolation using the RNeasy Mini kit (Qiagen) according to the manufacturer's instructions. RNA concentration was determined using the NanoDrop Spectrophotometer. cDNA synthesis was prepared using 1 µg total RNA with the High Capacity RNA-to-cDNA kit (Applied Biosystems) according to manufacturer's instructions. To determine the relative levels of Sf9 MIP18 mRNA in insect cells following treatment with an shRNA Sf9 MIP18 baculovirus, a RT-PCR was performed. The PCR was prepared using 2 µl of cDNA as template DNA with Sf9 MIP18 specific primers oRL 63 & 66 as described in *Table 2.2*.

2.3 General Cell Culture Methods

2.3.1 Cell Culture

Human embryonic kidney-293T (HEK-293T) and HeLa cells were grown in DMEM (Dulbecco's Modified Eagle Medium; Gibco) supplemented with 10% fetal calf serum (FCS; Gibco) at 37 °C and 5% CO_2. Cells were split biweekly in fresh medium upon reaching sub-confluency. Sf9 insect cells were grown in a suspension culture with shaking in HyClone™ SFX-Insect™ cell media (GE Healthcare) at 25°C. Insect cells were split triweekly by diluting culture to 0.5 x10^6 cells/ml.

2.3.2 Plasmid Transfection

HEK 293T cells were transfected using calcium phosphate, a widely used chemical transfection of human cells. The basic protocol entails mixing DNA in a buffered phosphate solution with calcium chloride, which generates DNA-calcium phosphate co-precipitates that then enter the cell *via* endocytosis. In brief, plasmid DNA (5 μg of each plasmid) was mixed with $CaCl_2$ (final 250 mM) in sterile water up to 250 μl. Next, 250 μl of 2x HBS buffer was added dropwise with low speed vortexing and incubated for 30 minutes at RT°. During the incubation the cell medium was changed to DMEM without FCS. Following the incubation, the transfection mixture was added to the cells dropwise, and allowed to further incubate for 4-6 hours. The medium was then removed from the cells, the cells were washed with PBS and resuspended in DMEM with 10% FCS. The cells were grown for 48 hours and harvested. Transfection of bacmids into Sf9 cells was done using TransIT®-LT1 transfection reagent (Mirus) according to the manufacturer's instructions.

2.3.3 RNA -Interference

For the transient knockdown of selected genes, HeLa cells were transfected with short interfering RNA duplexes (siRNA). To begin, HeLa cells were seeded 1:4 into a 6-well plate and grown overnight. The following morning (day one), the nearly confluent plate was transfected with siRNAs (final 25 nM) using DharmaFECT1 Transfection Reagent (Dharmacon). The cells were then incubated for 72 hours at 37°C and 5% CO_2. On day four, the cells were diluted 1:5 and re-seeded in a new 6-well plate and transfected again with siRNAs as described above. The cells were once again incubated for 72 hours. On day seven, the cells were harvested and protein depletion was determined by Western blotting. All siRNAs were synthesized by Microsynth and are listed in *Table 2.5*.

Table 2.5: List of siRNAs Used in this study

siRNA	Sequence (5' - 3')
siControl	**AGGUAGUGUAAUCGCCUUG (dTdT)**
siMMS19 # 2	**AGAAGAGACUGGUGCGCAA (dTdT)**
siMMS19 # 6	**ACCUGAUACUGUUCUAUGA (dTdT)**
siMIP18 # 5	**ACAAGCAACUUGCAGAUAA (dTdT)**
siMIP18 # 6	**UUAUUGGUCUGUCCAUCAA (dTdT)**

2.3.4 Baculoviruses

All baculoviruses were generated using the Bac to Bac® Baculovirus Expression System (Invitrogen). In general, there are three main steps of baculovirus generation: (i) transform the pFastBac™ based construct containing the gene of interest into DH10bac competent cells to generate recombinant bacmid, (ii) transfect the bacmid into Sf9 insects cells to produce recombinant baculovirus particles, and (iii) amplify and titer the baculoviral stock to use for recombinant protein expression.

2.3.4.1 Bacmid Generation

To produce recombinant bacmids, a pFastBac based Gateway® vector with specific tags was subcloned with the gene of interest by the LR reaction. The bacmid was then transformed into DH10bac competent cells as described above (*See 2.2.4).* The transformants were grown for 48 hours under selective antibiotic pressure, including IPTG and X-gal for white-blue screening. All white transformants were then analyzed by PCR according to the manufacturer's instructions, using the universal M13 forward and reverse primers. The positive clones were grown in 6 ml suspension culture overnight, and the bacmids were then isolated using the QIAmp DNA Mini Kit (Qiagen) and stored at -20 ˚C.

Alternatively, bacmids were generated *via* direct ligation of the pFastBac vector with the gene of interest. In this case, a shRNA specific for Sf9 MIP18, that was commercially produced by Vigene Biosciences. The shRNA was flanked by BamHI and HindIII restriction sites, which allowed direct ligation into the pFastBac vector. The ligation reaction was performed overnight at 16 ˚C with linearized vector (pFastBac) and insert (Sf9MIP18 shRNA) at a 1:3 ratio, with T4 Ligase (Promega) and 10x reaction buffer in a 20 µl reaction according to the manufacturer's instructions. Following the ligation, the mixture was transformed into DH10B competent bacteria and bacmids were isolated with the QIAmp DNA Mini kit as described above. In addition, the human DNA2 WT bacmid was kindly provided by Dr. Cosimo Pinto (University of Zurich).

2.3.4.2 Baculovirus Generation

To produce baculoviruses, the recombinant bacmids were transfected into Sf9 cells that were first seeded into a 6-well plate at a density of 2.25 x 10^6 cells/well and allowed to adhere to the plate for 30 minutes at RT°. Next, the transfection mix was prepared by combining 2.5 μg bacmid DNA with the transfection reagent at a 1:3 ratio (wt /vol) in 260 μl of SFX medium. The mix was incubated for 30 minutes at RT° and was then added to the cells dropwise. The transfected Sf9 cells were incubated for 96 hours at 25°C. Afterwards, the medium was recovered, clarified by centrifugation and filter sterilized with a 0.22 μM filter, resulting in the P1 baculoviral stock. Next, 5 ml of Sf9 cells were seeded in a culture flask at a density of 1.0 x10^6 cells/ml and allowed to adhere for 30 minutes at RT°C. Thereafter, 1.25 ml of the P1 stock was used to infect the cells, which were then incubated for 96 hours at 25°C. After 96 hours, the medium was recovered and filtered as described above, resulting in the P2 baculoviral stock. The titer of the P2 stock was determined by infecting 2.0 x10^6 adhered Sf9 cells in a 6-well plate with increasing amount of the baculovirus (0, 12.5, 25, 50, 100, 200 μl). The cells were incubated for 48 hours at 25°C. Next, the cells were harvested and lysed as described below (*See 2.4.1),* and protein expression was analyzed by Western blotting. To determine the proper baculovirus titer, the minimum volume of the baculovirus that resulted in maximal protein expression was considered the volume defining the multiplicity of infection (MOI) that is equal to (1/2 x10^6 cells). To amplify the baculovirus, Sf9 cells were seeded at 1 x10^6 cells/ml in a 50 ml suspension culture and infected with the P2 baculoviral stock at MOI= 0.1, incubated for 96 hours, and recovered and filtered as described above. To assure baculovirus stability, all baculoviral stocks were supplemented with 2% FCS (Gibco) and stored at 4°C.

2.4 Protein Isolation, Purification, and Analysis

2.4.1 Whole Cell Lysis

Whole cell lysates for human and insect cells were prepared by incubating freshly-harvested or frozen cell pellets with 5 PCV (packed-cell volume) of lysis buffer supplemented with cOmplete protease-inhibitor cocktail (Roche), for 30 minutes on ice with periodic vortexing. Next, the lysate was clarified by centrifugation at 17,200 x g for 30 minutes at 4°C. Afterwards, the supernatant was collected and used for further analysis or purification. When applicable, protein concentrations were estimated using the Bradford Assay.

2.4.2 Co-Immunoprecipitation: Protein-Protein Interaction analysis.

Whole cell lysates were collected from HEK-293T or Sf9/Sf21 insect cells that transiently overexpressed the proteins of interest either by plasmid transfection or baculovirus infection. For each IP sample, 15-20 µl M2 anti-flag affinity resin (Sigma) was added to 200-250 µl of the cleared lysate. The lysate-resin mixture was then incubated overnight on a rotary shaker at 4˚C. The following morning, the resin was collected and washed 3 times with lysis buffer. Lastly, the resin was boiled in 5 volumes of 1x Laemmli buffer, and protein interactions were analyzed by Western blotting.

2.4.3 Recombinant Protein Purification

Dna2 wild-type and mutant variants were expressed from a modified pGAL:DNA2 vector that contains two amino N-terminal tags (Flag and HA) and a C-terminal HIS_6 tag, in the protease-deficient *S. cerevisiae* strain WDH668. This protocol describes purification from a 4l (WT) or 8l (mutant variants) culture. Yeast cells were grown to OD_{600} = ~0.6 in a standard synthetic medium lacking uracil and supplemented with glycerol (3% vol/vol) and lactic acid (2% vol/vol) as carbon sources. Expression of Dna2 was induced by the addition of galactose (2% wt/vol) and the cells were grown for an additional 6 hours. All subsequent steps were performed at 4˚C. Pelleted cells were resuspended in 35 ml TBSG-PI buffer [25 mM Tris-HCl (pH 7.5), 300 mM NaCl, glycerol (10% vol/vol), 3 mM β-mercaptoethanol, 10 mM imidazole, 1 mM PMSF and cOmplete protease-inhibitor cocktail (Roche, 1 tablet/50 ml)] and lysed in a French press. The lysed cells were collected by centrifugation at 27,000 RPM for 45 minutes in the A27-8x 50 rotor in a Sorvall Lynx 6000 centrifuge (Thermo-Fischer). The cleared lysates were then incubated batch-wise with 5 ml packed Ni^{2+}-NTA agarose (Qiagen) for 1 hour. Following incubation, the resin was washed extensively with TBSG-PI high salt buffer (TBSG-PI buffer supplemented with NaCl for final concentration of 1M) and transferred to a 10 ml column. The bound proteins were eluted from the column with 250 mM imidazole in TBSG-PI. The fractions containing protein were pooled, diluted 1:8 with degassed dilution buffer (25 mM Tris-HCl (pH 7.5), 150 mM NaCl, glycerol (10% vol/vol), 3 mM β-mercaptoethanol, 1mM PMSF and cOmplete protease-inhibitor cocktail (Roche, 1 tablet/ 50 ml)) and incubated batch-wise with 500 µl of M2 anti-flag affinity resin (Sigma) for 45 minutes. Afterwards, the resin was washed extensively with degassed wash buffer [25 mM Tris-HCl (pH 7.5), 150 mM NaCl, glycerol (10% vol/vol), and 1 mM β-mercaptoethanol)] and transferred to a 5 ml column. Dna2 was eluted with wash buffer supplemented with 3x Flag peptide (200 µg/ml; Sigma). Fractions containing protein were pooled and small aliquots were frozen in liquid nitrogen and stored at -80˚C. The final protein concentration

was estimated by densitometry by comparison with a dilution series of BSA (New England BioLabs) on a 12% polyacrylamide gel stained with Coomassie blue. The protein yields were ~40-170 μg and concentrations of ~157-992 nM for Dna2 wild-type and mutant variants. (*Figure 4.1*). All Dna2 yeast strains and recombinant proteins yRPA ,Pol delta, yPCNA, yRFC, and Lig1 were kindly provided by Dr. Maryna Levikova (University of Zurich).

2.4.4 Western Blotting

For the analysis and detection of proteins from cell lysates, Western blots were performed. Proteins samples were boiled (95˚C for 5 minutes) in 5x Laemmli sample buffer and separated on 12% SDS-PAGE gels at 180 V for 45 minutes in 1x SDS running buffer. Afterwards, the proteins were transferred onto nitrocellulose membranes (GE Healthcare) at 100 V for 1 hour in 1x transfer buffer. Next, the efficient transfer of the proteins onto the membranes was confirmed by Ponceau-S staining. The membranes were then blocked in 5% milk-TBS-T solution for 30 minutes and incubated with primary antibody solution overnight at 4˚C. The following morning, the membranes were washed extensively in 1x TBS-T and incubated in the appropriate HRP-coupled secondary antibody for 1 hour at RT˚ (*Table 2.6)*. After the incubation, the membranes were once again washed extensively in 1x TBS-T and the protein signals were developed using the Fusion Solo Chemiluminescence Imager (Vilber Lourmat) following the incubation with ClarityTM Western ECL Blotting Substrate (Bio-Rad) or SuperSignalTM West Femto Maximum Sensitivity Substrate (ThermoFisher Scientific) per manufacturer's instructions.

Table 2.6: List of primary and secondary antibodies used in Western blots.

Primary Antibody	Raised In	Concentration Used	Supplier
Flag M2	Mouse	1:1000	F1804; Sigma-Aldrich
MMS19	Rabbit	1:1000	16015-1-AP; Proteintech
MIP18	Rabbit	1:500	20108-1-AP; Proteintech
RFC5	Goat	1:2000	ab3619; Abcam
RFC2	Mouse	1:500	ab88502; Abcam
RFC4	Mouse	1:1000	ab57917; Abcam
Secondary Antibody	Raised In	Concentration Used	Supplier
Mouse	Sheep	1:2500	NA931V; GE Healthcare
Rabbit	Donkey	1:2500	NA934V; GE Healthcare
Goat	Bovine	1:2500	Sc2350; Santa Cruz

2.5 Biochemical Assays

2.5.1 DNA Substrates

All oligonucleotides used for DNA substrate preparation were synthesized by Microsynth and are listed in *Tables 2.6* and *2.7*. DNA substrates used in biochemical assays contained either a FAM or radioactive label as indicated.

2.5.1.1 FAM Labeled DNA Substrates

The oligonucleotides were FAM labeled on the 3' or 5'-end during oligo synthesis as indicated *Table 2.6*. DNA substrates were annealed in a 50 µl reaction with a 1:1.5 ratio of labeled to unlabeled oligo in 10x DNA annealing buffer. The substrate mixture was then heated to 96˚C for 5 minutes and slowly brought down to 50˚C in a thermocycler. The substrates were then placed on the bench to slowly cool down to RT˚. The concentration of the DNA substrates was 200 nM and was used at a final concentration of 10 nM in biochemical assays.

2.5.1.2 Radioactively Labeled DNA Substrates

The three oligonucleotides used to prepare the flapped substrate are listed in *Table 2.7*. Oligonucleotide 292, which was used to generate the 30 nt flap, was ^{32}P-labeled at the 3' end with [alpha-^{32}P] cordycepin-5' triphosphate (PerkinElmer) using terminal transferase (TdT) (New England BioLabs) according to manufacturer's instructions. Unincorporated nucleotides were removed using MicroSpin G25 columns (GE Healthcare). The flapped substrates were annealed in a 31.25 µl reaction with a 1:2 ratio of labeled to unlabeled oligos in 10x TdT buffer as described above. The final concentration of the flapped substrate was 100 nM and was used at a final concentration of 1 nM in nuclease assays.

2.5.2 Nuclease Assays

Nuclease assays were performed in a 10 µl reaction volume containing, 25 mM Tris-Acetate (pH 7.5), 1 mM ATP, 1 mM DTT, 0.1 mg/ml BSA, 1 mM PEP, 80U/ml pyruvate kinase, 2 mM Magnesium Acetate, recombinant proteins and as indicated either 10 nM DNA substrate for FAM labeled substrates or 1 nM DNA substrate for radioactively labeled substrates. Where indicated, yRPA was present at 30 nM, which is sufficient to fully cover the entire ssDNA in the reaction. Reaction samples were incubated at 30˚C for 30 minutes, the reaction was halted by the addition of 2x stop buffer. The samples were then heated at 95˚C for 5 minutes and separated on 12 or 20% denaturing polyacrylamide gels (ratio acrylamide:bisacrylamide 19:1) in TBE as indicated in the results section.

Nuclease Assays with radioactively labeled were fixed in a solution containing 40% methanol, 10% acetic acid, and 5% glycerol for 30 minutes, without drying, the gels were exposed to storage phosphor screens (GE Healthcare) overnight. The following day, the screens were scanned by Typhoon Phosphor imager (GE Healthcare). In contrast, nuclease assays with FAM labeled substrates were scanned immediately after separation on a gel with the Typhoon Phosphor imager (FAM setting). The graphs were prepared in the GraphPad Prism7, using mean values from three independent experiments.

Table 2.6: Oligonucleotides for FAM labeled DNA substrates

Name	Length (nt)	Sequence (5'-3')
XO1/5' FAM *	61	GACGCTGCCGAATTCTACCAGTGCCTTGCTAGGACATCTTT GCCCACCTGCAGGTTCACCC
XO4/3' FAM *	62	ATCGATAGTCGGATCCTCTAGACAGCTCCATGTAGCAAGGC ACTGGTAGAATTCGGCAGCGT
FP42-5' FAM	42	GACGCTGCCGAATTCTACCAGTGCCTTG CTAGGACATCTTTG
FP42 COMP-Y	42	TTTTTTTTTTTTTTTTTTTTTTTTTTTTAGAATTCGGCAGCGTC
FP COMP-17	17	GACGCTGCCGAATTCTA

** Oligonucleotides both labeled and unlabeled used in DNA substrate preparation*

DNA substrates	Oligonucleotides
Y-structure: XO1 5'*FAM	XO1 5' FAM + XO4
Y-structure: XO4 3'*FAM	XO4 3' FAM + XO1
Y-structure (Y42): FP42 5*FAM	FP42 5' FAM + FP42 COMP-Y

Table 2.7: Oligonucleotides for radioactively labeled DNA Substrates.

Name	Length (nt)	Sequence (5'-3')
X12–4NC	50	GCGATAGTCTCTAGACAGCATGTCCTAGCAAGCCAGAATTC GGCAGGCTA
Flap 19 X12–4C	19	TAGCCTGCCGAATTCTGGC
292	61	GGTACTCAAGTGACGTCATAGACGATTACATT GCTAGGACATGCTGTCTAGAGACTATCGC

DNA substrates	Oligonucleotides
30 nt FLAP	292* 3' + X12-4NC + Flap 19 X12-4C

2.5.3 Helicase Assays

Helicase assays were performed in 10 μl reaction volume containing, 25 mM Tris-Acetate (pH 7.5), 1 mM ATP, 1 mM DTT, 0.1 mg/ml BSA, 0.5 mM Magnesium Chloride, 50 nM competitor oligo, recombinant proteins, and 10 nM FAM labeled DNA substrate. Reactions were incubated at 30˚C for 30 minutes and the reaction was halted by the addition of 2x helicase stop buffer. Reactions were then supplemented with 1 μl of Proteinase K (20mg/ml) and incubated for 10 minutes at 37˚C. Next, the control reaction was heated to 95˚C for 5 minutes, and all samples were separated on a 10% native polyacrylamide gel in TBE (ratio acrylamide:bisacrylamide 19:1). The gel was then scanned by the Typhoon Phosphor imager (FAM setting).The graphs were prepared in the GraphPad Prism7, using mean values from three independent experiments.

2.5.4 Replication Assays

Replication assays were performed with a 3.197 kb-long ssDNA plasmid (pRichi) based substrate with the pR_T30flap (5'- T*T*T*T*T*T*T*T*T*T*T*T*T*T*T*T*T*T*T*T*T*T*TACCA-3') oligo annealed to generate a 30 nt flap as previously described (Levikova & Cejka, 2015). In a 15 μl reaction volume, 25 mM Tris-acetate pH 8.5, 10 mM magnesium acetate, 125 mM NaCl, 1 mM ATP, 1 mM DTT, 0.1 mg/ml BSA, 1 mM phosphoenol pyruvate, 80 U/ml pyruvate kinase, 100 M dNTPs (each) and 6.4 nM (molecules, 100 ng) ssDNA substrate were mixed together. Afterwards, PCNA (20 nM), RFC (20 nM) and RPA (1 μM, concentration saturating 100% of DNA) were added to the reaction and pre-incubated for 1 min at 30˚C. Next, Pol δ (5 nM) Dna2 (as indicated) and Lig1 (20 nM) were added to the reaction and further incubated at 30˚C for 1 hour. The reactions were halted by the addition of 5 μl of 2% replication assay stop solution and supplemented with 1 μl of Proteinase K and incubated for 10 minutes at 37˚C. The reactions were then separated on a 1% agarose gel containing GelRed® (1:10,000 vol/vol; Biotium) and analyzed by an Alpha Imager gel imaging system. The experiments and pRichi ssDNA plasmid and pR_T30 flap oligo were kindly performed and provided by Dr. Maryna Levikova (University of Zurich). The graphs were prepared in the GraphPad Prism7, using mean values from three independent experiments.

2.6 Radioactive ^{55}Fe Incorporation

2.6.1 Yeast ^{55}Fe Incorporation

To obtain clear evidence that RFC5 binds an FeS cluster, an ^{55}Fe-incorporation assay was conducted as described previously (Pierik et al., 2009). In brief, human GFP-tagged RFC5 was constitutively expressed in a yeast strain in which Flag-tagged MMS19 is expressed in a galactose-inducible manner *(PGAL Flag-MMS19*). Following iron starvation, the yeast cells were radiolabeled with ^{55}Fe (PerkinElmer). Next, yeast cell extracts were prepared and GFP-RFC5 was immunopurified with GFP-Trap® agarose resin (Chromotek) for 1 hour on a rotary rotor at 4˚C. Next, the resin was washed extensively and then resuspended in 50 µl of sterile water and transferred to a counting tube and mixed with 1 ml of Ultima Gold™ liquid scintillation cocktail (PerkinElmer). The extent of ^{55}Fe incorporation was measured by liquid scintillation counting on the Tri-Carb 2000 CA (Packard) with settings appropriate for ^{3}H. In addition, to examine the dependency on MMS19 for iron incorporation, the assay was performed under normal (galactose-containing medium) conditions and MMS19-depleted (glucose-containing medium) conditions. RFC5 expression levels were evaluated by Western blotting to verify that any decrease in ^{55}Fe incorporation was not a result of RFC5 destabilization.

2.6.2 Sf9 ^{55}Fe Incorporation

The radiolabeling of Sf9 insect cells with ^{55}Fe is an efficient assay for the estimation of the *de novo* biogenesis of FeS cluster containing proteins *in vivo.* The Sf9 Fe incorporation assay was developed based on the protocol from Pierik and colleagues, who measured Fe incorporation in yeast cells (Pierik et al., 2009). To begin, 20 ml Sf9 suspension cultures are seeded at a density of 1.5 x10^6 cells/ml. Next, the cells were infected with the appropriate baculovirus according to its MOI. Next, the cells were radiolabeled with the addition of 200 µl of 0.1M Na ascorbate, which prevents the formation of ferric precipitates in the growth media, and 20 µl of $^{55}FeCl_3$ (PerkinElmer). The cells were then incubated for 48 hours at 25˚C. Afterwards, the cells were harvested by centrifugation (1500 RPM, 10 mins, 4˚C) and the supernatant discarded. To remove residual $^{55}FeCl_3$, cells were washed with 5 ml of citrate buffer [50 mM Na Citrate, 1 mM EDTA in 1x PBS] and spun down. Again, the supernatant was discarded and the cells were washed with 1x PBS to remove residual citrate buffer. Thereafter, the cell pellet was lysed as described above (*See 2.4.1).* The resulting lysate was then immunoprecipitated (IP) on 20 µl pre-equilibrated M2 Flag beads on a rotor at 4˚C for 1 hour. After the IP, the beads were washed 6x 5 minutes in lysis buffer. Meanwhile, the liquid scintillation tubes were prepared,

by adding 1 ml of Ultima Gold™ liquid scintillation cocktail to the counting tubes. After washing, the supernatant was removed and the beads were resuspended in 50 µl of sterile water and added to the counting tubes. The tubes were vortexed gently for 1 min/sample, then taken for counting on the Tri-Carb 2000 CA.^{55}Fe radioactivity associated with the beads was counted with settings appropriate for ^{3}H as described above. The remaining beads from the IP were stored in 40 µl of 2x loading dye. To check protein expression/ capture, 10 µl were loaded on a 12% SDS gel, and stained with Coomassie blue.

2.7 Bioinformatics

2.7.1 Multiple-Sequence Alignment

Primary Sequence alignment was performed by using Clustal Omega algorithms with default settings, accessed through Uniprot (*www.uniprot.org*). Accession Numbers of proteins: **RFC5:** B5DF29 (*R. norvegicus*), P40937 (*H. sapiens),* Q8CFZ9 (*M. musculus),* Q6DRK4 (*D. rerio*), and P38629 (*S. cerevisiae).* **RFC2:** P35250 (*H. sapiens);* **RFC3:** P40938 *(H. sapiens);* **RFC4:** P35249 *(H. sapiens).*

2.7.2 Protein Structure Analysis

Analysis of mouse DNA2 structure was performed using UCSF Chimera. Structure from (Zhou et al., 2015), PDB Code: 5EAX

2.7.3 Quantification of Biochemical Assays and Protein Purification

Nuclease and helicase activities were quantified using ImageJ software (NIH); product formation was calculated by measuring the remaining substrate compared to control samples; the integrated density parameter of each band was measured and adjusted by eliminating the integrated density value of the background. Purified proteins were also quantified with ImageJ by comparing the purified proteins with a dilution series of BSA.

3. Results

Aim 1: Identifying Potential Novel Nuclear FeS Cluster Proteins: RFC5

A common characteristic of all currently known nuclear FeS cluster proteins is their interaction with the MMS19-MIP18 complex, core components of the CIA machinery. RFC5 was identified as a potential interaction partner of MMS19 *via* mass spectrometry (Stehling et al., 2012). In addition Rfc3, the yeast counterpart to RFC5 was shown to be synthetic lethal with *mms19*Δ (Collins et al., 2007). Furthermore, *in silico* multiple sequence alignment revealed five conserved cysteine residues that could potentially function in coordinating an FeS cluster (*Figure 3.1).* Therefore, we hypothesized that RFC5 could potentially bind an FeS cluster as a cofactor.

3.1 RFC5 Interaction Study with CIA Machinery Components MMS19 & MIP18

To confirm the interaction between RFC5 and the CIA machinery, extracts from Sf9 or Sf21 insect cells transiently co-expressing RFC5 along with MMS19 or MIP18 were used for co-IP experiments. The constituents of the isolated complexes were then identified by Western blotting. Here we show that RFC5 physically interacts with both MMS19 and MIP18 independently and bidirectionally *in vitro* (*Figure 3.2).* In addition to co-IP experiments in insect cells, the physical interaction of RFC5 with MMS19 and MIP18 in HEK-293T cells was also tested. Cells were transfected using Calcium Phosphate. As before in insect cells, RFC5 was co-expressed with MMS19 and the putative complexes were isolated and analyzed by Western blotting. In initial experiments, we observed that the expression levels of RFC5 were very low *(see also Figure 3.3: WCE lanes 1,3,6).* Since it has been shown that RFC5 and RFC2 have a pairwise subunit interaction (Majka & Burgers, 2004), we additionally co-expressed the RFC2 subunit to test if RFC5 expression was stabilized, which indeed was the case *(Figure 3.3: WCE lanes 2,5,7).* When expressed in the presence of RFC2, RFC5 was pulled down by Flag-tagged MMS19 but not by Flag-tagged ALC1, which was used as a control in the co-IP experiments. Interestingly, RFC5 interaction with RFC2 does not interfere with its interaction with MMS19, indicating that the interaction between MMS19 and RFC5 is specific *(Figure 3.3).* A similar result was obtained when we tested the interaction of RFC5 with MMS19 and MIP18 simultaneously, utilizing a plasmid encoding Flag-tagged MMS19 and untagged MIP18 separated by the self-cleaving peptide T2A, allowing us to obtain approximately the same expression of MMS19 and MIP18 (Szymczak et al., 2004). These data show that RFC5 interacts with MMS19 and MIP18 suggesting that it may incorporate an FeS cluster as a cofactor.

```
TR|B5DF29|B5DF29_RAT   --MAAAPSQQQPRAARARNLPWVEKYRPQTLADLISHQDILSTIQKFISEDRLPHLLLYG 58
SP|P40937|RFC5_HUMAN   METSALKQQEQPAATKIRNLPWVEKYRPQTLNDLISHQDILSTIQKFINEDRLPHLLLYG 60
TR|Q8CFZ9|Q8CFZ9_MOUSE -------HASAHASAHASAHASAHASGPQTLADLISHQDILSTIQKFISEDRLPHLLLYG 53
TR|Q6DRK4|Q6DRK4_DANRE ------MASTSKTQPQARNLPWVEKYRPQTLDDLISHQDILSTIQKFISEDRLPHLLFYG 54
SP|P38629|RFC3_YEAST   -------MSTSTEKRSKENLPWVEKYRPETLDEVYGQNEVITTVRKFVDEGKLPHLLFYG 53

TR|B5DF29|B5DF29_RAT   PPGTGKTSTILACAKQLYKDKEFGSMVLELNASDDRGIDIVRGPILSFASTRTIFKRGFK 118
SP|P40937|RFC5_HUMAN   PPGTGKTSTILACAKQLYKDKEFGSMVLELNASDDRGIDIIRGPILSFASTRTIFKKGFK 120
TR|Q8CFZ9|Q8CFZ9_MOUSE PPGTGKTSTILACAKQLYKDKEFGSMVLELNASDDRGIDIVRGPILSFASTRTIFKKGFK 113
TR|Q6DRK4|Q6DRK4_DANRE PPGTGKTSTILACARQLYKDKEFNSMVLELNASDDRGIDVVRGPILSFASTRTIFKKGFK 114
SP|P38629|RFC3_YEAST   PPGTGKTSTIVALAREIYG-KNYSNMVLELNASDDRGIDVVRNQIKDFASTRQIFSKGFK 112

TR|B5DF29|B5DF29_RAT   LVILDEADAMTQDAQNALRRVIEKFTENTRFCLICNYLSKIIPALQSRCTRFRFGPLTPE 178
SP|P40937|RFC5_HUMAN   LVILDEADAMTQDAQNALRRVIEKFTENTRFCLICNYLSKIIPALQSRCTRFRFGPLTPE 18
TR|Q8CFZ9|Q8CFZ9_MOUSE LVILDEADAMTQDAQNALRRVIEKFTENTRFCLICNYLSKIIPALQSRCTRFRFGPLTPE 173
TR|Q6DRK4|Q6DRK4_DANRE LVILDEADAMTQDAQNALRRVIEKFTENTRFCLICNYLSKIIPALQSRCTRFRFGPLSQN 174
SP|P38629|RFC3_YEAST   LIILDEADAMTNAAQNALRRVIERYTKNTRFCVLANYAHKLTPALLSRCTRFRFQPLPQE 172

TR|B5DF29|B5DF29_RAT   LMVPRLEHVVQEENVDISEDGMKALVTLSSGDMRRALNILQSTNMAFG-----KVTEETV 233
SP|P40937|RFC5_HUMAN   LMVPRLEHVVEEEKVDISEDGMKALVTLSSGDMRRALNILQSTNMAFG-----KVTEETV 235
TR|Q8CFZ9|Q8CFZ9_MOUSE LMVPRLEHVVQEENVDISEDGMKALVTLSSGDMRRALNILQSTNMAFG-----KVTEETV 228
TR|Q6DRK4|Q6DRK4_DANRE QMIPRLEHVIQQESIDITPDGMKAIVTLSTGDMRRSLNILQSTHMAYG-----KVTEETV 229
SP|P38629|RFC3_YEAST   AIERRIANVLVHEKLKLSPNAEKALIELSNGDMRRVLNVLQSCKATLDNPDEDEISDDVI 232

TR|B5DF29|B5DF29_RAT   YTCTGHPLKTDIANILDWMLNQDFTTAYKNIMELKTLKGLALHDILTEVHLFVHRVDF-P 292
SP|P40937|RFC5_HUMAN   YTCTGHPLKSDIANILDWMLNQDFTTAYRNITELKTLKGLALHDILTEIHLFVHRVDF-P 294
TR|Q8CFZ9|Q8CFZ9_MOUSE YTCTGHPLKTDIANILDWMLNQDFTTAYKNIMELKTLKGLALHDILTEVHLFVHRVDF-P 287
TR|Q6DRK4|Q6DRK4_DANRE YTCTGHPLRSDIANILDWALNKDFTTAYNQILELKTLKGLALHDILTEVHLLIHRVDF-P 288
SP|P38629|RFC3_YEAST   YECCGAPRPSDLKAVLKSILEDDWGTAHYTLNKVRSAKGLALIDLIEGIVKILEDYELQN 292

TR|B5DF29|B5DF29_RAT   SSVRMHLLTKMADIEYRLSVGTSEKIQLSSLIAAFQVTRDLIVAEA-- 338
SP|P40937|RFC5_HUMAN   SSVRIHLLTKMADIEYRLSVGTNEKIQLSSLIAAFQVTRDLIVAEA-- 340
TR|Q8CFZ9|Q8CFZ9_MOUSE SSVRIHLLTKMADIEYRLSVGTSEKIQLSSLIAAFQVTRDLIVAEA-- 333
TR|Q6DRK4|Q6DRK4_DANRE PSIRMGLLIKLADIEYRLASGTSEKIQLSSMVAAFQAVRDIVVSDG-- 334
SP|P38629|RFC3_YEAST   EETRVHLLTKLADIEYSISKGGNDQIQGSAVIGAIKASFENETVKANV 340
```

Figure 3.1 Multiple Sequence Alignment of RFC5. Multiple sequence alignment of RFC5 reveals five conserved cysteines that may potentially function in FeS cluster coordination. Sequences aligned from rat, human, mouse, zebrafish, and yeast.

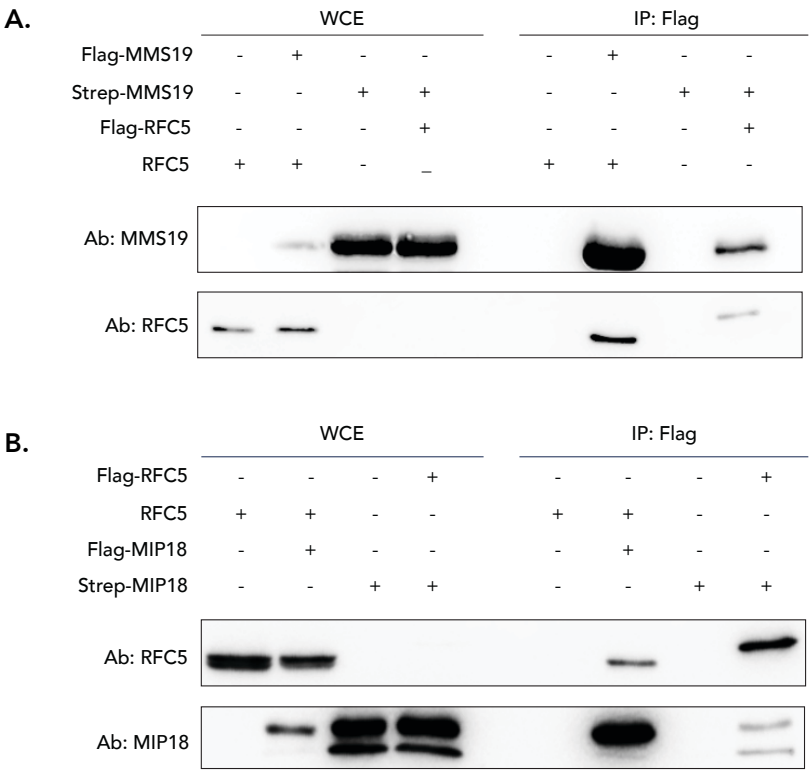

Figure 3.2 RFC5 Interacts with CIA Machinery Components MMS19/MIP18. (A.) Co-IP of RFC5 co-expressed with MMS19 in Sf21 insect cells. **(B.)** Co-IP of RFC5 co-expressed with MIP18 in Sf9 insect cells.

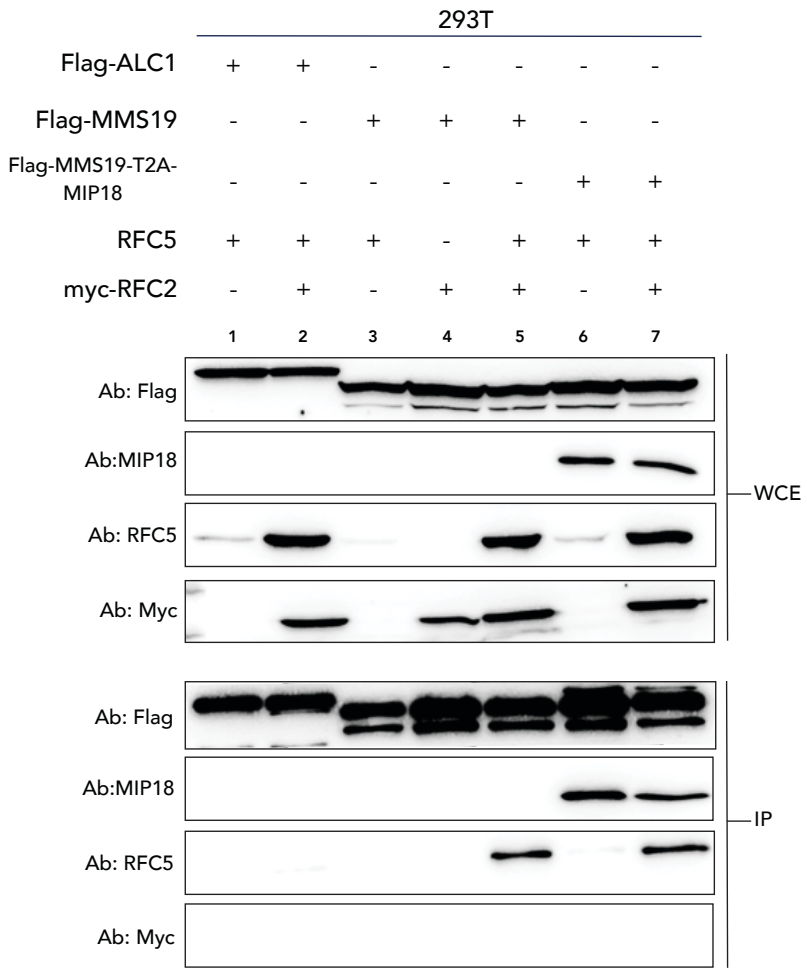

Figure 3.3 RFC5 Interacts with CIA Machinery Components MMS19/MIP18 in HEK 293T. Like in insect cells, RFC5 interacts with both MMS19 and MIP18. Co-expression of RFC2 stabilizes RFC5 expression but RFC2 does not interact with the CIA machinery.

3.2 Yeast ^{55}Fe Incorporation Assay with RFC5

To obtain clear evidence that RFC5 coordinates an FeS cluster, we performed an ^{55}Fe incorporation assay in yeast as described in *(Sec. 2.6)*. Human GFP-tagged RFC5 was overexpressed in a yeast strain in which Flag-tagged *MMS19* is expressed in a galactose-inducible manner *(P_{GAL} Flag-MMS19)*. The extent of ^{55}Fe incorporation was measured by liquid scintillation counting. In initial experiments GFP-RFC5 expression was unstable, which resulted in unreliable measurements (*data not shown*). Therefore, to enable stable expression of RFC5, we generated a GFP tagged RFC5 yeast strain coupled with RFC2 using the T2A peptide as described above. Using the newly-generated yeast strain, we re-performed the ^{55}Fe incorporation assays. Across four biological replicates we were able to detect the presence of iron in RFC5, albeit at low levels. In addition to low detection levels, the counts were highly variable across all experiments (*Figure 3.4A)*. However, after data normalization, we were able to demonstrate a significant difference in iron incorporation

between the MMS19 expressing (galactose-containing medium) and non-MMS19 expressing (glucose-containing medium) conditions *(Figure 3.4B)*. In addition, after Western blot analysis of the isolated complexes, we discovered that RFC5 expression was greatly stabilized in the presence of RFC2 (*Figure 3.4C)*. Although we were able to detect the presence of iron in RFC5, the low counts and high variability between experiments led us to seek another method to detect the presence of iron in RFC5 more reliably.

A.

Experiment #	Galactose (+ MMS19)	Glucose (-MMS19)
1	144	50
2	281	89
3	144	52
4	203	66

B.

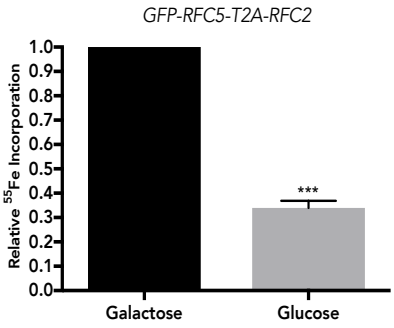

C.

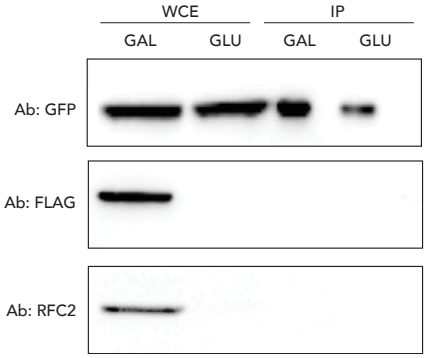

Figure 3.4 Yeast iron incorporation assay . **(A.)** Liquid scintillation counting measurements for RFC5 iron incorporation (Counts/min). **(B.)**Relative levels of ^{55}Fe incorporation in the presence (GAL) or absence (GLU) of MMS19 after data normalization. n=4; p: <0.001 **(C.)** Representative Western blot of the isolated RFC5 complexes. RFC5 expression levels are stabilized in the presence of RFC2.

3.3 ^{55}Fe Incorporation in Sf9 Insect Cells

Due to the challenges of expressing RFC5 in yeast for iron incorporation analysis, a new method to detect the presence of iron in candidate proteins was required. Therefore, we developed a new method using a cellular system closer related to humans. We made use of *Spodoptera frugiperda* Sf9 insect cells, which are widely used for protein expression and recombinant protein purification. To validate the assay, we analyzed the iron incorporation in a known FeS cluster protein, ChlR1. As a control we used ChlR1's FeS binding mutant C267S as described in *(Sec. 2.7)*. Our results demonstrated a nearly a 10-fold decrease in ^{55}Fe incorporation in the C267S mutant compared to ChlR1 WT. In addition, ^{55}Fe incorporation counts were higher than in yeast, which allowed us to see a clear difference between the WT and FeS binding mutant, proving to be a robust method for the detection of the *de novo* biogenesis of FeS cluster proteins *in vivo (Figure 3.5)*.

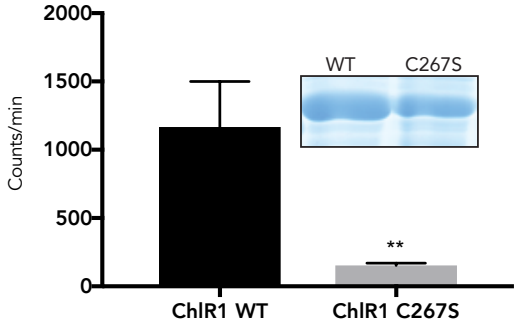

Figure 3.5 Sf9 ^{55}Fe Incorporation Assay Validation.
Counts per min in ChlR1 WT and FeS binding mutant C267S. The C267S mutant exhibits ~10 fold less incorporation compared to the WT. Inset: Protein Capture, 12% SDS; Coomassie blue staining. *n*= 3; p: 0.0062

To enable the stable expression of RFC5 in insect cells, we generated a Flag-tagged baculovirus coupled with RFC2, using the T2A peptide as described above. To ensure our construct resulted in stable RFC5 expression, we performed a series of interaction studies in HEK-293T cells. Plasmids encoding Flag-tagged RFC5, Myc-tagged RFC2 and Flag-tagged RFC5-T2A-RFC2 were transiently over expressed with MMS19, and the isolated complexes analyzed by Western blotting. As suspected, the expression of RFC5 was greatly stabilized in the presence of RFC2. Surprisingly, we found that the T2A peptide in the RFC5-T2A-RFC2 construct eliminated RFC5s interaction with MMS19 *(Figure 3.6)*. Therefore, we tested the iron incorporation in RFC5 alone and with the co-expression with RFC2, using ChlR1 WT as a positive control. Across three biological replicates, we were only able to detect background levels of iron in RFC5 when compared with the known FeS protein ChlR1 *(Figure 3.7)*. These data suggest that RFC5 is unlikely to coordinate an FeS cluster as a cofactor.

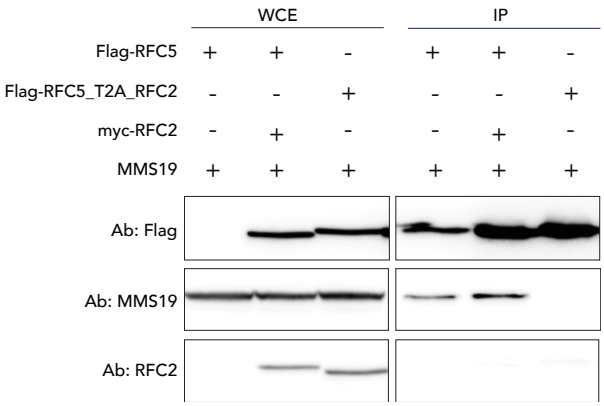

Figure 3.6 RFC5 T2A RFC2 Construct Eliminates MMS19 Interaction.
RFC5 stability is increased in the presence of RFC2. However, T2A peptide eliminates RFC5's interaction with MMS19.

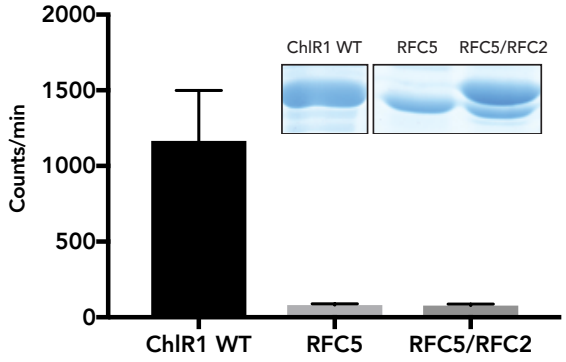

Figure 3.7 Sf9 ^{55}Fe Incorporation Assay: RFC5
Mean ^{55}Fe incorporation levels (Counts/min) in ChlR1 WT, RFC5 alone, and RFC5/RFC2. RFC5 ^{55}Fe incorporation only detects background levels; RFC5 likely does not coordinate FeS cluster Inset: Protein Capture, 12% SDS; Coomassie blue staining. *n*= 3

3.4 Knock-down of CIA Machinery Components MMS19/MIP18 Does Not Affect RFC5 Expression

Since it was previously shown that the loss of MMS19 resulted in lower expression levels for multiple FeS proteins, we reasoned that the transient knockdown of CIA machinery components MMS19 and/or MIP18 *via* siRNA treatment would destabilize RFC5, resulting in lower expression levels (Gari et al., 2012). Both MMS19 and MIP18 were knocked down using two siRNAs each as described in (*sec. 2.3.3).* Expression levels were analyzed by Western blotting. The siRNAs targeting MMS19 both effectively reduced expression levels in HeLa cells *(Figure 3.8).* The MIP18 knockdown was less efficient, but was significantly reduced in comparison to the control siRNA. Interestingly, MIP18 expression in MMS19 knockdown cells was also reduced, which is in line with a recent study that demonstrated MMS19 expression is required for stable MIP18 expression (Odermatt & Gari, 2017). Ultimately, the levels of RFC5 were unaffected by the knockdown of the CIA machinery components *(Figure 3.8).* Taken together with the Sf9 ^{55}Fe incorporation data, these results suggest that RFC5 is unlikely to coordinate an FeS cluster as a cofactor. Further studies will be required to identify the functional relevance of RFC5's interaction with the CIA machinery.

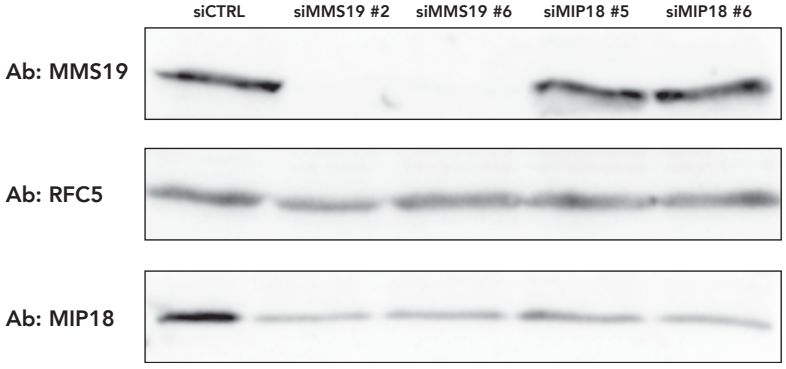

Figure 3.8 RFC5 expression levels following knockdown of CIA machinery components.
The transient knockdown of CIA machinery components MMS19 and MIP18 does not affect the expression of endogenous RFC5.

4. Results

Aim 2: Elucidating the Role of the Iron-Sulfur Cluster in the Nuclease/Helicase Dna2

4.1 Purification of Dna2

In 2012, Pokharel and Campbell confirmed Dna2 as a *bona fide* FeS cluster protein (Pokharel & Campbell, 2012). In this study, they showed that loss of the FeS cluster was detrimental to Dna2's nuclease and ATPase activities *in vitro*. However, considering the fragile nature of FeS clusters and their sensitivity to oxidation and long dialysis procedures, we asked whether the integrity of the FeS cluster was maintained in this earlier study. Therefore, wild-type, nuclease-dead (E675A), helicase-dead (K1080E), FeS binding mutant (C771A), double-mutants (C771A/E675A) and (C771A/K1080E) Dna2, were purified using an optimized protocol as described previously (Levikova et al., 2013)*(Figure 4.1) (See 2.4.2)*.

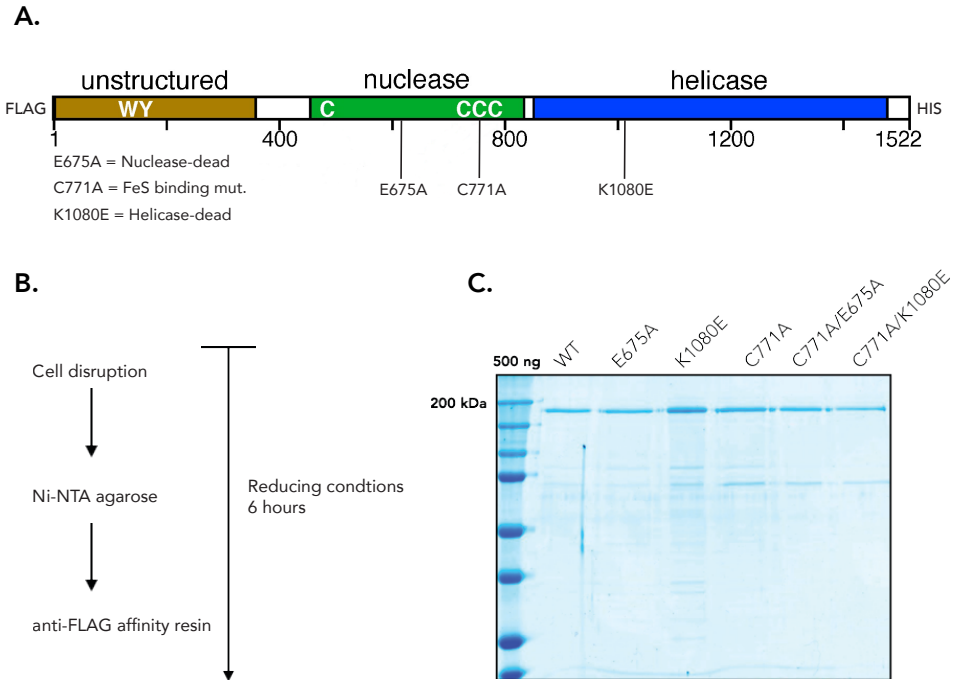

Figure 4.1 Dna2 Purification
(A.) Dna2 constructs with indicated point-mutations. **(B.)** Purification Schematic **(C.)** Wild-type and mutant proteins of Dna2

4.2 Biochemical Analysis

4.2.1 Dna2 Nuclease Assays

As noted above, previous studies have shown that, in the absence of the FeS cluster, Dna2 nuclease activity is almost completely lost (Pokharel & Campbell, 2012). Therefore, we tested our recombinant Dna2 preps and found that for the wild-type, maximum cleavage was observed at all protein concentrations, whereas the FeS (C771A) and FeS-helicase-dead (C771A/K1080E) double mutant showed impaired but not abolished nuclease activity. As expected, the FeS-nuclease-dead (C771A/E675A) double mutant showed no nuclease activity (*Figure 4.2*). Nuclease assays were performed using 3' FAM labeled oligo-based DNA substrates and analyzed on a denaturing gel.

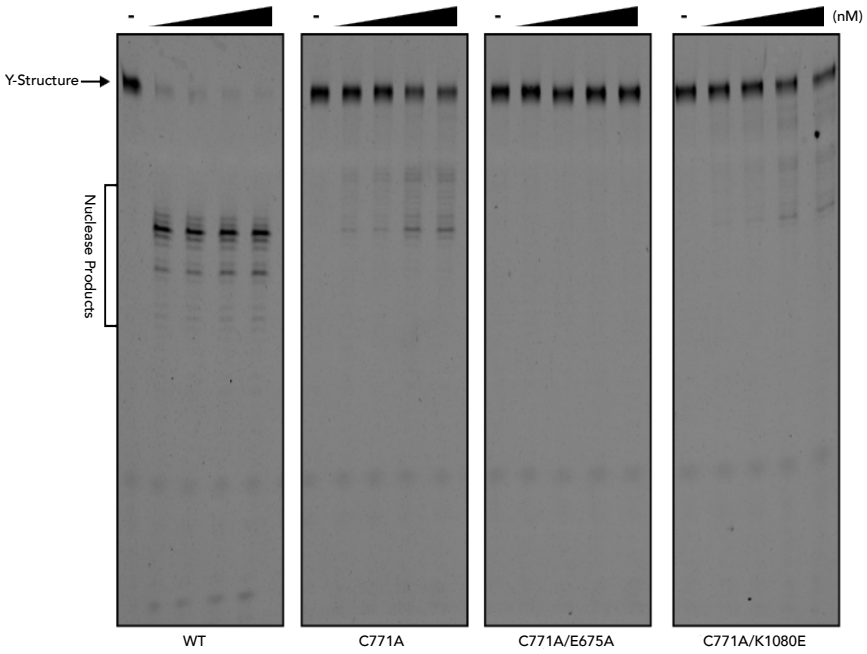

Figure 4.2 Nuclease activity of wild-type and mutant proteins (4-32nM). 10nM Y-structure DNA substrate was used in the nuclease reaction containing: 25mM Tris-Acetate (pH 7.5), 1mM dithiothreitol (DTT), 0.1mg/ml BSA, 1mM ATP, 2 mM Mg Acetate, 1mM phosphoenolpyruvic acid (PEP), and 80U/ml pyruvate kinase. 12% denaturing gel.

Next, we tested the speed at which the wild-type or FeS binding mutant (C771A) degrades its DNA substrate. Therefore, as described in (*Sec. 2.5.2)* we performed a time-course nuclease assay using 45nM of WT or FeS binding mutant Dna2. Wild-type Dna2 was able to degrade its substrates very rapidly, reaching maximum cleavage by 60 seconds, whereas for the FeS binding mutant significant substrate cleavage was only seen after 5 minutes, increasing steadily with time. *(Figure 4.3A).* These results indicate that the FeS cluster in Dna2 is required for rapid nuclease activity and that loss of the FeS cluster doesn't completely eliminate nuclease activity in Dna2.

Considering that the FeS binding mutant's (C771A) nuclease activity was concentration dependent, we then tested the minimum concentration required of wild-type Dna2 to reduce its nuclease activity to that of a maximum concentration of C771A Dna2. Therefore, we performed a nuclease assay as described in *(Sec. 2.5.2)*. Wild-type Dna2 was titrated between 0.125-32nM and C771A Dna2 4-32nM. These experiments revealed that wild-type Dna2's nuclease activity is comparable to 32nM of C771A Dna2 at a concentration of 0.5nM *(Figure 4.3B)*. Collectively, our results indicate the loss of the FeS cluster in Dna2 significantly reduces its nuclease activity but does not abrogate it completely.

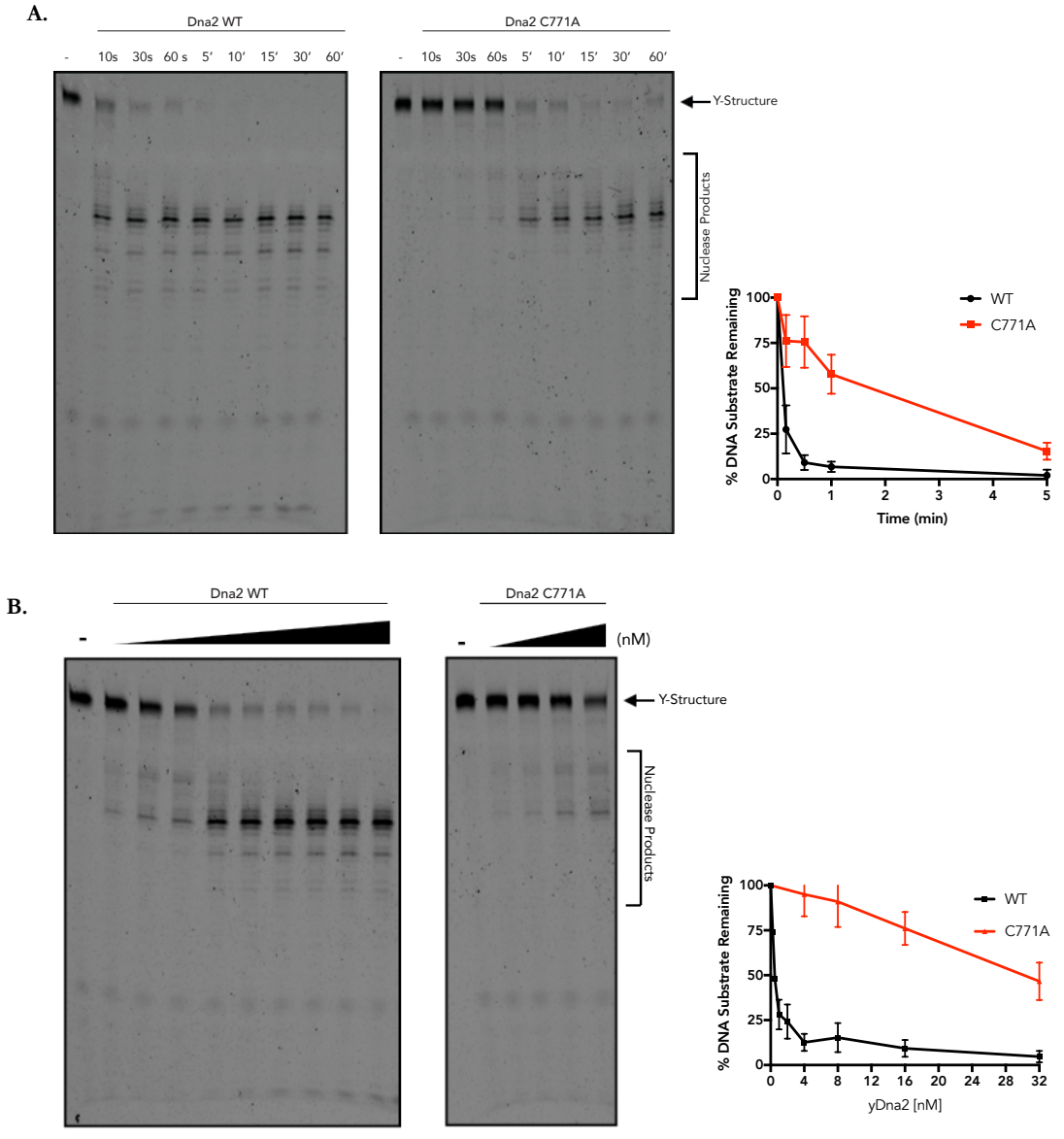

Figure 4.3 Nuclease Activity of WT and FeS Mutant (A.) Nuclease activity of 45nM wild-type (left panel) and FeS binding mutant (right panel), 100µl reaction volume, 10µl samples taken at indicated time points. Inset: Quantification: Averages shown *n*=3, error bars; s.e.m.**(B.)** Nuclease activity of wild-type, titrated between 0.125-32nM (left panel) and FeS binding mutant (right panel) titrated between 4-32nM; 10nM Y-structure DNA substrate was used in the nuclease reactions containing: 25mM Tris-Acetate (pH 7.5), 1mM dithiothreitol (DTT), 0.1mg/ml BSA, 1mM ATP, 2 mM Mg Acetate, 1mM phosphoenolpyruvic acid (PEP), and 80U/ml pyruvate kinase. Inset: Quantification:Averages shown *n*=3, error bars; s.e.m. 12% denaturing gel.

4.2.2 Dna2 Helicase Assays

The nuclease activity of Dna2 was reported to be required for all of its *in vivo* functions and considered its main functional role. However, Dna2 contains a Superfamily I helicase domain, shown to possess weak unwinding capability. It was later shown that Dna2 possesses cryptic but potent helicase activity comparable to a number of other helicases, only observable after nuclease inactivation (Levikova et al., 2013). These data suggested that the potent Dna2 nuclease activity inhibits substrate unwinding by cleaving 5' flaps required for helicase loading. Considering the reduction in nuclease activity after the loss of the FeS cluster, we hypothesized that loss of the FeS cluster may result in increased helicase activity. To test this, we performed helicase assays using recombinant nuclease-dead (E675A), FeS binding- (C771A) and double mutant (C771A/E675A) Dna2. In addition, to confirm that our reaction products were the result of ATP-dependent helicase activity, we tested helicase activity in the absence of ATP as described in *(Sec. 2.5.3)*.

As expected, the nuclease-dead (E675A) mutant exhibited potent helicase activity and reached a minimum of 50% unwinding at all protein concentrations. The FeS-nuclease-dead double mutant (C771A/E675A) exhibited reduced helicase activity in a concentration-dependent manner, which points to a critical role of the FeS cluster in sustaining helicase activity *(Figure 4.4A)*. Helicase reactions without ATP resulted in no unwinding, which was expected as Dna2 is an ATP-dependent helicase *(Figure 4.4B)*. Interestingly, the FeS binding mutant (C771A) exhibited slight helicase activity that decreased in a concentration-dependent manner, which was lost in the absence of ATP. Furthermore, the decrease in helicase activity in the C771A mutant was the result of simultaneous nuclease activity (*Figure 4.4C)*. Moreover, we investigated whether or not Dna2 WT exhibits helicase activity compared to the FeS binding mutant (C771A). Surprisingly, Dna2 WT exhibited helicase activity at low protein concentrations, while, as expected, Dna2 C771A exhibited only slight helicase activity *(Figure 4.5)*. Our data suggests that the loss of the FeS cluster in Dna2 does not stimulate Dna2's helicase activity, but rather is critical for both its nuclease and helicase activities.

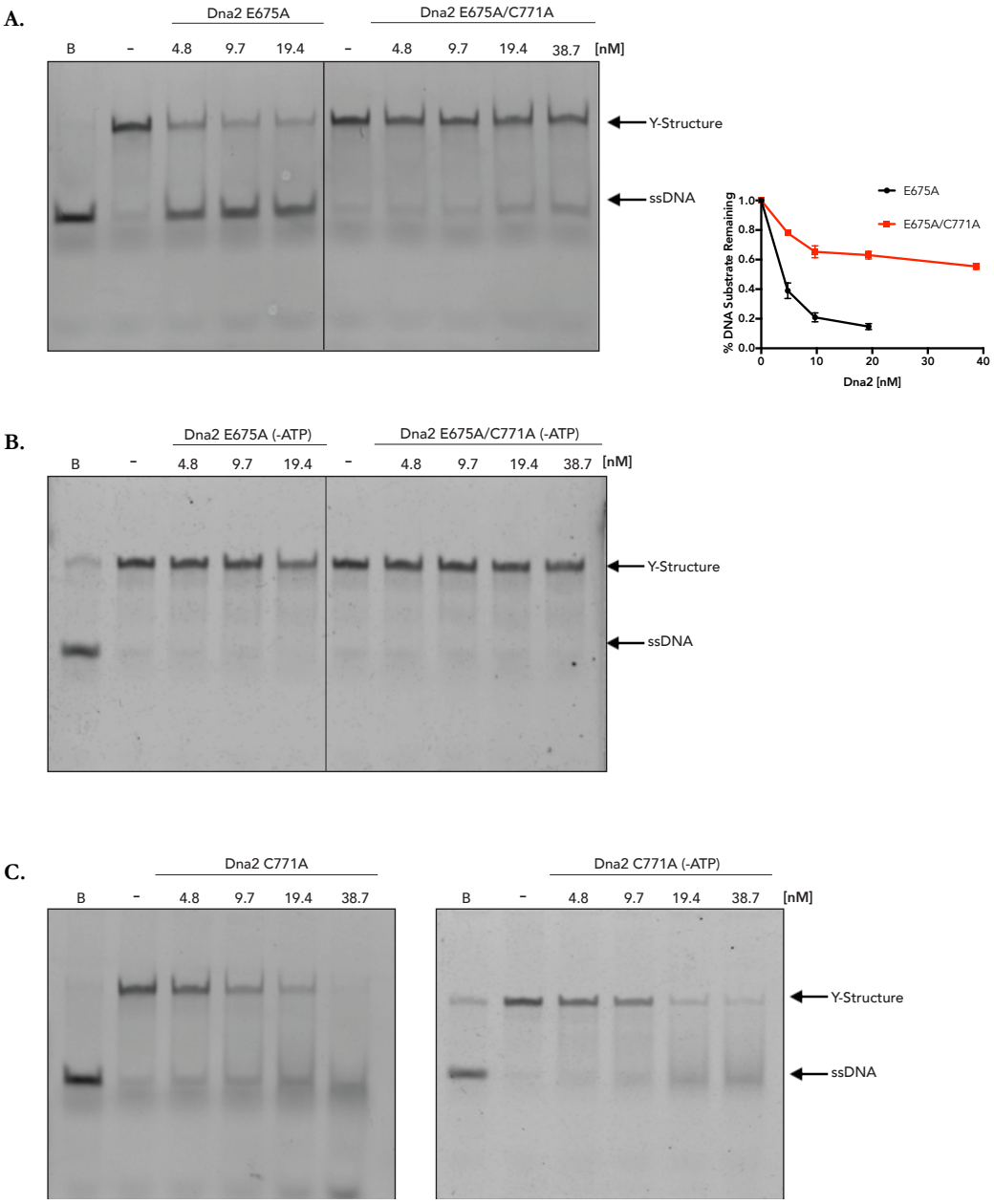

Figure 4.4 Dna2 Helicase Assays (A/B). Helicase activity of nuclease-dead (E675A) and FeS/nuclease-dead (C771A/E675A) with or without ATP. Inset A: Quantification of the E675A and E675A/C771A helicase activity. Averages shown *n*=3; error bars, s.e.m. **(C.)** Helicase activity of the FeS binding mutant (C771A) with or without ATP. Protein concentrations as indicated; 10nM 5'FAM labelled Y-structure DNA substrate was used in a 10µl reaction containing: 25mM Tris-Acetate (pH 7.5), 1mM dithiothreitol (DTT), 0.1mg/ml BSA, 2mM ATP, 1mM Mg Acetate and, 50nM of DNA competitor. Reactions incubated at 30 ˚C for 30 minutes. The reaction was stopped by addition of 2X stop solution (7% Ficoll 400, 20mM Tris- Hcl (pH 7.5), 20mM EDTA, 0.2% SDS, bromophenol blue, and 10mg/ml

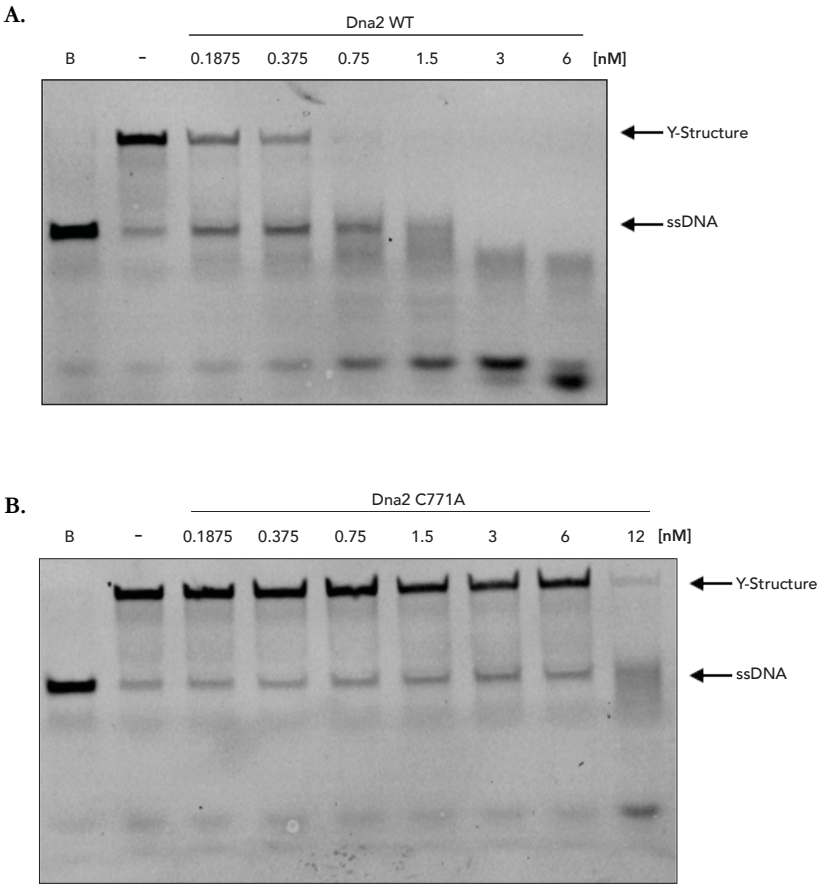

Figure 4.5 Dna2 Helicase Assays WT and FeS Mutant (A/B). Helicase activity of Dna2 WT. **(B.)** Helicase activity of the FeS binding mutant (C771A). Protein concentrations as indicated; 10nM 5'FAM labelled Y-structure DNA substrate as described in *Figure 4.4*.

4.2.3 Okazaki Fragment Maturation

During DNA replication, lagging strand synthesis occurs in short stretches termed Okazaki fragments. Prior to the adjacent fragments ligation, any flaps resulting from the displacement of the 5' end of the Okazaki fragment must be resected. It has been shown that Dna2 functions upstream of Fen1 in processing flaps coated by RPA, resulting in a shorter flap that is then processed by Fen1. However, it was later shown that Dna2 can cleave at or near the base of the flap without the further requirement for Fen1 processing (Levikova & Cejka, 2015). Since the latter study had significantly more active Dna2 rapidly purified under reducing conditions, we hypothesized that the integrity of the FeS cluster in Dna2 may be required for cleavage at or near the base, and that the FeS cluster may regulate the cleavage site of Dna2 in Okazaki fragment processing. To test this, we used recombinant wild-type and 10 times the concentration of the FeS binding mutant (C771A) Dna2 in a nuclease assay that utilizes a substrate mimicking a structure that arises upon displacement synthesis during Okazaki fragment processing *(Figure 4.6A)* (Levikova & Cejka, 2015). To assess Dna2 WT and Dna2 C771A's ability to cleave at the base of an Okazaki-like fragment, we performed nuclease assays as described in (*Sec. 2.5.2),* using 1nM

flapped substrate in the presence of RPA and analyzed them on a denaturing gel. As expected, the majority of Dna2 WT's cleavage products are 33 nucleotides long, indicating cleavage at or near the base. In contrast, Dna2 C771A is unable to efficiently cleave at the base, where the majority of cleavage products are larger than 35 nucleotides, despite a similar rate of nuclease activity (*Figure 4.6B*).

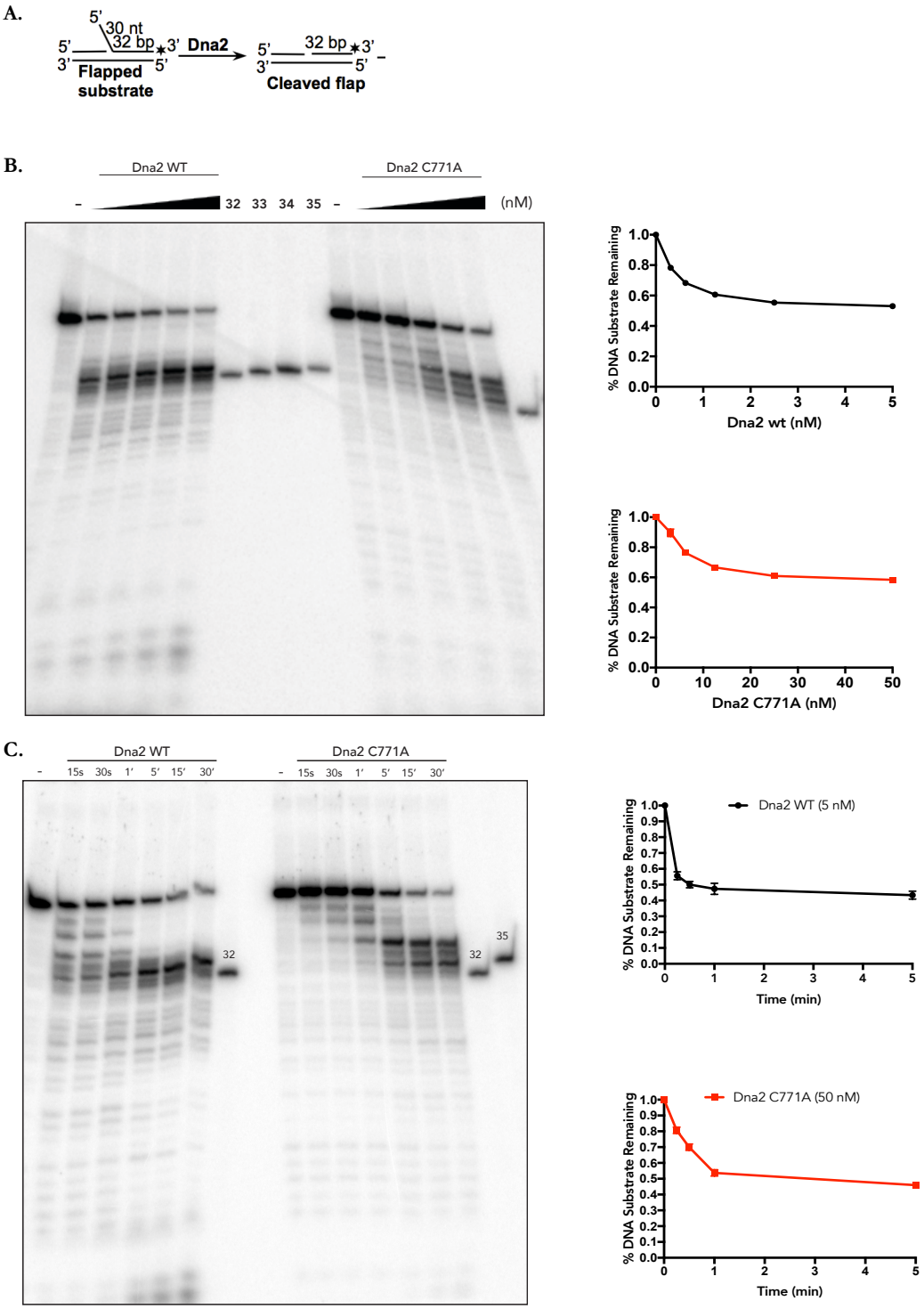

Figure 4.6 Okazaki Fragment Maturation Nuclease Assay (A). 30 nucleotide flap substrate that mimics a structure that arises upon displacement synthesis during Okazaki Fragment processing. **(B.)** Wild-type (0.3125-5nM) Dna2 and FeS binding mutant (3.125-50 nM), exhibit different cleavage patterns. Inset: Quantification of nuclease activity. Averages shown *n*=3; error bars, s.e.m. Nuclease reaction carried out as described in *Figure 3*. **(C.)** Time course experiments with 5nM WT and 50nM C771A. WT and C771A exhibit similar cleavage pattern in early time points, but the C771A is unable to efficiently cleave at the base at any time point, despite an overall similar rate in nuclease activity. Inset: Quantification:Averages shown *n*=3; error bars, s.e.m. 20% denaturing gel

Next, we investigated the cleavage dynamics between 5nM Dna2 WT and 50nM C771A in time course experiments. Both WT and the C771A mutant exhibited a similar rate of nuclease activity. However, while Dna2 WT cleaved a majority of its products at or near the base already at the earliest time points, the C771A mutant was unable to cleave efficiently at or near the base and instead exhibited cleavage products mainly away from the base - even at the latest time points *(Figure 4.6C)*. These data suggest that the integrity of the FeS cluster is critical for Dna2 to cleave efficiently at the base of a 5' flap.

Therefore, due to the fact that, during replication, flap processing is coupled with DNA synthesis by Pol δ, a plasmid-based ssDNA substrate which contains a 30 nt long ssDNA flap was used in a replication-coupled nuclease assay (performed by Dr. Maryna Levikova, UZH) that contains RFC, PCNA, RPA, and Lig1 *(Sec. 2.5.4)*. In this assay, the reaction is initiated when the replisome proteins are incubated with the substrate, generating a dsDNA open circular DNA intermediate. The open circular DNA intermediate can be further converted to a dsDNA closed circular product by the addition of Dna2 and Lig1. If Dna2 efficiently cleaves at or near the base, further processing by Pol δ through its synthesis or proofreading exonuclease activities will create a ligatable substrate that is ligated by Lig1 *(Figure 4.7A)*. As expected, Dna2 WT was able to cleave at or near the base, creating a ligatable substrate. In contrast, Dna2 C771A was unable to efficiently cleave at the base, which left non-ligatable substrates (*Figure 4.7B)*. Collectively, these results suggest that the FeS cluster in Dna2 is essential for regulating its cleavage site *in vitro*.

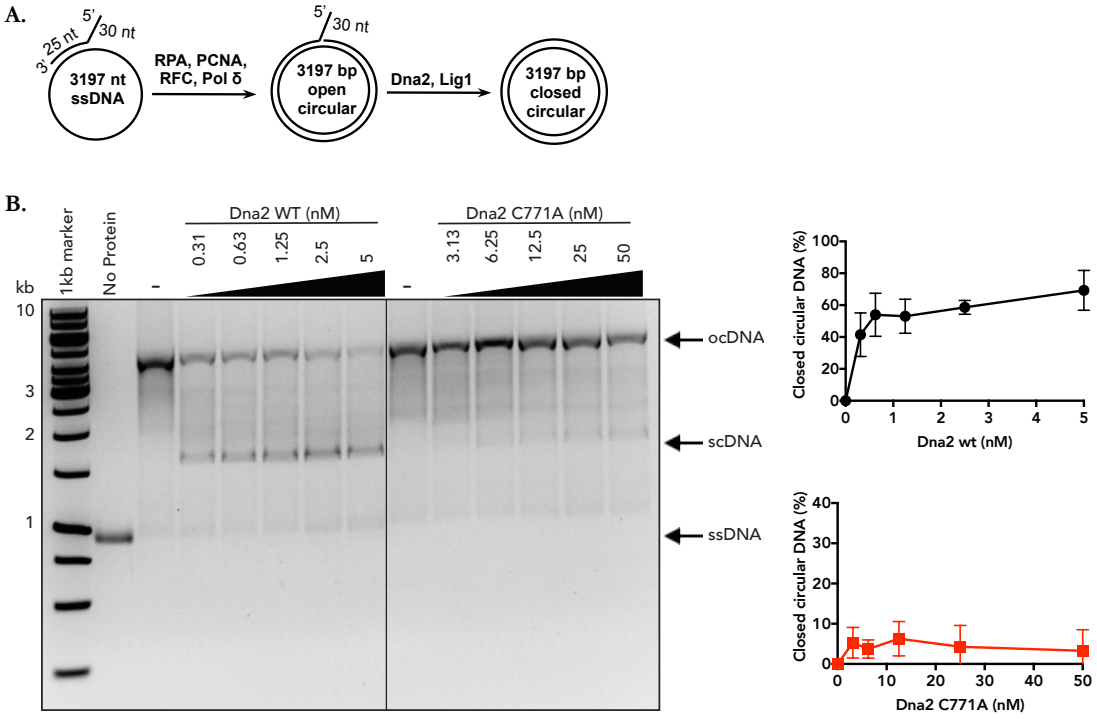

Figure 4.7 Replication Assay (A). Replication Assay with a 30nt flapped primer. **(B.)** Dna2 is required for the completion of replication of a substrate containing a 5' ssDNA flap of 30 nt in length. Reactions contained pol δ, PCNA, RFC, RPA, Lig1 and Dna2 as indicated. Positions of substrate ssDNA, open circular intermediate (ocDNA) and closed circular final product (scDNA) are indicated. Final product appears in a Dna2 concentration dependent manner. Inset: Quantitation of data; Averages shown, $n = 3$; error bars, s.e.m.

4.2.4 Using Sf9 Iron Incorporation To Characterize hDNA2

Until now, our studies focused on yeast Dna2, but in light of the growing number of nuclear FeS cluster proteins that function in various DNA-related activities and the implication of some of these proteins in human disease, we wanted to begin to characterize human DNA2. Therefore, using our newly developed Sf9 iron incorporation assay, we first tested to see if hDNA2 is a *bona fide* FeS cluster protein. Across three biological replicates, our results indicate that hDNA2 is indeed an FeS cluster protein when compared to the FeS binding mutant (C396S) *(Figure 4.8)*.

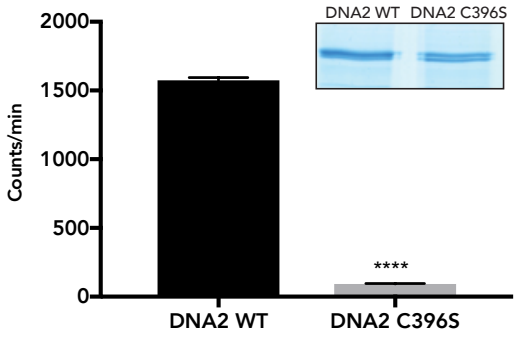

Figure 4.8 Sf9 ^{55}Fe Incorporation Assay: DNA2
Mean ^{55}Fe incorporation levels (Counts/min) in DNA2 WT and C396S. ^{55}Fe incorporation Inset: Protein Capture, 12% SDS; Coomassie blue

In addition, as stated above, FeS cluster protein biogenesis requires CIA machinery proteins MMS19 and MIP18 for the specific insertion of the FeS cluster *via* an unknown mechanism. Therefore, we wanted to develop a transient knockdown system of CIA machinery protein MIP18, taking advantage of a short-hairpin RNA that targets endogenous Sf9 MIP18. Unfortunately the entire Sf9 genome is not annotated; however, starting from a partially annotated sequence of MIP18 found in the Spodobase (Sf9 genome database), we had an shRNA synthesized that allows the direct ligation into the pFASTBac1 vector for baculovirus production. To test the effect of Sf9 MIP18 knockdown, we performed Fe incorporation experiments with wild-type human DNA2 non/co-infected with the shRNA-MIP18. As a control we used the FeS binding mutant DNA2 C396S. In parallel, we also by overexpressing human MIP18, attempted a rescue following the knockdown of the endogenous MIP18. Knockdown of endogenous MIP18 was confirmed by RT-PCR *(Figure 4.9C)* (*Sec. 2.2.7)*. As expected, DNA2 WT untreated with shRNA had efficient iron incorporation in comparison to the FeS binding mutant DNA2 C396S. Furthermore, DNA2 WT treated with shRNA saw greatly reduced iron incorporation, with a partial rescue with the co-infection of human MIP18 *(Figure 4.9A/B)*. Taken together, our data show hDNA2 to be a *bona fide* FeS cluster protein that incorporates iron *via* interaction with the Sf9 CIA machinery components.

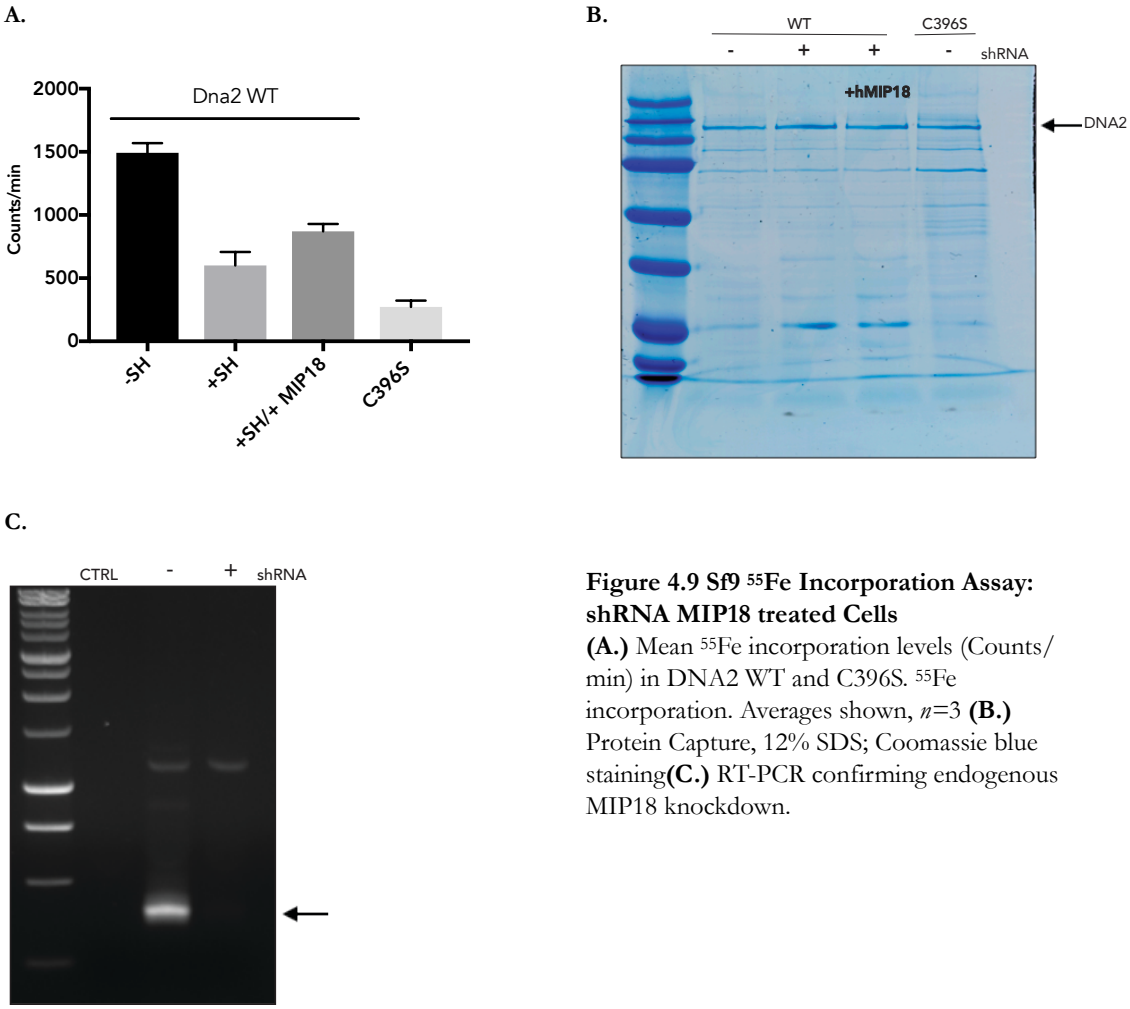

Figure 4.9 Sf9 ^{55}Fe Incorporation Assay: shRNA MIP18 treated Cells
(A.) Mean ^{55}Fe incorporation levels (Counts/min) in DNA2 WT and C396S. ^{55}Fe incorporation. Averages shown, n=3 **(B.)** Protein Capture, 12% SDS; Coomassie blue staining**(C.)** RT-PCR confirming endogenous MIP18 knockdown.

5. Discussion

Aim 1: Identifying Potential Novel Nuclear FeS Cluster Proteins: RFC5

5.1 RFC5 Interaction with the CIA Machinery

In this project, we aimed to investigate whether RFC5 coordinates an FeS cluster as a co-factor. As stated before, RFC5 was chosen as a candidate protein due to its identification as a potential interaction partner of MMS19 *via* mass spectrometry experiments and the observed synthetic lethality of RFC5's yeast counterpart Rfc3 with *mms19*Δ. To confirm RFC5's interaction with MMS19 and MIP18 we performed co-IP experiments in both Sf9 insect and HEK-293T cells, that revealed that RFC5 indeed interacts independently with both MMS19 and MIP18 *(Figure 3.2)*. However, when we attempted to detect the presence of iron in RFC5 *via* ^{55}Fe incorporation assays, our data revealed that RFC5 is unlikely to coordinate an FeS cluster as a co-factor. If RFC5 is indeed not an FeS cluster protein, more studies will be required to identify the relevance of RFC5's interaction with the CIA machinery.

Considering that nuclear FeS cluster protein biogenesis occurs in the cytoplasm *via* the CIA machinery, it would be important to identify in which cellular compartment the RFC5-CIA machinery interaction takes place, as MMS19 has also been shown to localize to the nucleus (Ito et al., 2010). Furthermore, it is also entirely possible that the interaction was a false positive, but the observed synthetic lethality of Rfc3 with *mms19*Δ points to a true interaction.

5.2 RFC5 Is Unlikely to Coordinate an FeS Cluster

As noted above, after we confirmed RFC5's interaction with MMS19 we attempted to detect the presence of iron in RFC5. ^{55}Fe incorporation assays in both yeast and Sf9 cells revealed RFC5 did not incorporate iron *(Figure 3.4 and Figure 3.7)*. Considering that RFC5 is a member of a heteropentameric complex, we hypothesized that the other small subunits of RFC could be required for the coordination of an FeS cluster, as it was shown that the four small subunits are required to form the holo-complex (Uhlmann et al., 1997). The FeS cluster protein XPD must first obtain its FeS cluster before its integration into an active TFIIH complex, but our data suggest that this is likely not the case with RFC5 (Vashisht et al., 2015). Therefore, our hypothesis is supported by the observation that the FeS cluster protein Primase (PriL) first forms its holocomplex with the non-FeS cluster containing small subunit (PriS) before its interaction with MMS19 and its subsequent coordination of an FeS cluster, inferred by the equal number of peptides of both the large and small subunits seen in MMS19 interaction mass spectrometry analysis (Stehling et al., 2012). Therefore, we attempted to produce baculoviruses for RFC3, RFC4,

and RFC1 to complete the complex. However, this presented the challenge of obtaining approximately equal amounts of each subunit, due to the need for separate viruses, as our previous experiments showed making a single virus using the T2A peptide would not be applicable here. As a consequence, we were unable to obtain conditions, to optimally express all subunits. In the end, the data we obtained suggested that RFC5 is unlikely to coordinate an FeS cluster. However, with addition of the small subunits (RFC2,3,4) perhaps the RFC complex together could coordinate an FeS cluster. The amino acid sequence of the four small subunits were analyzed and revealed that RFC3, RFC4, and RFC5 contain a *CXXC* motif at amino acids: 230-233, 177-180 and, 152-155 respectively. This motif has been shown to be important for FeS cluster coordination in a number of proteins that bind an FeS cluster in a labile fashion. (Bandyopadhyay et al., 2008; Netz et al., 2012; Sheftel et al., 2009). Therefore, it is tempting to speculate whether the RFC complex may coordinate an FeS cluster also in this fashion.

6. Discussion

Aim 2: Elucidating the Role of the Iron-Sulfur Cluster in the Nuclease/Helicase Dna2

6.1 FeS Cluster in Dna2 Is Essential For its Nuclease and Helicase Activities

In this project, we investigated the role of the FeS cluster in the nuclease/helicase Dna2. The role of the FeS cluster in Dna2 was previously investigated by Pokharel and Campbell, where they confirmed Dna2 to be an FeS cluster protein. Furthermore, their biochemical analysis revealed that loss of the FeS cluster was detrimental to its nuclease activity, but caused no defects in DNA binding and protein structure, as indicated by limited protease digestion experiments. Interestingly, the loss of the FeS cluster also reduced its ATPase activity, even though the ATPase domain is located in the C-terminal helicase domain (Pokharel & Campbell, 2012). Considering the fragile nature of FeS clusters and the threat of oxidation, coupled with advancements in protein purification and FeS cluster biology, we asked whether the integrity of the FeS cluster was maintained during purification in this earlier study. Therefore, we purified Dna2 and various mutants with an optimized protocol and tested their biochemical activities *in vitro*. Our data revealed an essential role of the FeS cluster in mediating both its nuclease and helicase activities.

6.2 Dna2's FeS Cluster Is Required For Potent Nuclease Activity

As stated before, a previous study on the FeS cluster in Dna2 showed that the loss of the FeS cluster eliminated Dna2's nuclease activity (Pokharel & Campbell, 2012). However, in contrast to this finding, we show that the loss of the FeS cluster significantly reduces Dna2's nuclease activity, but does not eliminate nuclease activity *(Figure 4.3)*. The FeS cluster in Dna2 has largely been considered a structural element, so the reduction in nuclease activity could be due to a structural conformational change. However, it was shown previously that DNA binding and overall structure was unaffected by the loss of the FeS cluster (Pokharel & Campbell, 2012). In our study, we did not address whether DNA binding or structure was affected, but it would be interesting to determine if our new optimized preps behave differently to those from the previous study. In the end, our data suggests the FeS cluster in Dna2 is required for potent nuclease activity.

6.3 Loss of the FeS Cluster in Dna2 Does Not Stimulate Helicase Activity.

Dna2 contains a Superfamily I helicase domain, shown to possess weak unwinding capability. However, it was later shown that upon nuclease inactivation, Dna2 possesses potent helicase activity that is comparable to a number of other helicases such as Sgs1 (Levikova et al., 2013). These data suggested that Dna2's helicase activity was masked

due to potent nuclease activity that cleaves 5' flaps required for helicase loading. Therefore, we hypothesized that the reduction in nuclease activity after FeS cluster loss could potentially stimulate helicase activity. Our data showed, that Dna2 has potent helicase activity upon nuclease inactivation as expected *(Figure 4.4)* However, the double nuclease-dead/FeS (E675A/C771A) and (C771A) mutant exhibited little to no helicase activity, indicating that the FeS cluster is required for helicase activity and that the loss of the FeS cluster does not stimulate helicase activity *via* reduction in nuclease activity *(Figure 4.4)*

6.4 The Role of Dna2's FeS Cluster in Okazaki Fragment Maturation

Dna2 has been shown to be an essential enzyme during DNA replication, where it has been shown to function during Okazaki fragment maturation (Budd et al., 1995). The general consensus of Dna2 function during Okazaki fragment maturation was to resect 5' DNA flaps upstream of Fen1 that are coated by RPA, which results in a shorter substrate that is then processed by Fen1. However, it was later shown that Dna2 can cleave at or near the base of the flap without the further requirement of Fen1 processing, challenging the "two-nuclease" model (Levikova & Cejka, 2015). We hypothesized that the integrity of the FeS cluster in Dna2 may be required for cleavage at or near the base, and that the FeS cluster may regulate the cleavage site of Dna2 in Okazaki fragment processing. To test this, we used recombinant wild-type and 10 times the concentration of the FeS binding mutant (C771A) Dna2 in a nuclease assay, which utilized a substrate mimicking a structure that arises upon displacement synthesis during Okazaki fragment processing *(Figure 4.6A)* (Levikova & Cejka, 2015). Here we show that recombinant Dna2 WT cleaves efficiently at or near the base of the 5' flap with majority of cleavage products being 32 nucleotides +/- 1 nucleotide long. In contrast, Dna2 C771A was unable to efficiently cleave at the base, where the majority of cleavage products are larger than 32 nucleotides, despite a similar rate of nuclease activity (*Figure 4.6B).* In addition, we performed time-course experiments between 5nM Dna2 WT and 50nM C771A. Our data revealed that both WT and the C771A exhibited a similar rate of nuclease activity. Over the course of the experiment qualitative differences in cleavage were observed, where Dna2 WT cleaved a majority of its products at or near the base, even at the earliest time points, whereas the C771A mutant cleaved the DNA substrate more indiscriminately, with cleavage products away from the base of the flap - even at the latest time points *(Figure 4.6C).* These data suggest that the integrity of the FeS cluster is critical for Dna2 to cleave efficiently at the base of a 5' flap. Next, we tested flap processing coupled with DNA synthesis by Pol δ, using a plasmid-based ssDNA substrate containing a 30 nt long ssDNA flap, using a replication-coupled nuclease assay (performed by Dr. Maryna Levikova, UZH) that contains RFC, PCNA, RPA, and Lig1 *(Sec. 2.5.4).* As expected, Dna2 WT was very efficient in flap processing by

allowing a nearly complete Okazaki fragment maturation, assisted by Pol δ's polymerase and 3'-5' exonuclease activities. In contrast, Dna2 C771A was unable to efficiently cleave at or near the base, which left non-ligatable substrates *(Figure 4.7B).* Collectively, these results suggest that the FeS cluster in Dna2 is essential for regulating its cleavage site *in vitro.*

6.5 FeS Cluster in Dna2: A Structural Element?

In this project we aimed to investigate the role of the FeS cluster in Dna2. Our results from biochemical analysis revealed the FeS cluster to be critical for both its nuclease and helicase activities. Furthermore, the FeS cluster was found to be essential in regulating the cleavage site during Okazaki fragment processing *in vitro.* Taken together, our results indicate that Dna2's activities can be regulated *via* its FeS cluster. However, a recent study of the the crystal structure of mouse Dna2 showed that the DNA is threaded through Dna2 *via* a narrow tunnel *(Figure 6.1)* (Zhou et al., 2015). Therefore, it is possible that the loss of the FeS cluster, which is located in the nuclease domain, could cause a conformational change, abrogating the threading of Dna2 onto DNA, which in turn reduces Dna2's nuclease activity. Furthermore, we saw a significant reduction in helicase activity of Dna2 in the double nuclease-dead/FeS binding mutant (E675A/C771A). Thus, it is also possible that this is due to the changes in Dna2's structure after FeS cluster loss, despite the fact the helicase domain is quite distant from the FeS binding domain. However, considering the essential role Dna2 plays in replication, the regulation of Dna2's activities through its FeS cluster could be by design. That is, when the replisome encounters DNA damage, local conditions could oxidize Dna2's FeS cluster, which in turn would reduce its nuclease activity and prevent helicase activity, allowing for the slow down of from progression so the damage can be repaired, a phenomenon that has been previously reported as a means to protect genome integrity (Iyer & Rhind, 2017). However, further studies, such as DNA fiber analysis to measure fork progression would be required to validate this hypothesis. Although it was tempting to speculate that the redox state of Dna2's FeS cluster plays a role in regulating the interplay between its nuclease and helicase activities, our data didn't support this notion. Moreover, it has been recently shown that Dna2 is SUMOylated in its N-terminal domain and that this modification abrogated Dna2's nuclease activity but not its helicase or ATPase activities (Levikova & Cejka, in press). Therefore, it is highly likely the interplay between Dna2's nuclease and helicase activities is determined by its post-translational modification status by SUMOylation.

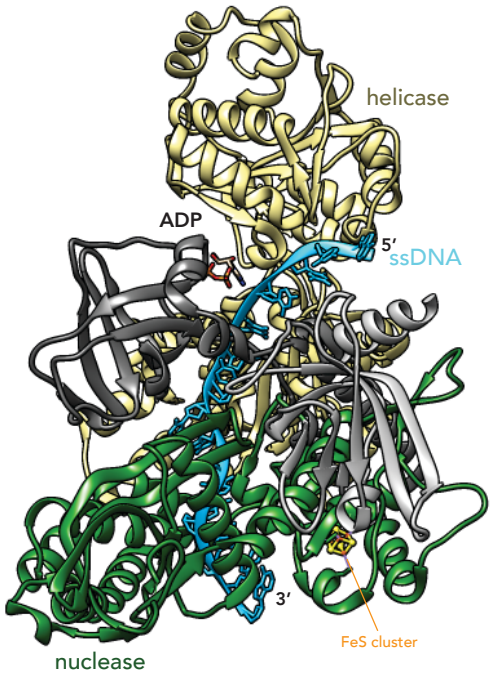

Figure 6.1 Crystal Structure of mDna2
Crystal structure of the Dna2-ssDNA complex. ssDNA depicted in blue. PDB Code: 5EAX (Zhou et al., 2015)

6.6 Dna2 Biochemical Analysis Outlook

In this study, we investigated the role of the FeS cluster in Dna2 and how it may regulate Dna2's cellular activities. Our data revealed an essential role in both Dna2's nuclease and helicase activities *in vitro*. Furthermore, the FeS cluster was critical for cleavage site regulation during the processing of Okazaki fragments. However, to obtain a complete picture on how Dna2's FeS cluster regulates its cellular activities, we've identified the following experiments that are critical to extend or confirm our preliminary results:

1. Purification of Dna2 WT from a *mms19*Δ background- In this construct, the absence of endogenous MMS19 would allow us to test Dna2 WT without the coordination of an FeS cluster. With this new construct, we can directly compare the biochemical activities of the FeS binding mutant, confirming our results we obtained showing a critical role of the FeS cluster in both nuclease and helicase activities.

2. DNA Binding - In our study we did not address DNA binding as it was shown not to be affected in a previous study by Pokharel and Campbell (Pokharel & Campbell, 2012). However, considering the large impact of the loss of the FeS cluster on Dna2's nuclease and helicase activities, it will be critical to address whether the reduction in nuclease and helicase activity is due to less stable DNA binding.

3. RPA Interaction Study- In our Okazaki fragment processing experiments, we showed that the FeS binding mutant was unable to cleave 5' flaps at or near the base in comparison with the WT. Considering that RPA has been shown to enhance Dna2 activity, we want to address whether the difference in cleavage is not due to a loss in Dna2-RPA interaction.

4. Role of FeS cluster in long rage resection- It has been shown that hydrolysis of ATP is important for Dna2's ability to translocate to the base of a 5' flap generated by the Sgs1 helicase in an *exo1*Δ background (Miller et al., 2017). Therefore, considering how the loss of the FeS cluster abolished helicase activity, it would be interesting to see if the loss of the FeS cluster also plays a role in Dna2's ability to translocate along a 5' flap, as the abolished helicase activity infers a loss in ATPase activity.

6.7 Using Sf9 Iron Incorporation To Characterize Human DNA2

In our studies we focused on yeast Dna2, but in light of the growing number of nuclear FeS cluster proteins that function in DNA metabolism and the implication of some of these proteins in human disease, we began to characterize human DNA2. First, we confirmed hDNA2 to be a *bona fide* FeS cluster protein by Sf9 iron incorporation *(Figure 4.8)*. Next, to test hDNA2 iron incorporation upon the knockdown of endogenous Sf9 MIP18, we performed experiments with wild-type human DNA2 non/co-infected with the shRNA-MIP18. In parallel, we overexpressed human MIP18 in shRNA treated DNA2 WT cells to attempt a rescue following the knockdown of the endogenous MIP18.*(Figure 4.9C) (Sec. 2.2.7)*. As expected, DNA2 WT untreated with shRNA, had efficient iron incorporation in comparison to the FeS binding mutant DNA2 C396S. Furthermore, DNA2 WT treated with shRNA saw greatly reduced iron incorporation, with a partial rescue with the co-infection of human MIP18 *(Figure 4.9A/B)*. Taken together, our data show hDNA2 to be a *bona fide* FeS cluster protein, that incorporates iron *via* interaction with the Sf9 CIA machinery components.

Moving forward we aim to optimize protein expression levels and MIP18 rescue, which will allow us to obtain clearer differences in iron incorporation. Furthermore, considering that MIP18 was originally identified in a proteome-wide screen for factors that contain hyperreactive cysteines (Weerapana et al., 2010), we aim to produce a MIP18 baculovirus with a point mutation in this cysteine residue, to investigate whether MIP18 is involved in the transient binding of an FeS cluster and the transfer to apoproteins. In the end, the Sf9 iron incorporation will allow us to i) identify and characterize known and unknown FeS cluster proteins and ii) with the knockdown and rescue experiments further elucidate how FeS cluster biogenesis occurs. Collectively, these experiments, will allow us to

obtain more information on how FeS clusters in DNA metabolizing proteins function and the role they play in preserving genomic integrity.

7. Bibliography

Abbas, T., Keaton, M. A., et al. (2013). Genomic instability in cancer. *Cold Spring Harb Perspect Biol,* 5(3), a012914.

Aguilera, A., & García-Muse, T. (2013). Causes of genome instability. *Annu Rev Genet,* 47, 1-32.

Alberts, B., Johnson, A., et al. (2015). Molecular Biology of The Cell. *Garland Science*.

Andegeko, Y., Moyal, L., et al. (2001). Nuclear retention of ATM at sites of DNA double strand breaks. *J Biol Chem,* 276(41), 38224-38230.

Awasthi, P., Foiani, M., et al. (2015). ATM and ATR signaling at a glance. *Journal of Cell Science,* 128(23), 4255-4262.

Ayyagari, R., Gomes, X. V., et al. (2003). Okazaki fragment maturation in yeast. I. Distribution of functions between FEN1 AND DNA2. *J Biol Chem,* 278(3), 1618-1625.

Bae, S. H., & Seo, Y. S. (2000). Characterization of the enzymatic properties of the yeast Dna2 Helicase/endonuclease suggests a new model for Okazaki fragment processing. *Journal of Biological Chemistry,* 275(48), 38022-38031.

Bae, S. H., Bae, K. H., et al. (2001). RPA governs endonuclease switching during processing of Okazaki fragments in eukaryotes. *Nature,* 412, 456-461.

Bae, S. H., Choi, E., et al. (1998). Dna2 of *Saccharomyces cerevisiae* Possesses a Single-stranded DNA-specific Endonuclease Activity That Is Able to Act on Double-stranded DNA in the Presence of ATP. *J Biol Chem,* 273(41), 26880-26890.

Balakrishnan, L., & Bambara, R. A. (2011). Eukaryotic lagging strand DNA replication employs a multi-pathway mechanism that protects genome integrity. *J Biol Chem,* 286(9), 6865-6870.

Balakrishnan, L., & Bambara, R. A. (2013). Flap endonuclease 1. *Annu Rev Biochem,* 82, 119-138.

Balakrishnan, L., Polaczek, P., et al. (2010). Dna2 exhibits a unique strand end-dependent helicase function. *J Biol Chem,* 285(50), 38861-38868.

Bandyopadhyay, S., Chandramouli, K., et al. (2008). Iron-sulfur cluster biosynthesis. *Biochem Soc Trans,* 36(Pt 6), 1112-1119.

Barras, F. (2017). Iron-Sulfur Proteins: Structure, Function and Biogenesis. *eLS. John Wiley & Sons, Ltd*, 1-9.

Bartkova, J., Horejsí, Z., et al. (2005). DNA damage response as a candidate anti-cancer barrier in early human tumorigenesis. *Nature,* 434, 864-870.

Bermudez, V. P., Lindsey-Boltz, L. A., et al. (2003). Loading of the human 9-1-1 checkpoint complex onto DNA by the checkpoint clamp loader hRad17-replication factor C complex in vitro. *Proc. Natl. Acad. Sci. U.S.A.,* 100(4), 1633-1638.

Bhargava, R., Onyango, D. O., et al. (2016). Regulation of Single-Strand Annealing and its Role in Genome Maintenance. *Trends Genet,* 32(9), 566-575.

Bizard, A. H., & Hickson, I. D. (2014). The Dissolution of Double Holliday Junctions. *Cold Spring Harb Perspect Biol,* 6(7), a01647.

Boal, A. K., Yavin, E., et al. (2007). DNA repair glycosylases with a [4Fe-4S] cluster: a redox cofactor for DNA-mediated charge transport? *J. Inorg. Biochem.,* 101(11-12), 1913-1921.

Boal, A. K., Yarvin, E., et al. (2005). DNA-Bound Redox Activity of DNA Repair Glycosylases Cotaining [4Fe-4S] Clusters. *Biochemistry,* 44(23), 8397-8407.

Boal, A. K., Genereux, J. C., et al. (2009). Redox signaling between DNA repair proteins for efficient lesion detection. *Proc. Natl. Acad. Sci. U.S.A,* 106(36), 15237-15242.

Boon, E. M., Ceres, D. M., et al. (2000). Mutation detection by electrocatalysis at DNA-modified electrodes. *Nat Biotechnol,* 18(10), 1096-1100.

Budd, M. E., & Campbell, J. L. (1995). A yeast gene required for DNA repliction encodes a protein with homology to DNA helicases. *Proc. Natl. Acad. Sci. U.S.A,* 92, 7642-7646.

Budd, M. E., & Campbell, J. L. (1997). A Yeast Replicative Helicase, Dna2 Helicase, Interacts with Yeast FEN-1 Nuclease in Carrying Out Its Essential Function. *Molecular and Cellular Biology,* 17(4), 2136-2142.

Budd, M. E., & Campbell, J. L. (2000). The pattern of sensitivity of yeast *dna2* mutants to DNA damaging agents suggests a role in DSB and postreplication repair pathways. *Mutation Research,* 459(3), 173-186.

Budd, M. E., Choe, W. C., et al. (1995). *DNA2* Encodes a DNA Helicase Essential for Replication of Eukaryotic Chromosomes. *J Biol Chem,* 270(45), 26766-26769.

Budd, M. E., Choe, W. C., et al. (2000). The nuclease activity of the yeast DNA2 protein, which is related to the RecB-like nucleases, is essential *in vivo*. *J Biol Chem,* 275(22), 16518-16529.

Budd, M. E., Reis, C. C., et al. (2006). Evidence suggesting that Pif1 helicase functions in DNA replication with the Dna2 helicase/nuclease and DNA polymerase delta. *Mol Cell Biol,* 26(7), 2490-2500.

Budd, M. E., Tong, A. H., et al. (2005). A network of multi-tasking proteins at the DNA replication fork preserves genome stability. *PLoS Genet,* 1(6), e61.

Burgers, P. M. (2009). Polymerase dynamics at the eukaryotic DNA replication fork. *J Biol Chem,* 284(7), 4041-4045.

Burgers, P. M. J., & Kunkel, T. A. (2017). Eukaryotic DNA Replication Fork. *Annual Review of Biochemistry,* 86, 417-438.

Capo-Chichi, J. M., Bharti, S. K., et al. (2013). Identification and biochemical characterization of a novel mutation in DDX11 causing Warsaw breakage syndrome. *Hum Mutat,* 34(1), 103-107.

Carson, C., Schwartz, R. A., et al. (2003). The Mre11 complex is required for ATM activation and the G2/M checkpoint. *EMBO Journal,* 22(24), 6610-6620.

Cejka, P., Cannavo, E., et al. (2010). DNA end resection by Dna2-Sgs1-RPA and its stimulation by Top3-Rmi1 and Mre11-Rad50-Xrs2. *Nature,* 467(7311), 112-116.

Chapman, J. R., Taylor, M. R., et al. (2012). Playing the end game: DNA double-strand break repair pathway choice. *Mol Cell,* 47(4), 497-510.

Ciccia, A., & Elledge, S. J. (2010). The DNA Damage Response: Making It Safe to Play with Knives. *Mol. Cell,* 40(2), 179-204.

Collins, S. R., Miller, K. M., et al. (2007). Functional dissection of protein complexes involved in yeast chromosome biology using a genetic interaction map. *Nature,* 446(7137), 806-810.

Daee, D., & Myung, K. (2010). Small RFC subunits make a big difference. *Cell Cycle,* 9(22), 4429.

Davis, A. J., & Chen, D. J. (2013). DNA double strand break repair via non-homologous end-joining. *Transl Cancer Res,* 2(3), 130-143.

DePamphilis, M. L., Blow, J. J., et al. (2006). Regulating the licensing of DNA replication origins in metazoa. *Curr Opin Cell Biol,* 18(3), 231-239.

Dos Santos, P. C., & Dean, D. R. (2017). Iron-Sulfur Clusters in Chemistry and Biology: Chapter 1: A retrospective on the discovery of [Fe-S] cluster biosynthetic machineries in Azobacter vinelandii (T. A. Rouault Ed. Vol. 2: Biochemistry, Biosynthesis, and Human Diseases). Berlin/Boston: De Gruyter.

Formosa, T., & Nittis, T. (1999). *Dna2*Mutants Reveal Interactions with Dna Polymerase α and Ctf4, a Pol α Acessory Factor, and Show That Full Dna2 Helicase Activity Is Not Essential for Growth. *Genetics,* 151(4), 1459-1470.

Garg, P., & Burgers, P. M. (2005). DNA polymerases that propagate the eukaryotic DNA replication fork. *Crit Rev Biochem Mol Biol,* 40(2), 115-128.

Garg, P., Stith, C. M., et al. (2004). Idling by DNA polymerase delta maintains a ligatable nick during lagging-strand DNA replication. *Genes Dev,* 18(22), 2764-2773.

Gari, K., León Ortiz, A. M., et al. (2012). MMS19 links cytoplasmic iron-sulfur cluster assembly to DNA metabolism. *Science,* 337(6091), 243-245.

Georgescu, R. E., Langston, L., et al. (2014). Mechanism of asymmetric polymerase assembly at the eukaryotic replication fork. *Nat Struct Mol Biol,* 21(8), 664-670.

Gerik, K. J., Li, X., et al. (1998). Characterization of the Two Small Subunits of *Saccharomyces cerevisiae* DNA Polymerase Delta. *Journal of Biological Chemistry,* 273(31), 19747-19755.

Gorgoulis, V. G., Vassiliou, L.-V. F., et al. (2005). Activation of the DNA damage checkpoint and genomic instability in human precancerous lesions. *Nature,* 434, 907-913.

Gottlieb, T., & Jackson, S. P. (1993). The DNA-dependent protein kinase: requirement for DNA ends and association with Ku antigen. *Cell,* 72, 131-142.

Halazonetis, T. D., Gorgoulis, V. G., et al. (2008). An Oncogene-Induced DNA Damage Model for Cancer Development. *Science,* 319, 1352-1355.

Hedglin, M., Kumar, R., et al. (2013). Replication Clamps and Clamp Loaders. *Cold Spring Harbor Perspectives in Biology,* 5(4), a010165-a010165.

Hoeijmakers, J. H. J. (2001). Genome maintenance mechanisms for preventing cancer. *Nature,* 411(6835), 366-374.

Hoeijmakers, J. H. J. (2009). Dna Damage, Aging, and Cancer. *The New England Journal of Medicine,* 361(15), 1475-1485.

Huertas, P., Cortes-Ledesma, F., et al. (2008). CDK targets Sae2 to control DNA-end resection and homologous recombination. *Nature,* 455(7213), 689-692.

Imlay, J. A. (2006). Iron-Sulphur clusters and the problem with oxygen. *Molecular Microbiology,* 59(4), 1073-1082.

Ito, S., Tan, L. J., et al. (2010). MMXD, a TFIIH-independent XPD-MMS19 protein complex involved in chromosome segregation. *Mol Cell,* 39(4), 632-640.

Iyama, T., & Wilson III, D. M. (2013). DNA repair mechanisms in dividing and non-dividing cells. *DNA Repair,* 12(8), 620-636.

Iyer, D. R., & Rhind, N. (2017). Replication fork slowing and stalling are distinct, checkpoint-independent consequences of replicating damaged DNA. *PLoS Genet,* 13(8), e1006958.

Jasin, M., & Rothstein, R. (2013). Repair of strand breaks by homologous recombination. *Cold Spring Harb Perspect Biol,* 5(11), a012740.

Johansson, E., Garg, P., et al. (2004). The Pol32 subunit of DNA polymerase delta contains separable domains for processive replication and proliferating cell nuclear antigen (PCNA) binding. *J Biol Chem,* 279(3), 1907-1915.

Johnson, A., Yao, N. Y., et al. (2006). The replication factor C clamp loader requires arginine finger sensors to drive DNA binding and proliferating cell nuclear antigen loading. *Journal of Biological Chemistry,* 281(46), 35531-35543.

Johnson, R. E., Klassen, R., et al. (2015). A Major Role of DNA Polymerase delta in Replication of Both the Leading and Lagging DNA Strands. *Mol Cell,* 59(2), 163-175.

Kelley, S. O., & Barton, J. K. (1999). Electron transfer between bases in double helical DNA. *Science,* 283, 375-381.

Kotula, E., Faigle, W., et al. (2013). DNA-PK target identification reveals novel links between DNA repair signaling and cytoskeletal regulation. *PLoS One,* 8(11), e80313.

Krejci, L., Altmannova, V., et al. (2012). Homologous recombination and its regulation. *Nucleic Acids Res,* 40(13), 5795-5818.

Kubota, T., Nishimura, K., et al. (2013). The Elg1 Replication Factor C-like Complex Functions in PCNA Unloading during DNA Replication. *Mol. Cell,* 50(2), 273-280.

Kuo, C. L., Huang, N. H., et al. (1983). Isolation of yeast DNA replication mutants in permeabilized cells. *Proc. Natl. Acad. Sci. U.S.A,* 80, 6465-6469.

Le Guen, T., Jullien, L., et al. (2013). Human RTEL1 deficiency causes Hoyeraal-Hreidarsson syndrome with short telomeres and genome instability. *Hum Mol Genet,* 22(16), 3239-3249.

Lee, K.-y., Fu, H., et al. (2013). ATAD5 regulates the lifespan of DNA replication factories by modulating PCNA level on the chromatin. *The Journal of Cell Biology,* 200(1), 31-44.

Lee, K. H., Kim, D. W., et al. (2000). The endonuclease activity of the yeast Dna2 enzyme is essential *in vivo*. *Nucleic Acids Res,* 28(15), 2873-2881.

Lehmann, A. (2003). DNA repair-deficient diseases, xeroderma pigmentosum, Cockayne syndrome and trichothiodystrophy. *Biochimie,* 85(11), 1101-1111.

Levikova, M., & Cejka, P. (2015). The *Saccharomyces cerevisiae* Dna2 can function as a sole nuclease in the processing of Okazaki fragments in DNA replication. *Nucleic Acids Research,* 43(16), 7888-7897.

Levikova, M., Klaue, D., et al. (2013). Nuclease activity of *Saccharomyces cerevisiae* Dna2 inhibits its potent DNA helicase activity. *Proceedings of the National Academy of Sciences,* 110(22), E1992-2001.

Lill, R. (2009). Function and biogenesis of iron–sulphur proteins. *Nature,* 460(7257), 831-838.

Lill, R., & Mühlenhoff, U. (2008). Maturation of iron-sulfur proteins in eukaryotes: mechanisms, connected processes, and diseases. *Annu Rev Biochem,* 77, 669-700.

Loeb, L. A. (2011). Human cancers express mutator phenotypes: origin, consequences and targeting. *Nat Rev Cancer,* 11(6), 450-457.

Majka, J., & Burgers, P. M. J. (2004). The PCNA-RFC Families of DNA Clamps and Clamp Loaders. *Prog. Nucleic Acid Res. Mol. Biol.*, 1-34.

Maréchal, A., & Zou, L. (2013). DNA Damage Sensing by the ATM and ATR Kinases. *Cold Spring Harbor Perspectives in Biology,* 5(9), a012716-a012716.

Marzahn, M. R., Hayner, J. N., et al. (2014). The ATP sites of AAA+ clamp loaders work together as a switch to assemble clamps on DNA. *J. Biol. Chem.,* 289(9), 5537-5548.

Masai, H., Matsumoto, S., et al. (2010). Eukaryotic chromosome DNA replication: where, when, and how? *Annu Rev Biochem,* 79, 89-130.

Matsuoka, S., Ballif, B. A., et al. (2007). ATM and ATR substrate analysis reveals extensive protein networks responsive to DNA damage. *Science,* 316, 1160-1166.

McVey, M., Khodaverdian, V. Y., et al. (2016). Eukaryotic DNA Polymerases in Homologous Recombination. *Annu Rev Genet,* 50, 393-421.

Mehta, A., & Haber, J. E. (2014). Sources of DNA double-strand breaks and models of recombinational DNA repair. *Cold Spring Harb Perspect Biol,* 6(9), a016428.

Miller, A. S., Daley, J. M., et al. (2017). A novel role of the Dna2 translocase function in DNA break resection. *Genes & Development*.

Mimitou, E. P., & Symington, L. S. (2008). Sae2, Exo1 and Sgs1 collaborate in DNA double-strand break processing. *Nature,* 455(7214), 770-774.

Negrini, S., Gorgoulis, V. G., et al. (2010). Genomic instability--an evolving hallmark of cancer. *Nat Rev Mol Cell Biol,* 11(3), 220-228.

Netz, D. J., Pierik, A. J., et al. (2012). A bridging [4Fe-4S] cluster and nucleotide binding are essential for function of the Cfd1-Nbp35 complex as a scaffold in iron-sulfur protein maturation. *J Biol Chem,* 287(15), 12365-12378.

Netz, D. J. A., Pierik, A. J., et al. (2007). The Cfd1-Npb35 complex acts as a scaffold for iron-sulfur protein assembly in the yeast cytosol. *Nat Chem Biol,* 3(5), 278-286.

Netz, D. J. A., Mascarenhas, J., et al. (2013). Maturation of cytosolic and nuclear iron-sulfur proteins. *Trends Cell Biol.*

Netz, D. J. A., Stith, C. M., et al. (2012). Eukaryotic DNA polymerases require an iron-sulfur cluster for the formation of active complexes. *Nat. Chem. Biol.,* 8(1), 125-132.

Núñez, M. E., Hall, D. B., et al. (1999). Long-range oxidative damage to DNA: Effects of distance and sequence. *Chem. Biol.,* 6(2), 85-97.

O'Brien, E., Holt, M. E., et al. (2017). The [4Fe4S] cluster of human DNA primase functions as a redox switch using DNA charge transport. *Science,* 355(6327)

Odermatt, D. C., & Gari, K. (2017). The CIA Targeting Complex Is Highly Regulated and Provides Two Distinct Binding Sites for Client Iron- Sulfur Proteins. *CellReports,* 18(6), 1434-1443.

Paul, V. D., & Lill, R. (2015). Biogenesis of cytosolic and nuclear iron-sulfur proteins and their role in genome stability. *Biochimica et Biophysica Acta,* 1853(6), 1528-1539.

Pierik, A. J., Netz, D. J. A., et al. (2009). Analysis of iron–sulfur protein maturation in eukaryotes. *Nat Protoc,* 4(5), 753-766.

Pike, J. E., Burgers, P. M., et al. (2009). Pif1 helicase lengthens some Okazaki fragment flaps necessitating Dna2 nuclease/helicase action in the two-nuclease processing pathway. *J Biol Chem,* 284(37), 25170-25180.

Pokharel, S., & Campbell, J. L. (2012). Cross talk between the nuclease and helicase activities of Dna2: role of an essential iron-sulfur cluster domain. *Nucleic Acids Research,* 40(16), 7821-7830.

Reagan, M. S., Pittenger, C., et al. (1995). Characterization of a Mutant Strain of *Saccharomyces cerevisiae* with a Deletion of the *RAD27* Gene, a Structural Homolog of the*RAD2*Nucleotide Excision Repair Gene. *Journal of Bacteriology,* 177(2), 364-371.

Rees, D. C. (2002). Great metalloclusters in enzymology. *Annu Rev Biochem,* 71, 221-246.

Rees, D. C., & Howard, J. B. (2003). The interface between the biological and inorganic worlds: iron-sulfur metalloclusters. *Science,* 300(5621), 929-931.

Rossi, M. L., Pike, J. E., et al. (2008). Pif1 helicase directs eukaryotic Okazaki fragments toward the two-nuclease cleavage pathway for primer removal. *J Biol Chem,* 283(41), 27483-27493.

Rouault, T. A. (2015). Mammalian iron-sulphur proteins: novel insights into biogenesis and function. *Nat Rev Mol Cell Biol,* 16(1), 45-55.

Rudolf, J., Makrantoni, V., et al. (2006). The DNA repair helicases XPD and FancJ have essential iron-sulfur domains. *Mol Cell,* 23(6), 801-808.

Salk, J. J., Fox, E. J., et al. (2010). Mutational heterogeneity in human cancers: origin and consequences. *Annu Rev Pathol,* 5, 51-75.

Schwartz, E. K., & Heyer, W. D. (2011). Processing of joint molecule intermediates by structure-selective endonucleases during homologous recombination in eukaryotes. *Chromosoma,* 120(2), 109-127.

Sclafani, R. A., & Holzen, T. M. (2007). Cell cycle regulation of DNA replication. *Annu Rev Genet,* 41, 237-280.

Seki, M., Takeda, Y., et al. (2013). IOP1 protein is an external component of the human cytosolic iron-sulfur cluster assembly (CIA) machinery and functions in the MMS19 protein-dependent CIA pathway. *J. Biol. Chem.,* 288(23), 16680-16689.

Sheftel, A. D., Stehling, O., et al. (2009). Human ind1, an iron-sulfur cluster assembly factor for respiratory complex I. *Mol Cell Biol,* 29(22), 6059-6073.

Shiloh, Y. (2003). ATM and related protein kinases: safeguarding genome integrity. *Nat Rev Cancer,* 3, 155-168.

Skibbens, R. V. (2005). Unzipped and loaded: the role of DNA helicases and RFC clamp-loading complexes in sister chromatid cohesion. *The Journal of Cell Biology,* 169(6), 841-846.

Sommers, C. H., Miller, E. J., et al. (1995). Conditional Lethality of Null Mutations in *RTH1* that Encodes the Yeast Counterpart of a Mammalian 5'- to 3'-Exonuclease Required for Lagging Strand DNA Synthesis in Reconstituted Systems. *Journal of Biological Chemistry,* 270(9), 4193-4196.

Stehling, O., Vashisht, A. A., et al. (2012). MMS19 assembles iron-sulfur proteins required for DNA metabolism and genomic integrity. *Science,* 337(6091), 195-199.

Stewart, J. A., Campbell, J. L., et al. (2010). Dna2 is a structure-specific nuclease, with affinity for 5'-flap intermediates. *Nucleic Acids Res,* 38(3), 920-930.

Stith, C. M., Sterling, J., et al. (2008). Flexibility of eukaryotic Okazaki fragment maturation through regulated strand displacement synthesis. *J Biol Chem,* 283(49), 34129-34140.

Symington, L. S., & Gautier, J. (2011). Double-strand break end resection and repair pathway choice. *Annu Rev Genet,* 45, 247-271.

Szymczak, A. L., Workman, C. J., et al. (2004). Correction of multi-gene deficiency in vivo using a single self-cleaving 2A peptide–based retroviral vector. *Nat Biotechnol,* 22(5), 589-594.

Técher, H., Koundrioukoff, S., et al. (2017). The impact of replication stress on replication dynamics and DNA damage in vertebrate cells. *Nature Publishing Group,* 18(9), 535-550.

Thompson, J. A., Marzahn, M. R., et al. (2012). Replication factor C is a more effective proliferating cell nuclear antigen (PCNA) opener than the checkpoint clamp loader, Rad24-RFC. *J Biol Chem,* 287(3), 2203-2209.

Uhlmann, F., Gibbs, E., et al. (1997). Identification of regions within the four small subunits of human replication factor C required for complex formation and DNA replication. *Journal of Biological Chemistry,* 272(15), 10065-10071.

van der Lelij, P., Chrzanowska, K. H., et al. (2010). Warsaw breakage syndrome, a cohesinopathy associated with mutations in the XPD helicase family member DDX11/ChlR1. *Am J Hum Genet,* 86(2), 262-266.

van Wietmarschen, N., Moradian, A., et al. (2012). The mammalian proteins MMS19, MIP18, and ANT2 are involved in cytoplasmic iron-sulfur cluster protein assembly. *J Biol Chem,* 287(52), 43351-43358.

Vannier, J. B., Sarek, G., et al. (2014). RTEL1: functions of a disease-associated helicase. *Trends Cell Biol,* 24(7), 416-425.

Vashisht, A. A., Yu, C. C., et al. (2015). The Association of the Xeroderma Pigmentosum Group D DNA Helicase (XPD) with Transcription Factor IIH Is Regulated by the Cytosolic Iron-Sulfur Cluster Assembly Pathway. *J. Biol. Chem.,* 290(22), 14218-14225.

Wanrooij, P. H., & Burgers, P. M. (2015). Yet another job for Dna2: Checkpoint activation. *DNA Repair,* 32, 17-23.

Weerapana, E., Wang, C., et al. (2010). Quantitative reactivity profiling predicts functional cysteines in proteomes. *Nature,* 468(7325), 790-795.

White, M. F. (2009). Structure, function and evolution of the XPD family of iron-sulfur-containing 5'-->3' DNA helicases. *Biochem Soc Trans,* 37(Pt 3), 547-551.

White, M. F., & Dillingham, M. S. (2012). Iron-sulphur clusters in nucleic acid processing enzymes. *Curr Opin Struct Biol,* 22(1), 94-100.

Wrensch, M., Jenkins, R. B., et al. (2009). Variants in the CDKN2B and RTEL1 regions are associated with high-grade glioma susceptibility. *Nat Genet,* 41(8), 905-908.

Wu, Y., & Brosh, R. M. (2012). DNA helicase and helicase-nuclease enzymes with a conserved iron-sulfur cluster. *Nucleic Acids Research,* 40(10), 4247-4260.

Wu, Y., Sommers, J. A., et al. (2010). Fanconi anemia group J mutation abolishes its DNA repair function by uncoupling DNA translocation from helicase activity or disruption of protein-DNA complexes. *Blood,* 116(19), 3780-3791.

Yang, X. H., & Zou, L. (2006). Recruitment of ATR−ATRIP, Rad17, and 9−1−1 Complexes to DNA Damage. *Methods in Enzymology,* 409, 118-131.

Yao, Y., & Dai, W. (2014). Genomic Instability and Cancer. *J Carcinog Mutagen,* 5.

Yeeles, J. T. P., Cammack, R., et al. (2009). An Iron-Sulfur Cluster Is Essential for the Binding of Broken DNA by AddAB-type Helicase-Nucleases. *Journal of Biological Chemistry,* 284(12), 7746-7755.

Zeman, M. K., & Cimprich, K. A. (2014). Causes and consequences of replication stress. *Nat. Cell Biol.,* 16(1), 2-9.

Zhang, C. (2014). Essential functions of iron-requiring proteins in DNA replication, repair and cell cycle control. *Protein Cell,* 5(10), 750-760.

Zhou, C., Pourmal, S., et al. (2015). Dna2 nuclease-helicase structure, mechanism and regulation by Rpa. *Elife,* 4, 213.

Zhu, Z., Chung, W.-H., et al. (2008). Sgs1 Helicase and Two Nucleases Dna2 and Exo1 Resect DNA Double-Strand Break Ends. *Cell,* 134(6), 981-994.

Zou, L., & Elledge, S. J. (2003). Sensing DNA Damage Through ATRIP Recognition of RPA-ssDNA Complexes. *Science,* 300, 1542-1548.